

1977

Response Of The Laminar Layer On A Flat Plate To Free Stream Disturbances

Hassan Mohamed Badr

Follow this and additional works at: <https://ir.lib.uwo.ca/digitizedtheses>

Recommended Citation

Badr, Hassan Mohamed, "Response Of The Laminar Layer On A Flat Plate To Free Stream Disturbances" (1977). *Digitized Theses*. 1000.

<https://ir.lib.uwo.ca/digitizedtheses/1000>

This Dissertation is brought to you for free and open access by the Digitized Special Collections at Scholarship@Western. It has been accepted for inclusion in Digitized Theses by an authorized administrator of Scholarship@Western. For more information, please contact tadam@uwo.ca, wlsadmin@uwo.ca.



National Library of Canada

Cataloguing Branch
Canadian Theses Division

Ottawa, Canada
K1A 0N4

Bibliothèque nationale du Canada

Direction du catalogage
Division des thèses canadiennes

NOTICE

The quality of this microfiche is heavily dependent upon the quality of the original thesis submitted for microfilming. Every effort has been made to ensure the highest quality of reproduction possible.

If pages are missing, contact the university which granted the degree.

Some pages may have indistinct print especially if the original pages were typed with a poor typewriter ribbon or if the university sent us a poor photocopy.

Previously copyrighted materials (journal articles, published tests, etc.) are not filmed.

Reproduction in full or in part of this film is governed by the Canadian Copyright Act, R.S.C. 1970, c. C-30. Please read the authorization forms which accompany this thesis.

**THIS DISSERTATION
HAS BEEN MICROFILMED
EXACTLY AS RECEIVED**

AVIS

La qualité de cette microfiche dépend grandement de la qualité de la thèse soumise au microfilmage. Nous avons tout fait pour assurer une qualité supérieure de reproduction.

S'il manque des pages, veuillez communiquer avec l'université qui a conféré le grade.

La qualité d'impression de certaines pages peut laisser à désirer, surtout si les pages originales ont été dactylographiées à l'aide d'un ruban usé ou si l'université nous a fait parvenir une photocopie de mauvaise qualité.

Les documents qui font déjà l'objet d'un droit d'auteur (articles de revue, examens publiés, etc.) ne sont pas microfilmés.

La reproduction, même partielle, de ce microfilm est soumise à la Loi canadienne sur le droit d'auteur, SRC 1970, c. C-30. Veuillez prendre connaissance des formules d'autorisation qui accompagnent cette thèse.

**LA THÈSE A ÉTÉ
MICROFILMÉE TELLE QUE
NOUS L'AVONS REÇUE**

RESPONSE OF THE LAMINAR LAYER
ON A FLAT PLATE TO FREE STREAM
DISTURBANCES

by

Hassan Mohamed Badr

Faculty of Engineering Science

Submitted in partial fulfillment
of the requirements for the degree of
Doctor of Philosophy

Faculty of Graduate Studies
The University of Western Ontario

London, Ontario

March, 1977



Hassan Mohamed Badr 1977.

ABSTRACT

The effect of free stream turbulence and other unsteady rotational flows on the laminar boundary layer growing on a flat plate were studied.

The response of the laminar boundary layer over a flat plate to a single two-dimensional rotational disturbance was first investigated. In this problem the rotational disturbance was simulated by a modified Rankine vortex which was superimposed on the oncoming uniform stream.

A variational-finite element method for solving the governing equations of viscous fluid motion was introduced and then used to obtain the variation of the velocity field with time when the vortex approached the flow domain, impinged on the plate and then the disturbance generated convected downstream allowing the flow field to regain the original steady state. The resulting time variations of the pressure, viscous shear forces, lift and drag forces and pitching moments were shown to be consistent with the physical situation of the problem.

The effect of free stream pseudo-turbulence on the viscous laminar layer growing on a flat plate was also investigated.

The approach was to use a relatively new computer simulation technique to generate pseudo-turbulence which provided the outer boundary conditions for the flow over the flat plate. In this turbulence model, real vortices, randomly distributed representing the turbulent eddy were convected along in the uniform stream similarly as in Taylor's "frozen pattern" model of turbulence. The variational approach was used to solve the governing equations of motion near the plate. The time variations of velocity and vorticity at different points in the flow field, together with the variation of the lift and drag coefficients with time were presented.

The finite element approach was shown to be extremely stable and the results obtained when compared with the available data were shown to be very satisfactory.

ACKNOWLEDGEMENTS

I would like to express my sincere thanks to Professor T.E. Base for suggesting the topic of the thesis, and for his encouragement, advice and close guidance during the course of the investigation.

The financial support received from The Egyptian Ministry of Education and from The University of Western Ontario was gratefully appreciated.

Appreciation is also expressed to other members of the Faculty of Engineering Science and the Department of Applied Mathematics for their helpful discussions and to Mrs. Cindy Reid for typing the thesis.

Thanks and appreciation to my wife, Tahia, for providing a tolerant and comfortable atmosphere at home which is a key factor in the completion of this work.

TABLE OF CONTENTS

	Page
CERTIFICATE OF EXAMINATION	ii
ABSTRACT	iii
ACKNOWLEDGEMENTS	v
TABLE OF CONTENTS	vi
LIST OF TABLES	xi
LIST OF FIGURES	xii
NOMENCLATURE	xiv
CHAPTER 1 - INTRODUCTION	1
1.1 General Introduction	1
1.2 The Governing Equations	2
1.3 Review of the Previous Work	4
1.4 The Present Work	7
CHAPTER 2 - THE FINITE-DIFFERENCE TECHNIQUE	11
2.1 Introduction	11
2.2 Review of the Finite-Difference Methods in Solving Viscous Flow Problems	13
2.3 Vorticity-Stream Function Equations	20
2.4 The Finite-Difference Formulation	20
2.4.1 The First Scheme (Fully Explicit)	21
2.4.2 The Second Scheme (Fully Implicit)	23

2.5	Solution of the Stream Function Equation	25
2.6	The Effect of a Two-Dimensional Rotational Distur- bance on the Laminar Boundary Layer Over a Flat Plate	26
2.7	Boundary Conditions for the Vorticity and Stream Function	28
2.7.1	The Upstream Boundary	29
2.7.2	The Boundary Conditions at the Two Sides of the Flow Field	30
2.7.3	The Boundary Conditions on the Flat Plate	31
2.7.4	The Downstream Boundary Conditions	32
2.8	Mathematical Model of a Two-Dimensional Rotational Disturbance	33
2.9	Procedure of Solution	35
2.9.1	Procedure of Computations When Using the Explicit Scheme	36
2.9.2	Procedure of Computations When Using the Implicit Scheme	36
2.9.3	Procedure of Calculations to Obtain the Steady Velocity Field Around a Flat Plate in Uniform Flow	38
2.9.4	Procedure of Calculations When Studying the Effect of the Rotational Disturbance on the Laminar Layer Over the Plate	39

2.9.5	A Test Problem	40
2.10	Discussion of the Method of Solution and Results	41
CHAPTER 3 - LITERATURE SURVEY OF THE USE OF THE FINITE		
ELEMENT METHODS IN SOLVING FLUID FLOW PROBLEMS ..		
		43
3.1	Introduction	43
3.2	Review of Some Finite Element Applications in Solving	
	Flow Problems	44
3.2.1	Incompressible Inviscid Flow Problems	45
3.2.2	Slow Creeping Flows	47
3.2.3	The Two-Dimensional Steady Flow of a Viscous	
	Fluid	48
3.2.4	The Two-Dimensional Unsteady Flow of a Viscous	
	Fluid	51
3.2.5	Steady Two-Dimensional Flow of a Viscous Fluid	
	With Temperature Variation	55
CHAPTER 4 - FINITE ELEMENT FORMULATION AND METHOD OF SOLUTION		
		58
4.1	Introduction to the Finite Element Approach	58
4.2	The Governing Equations of Viscous Flow	62
4.3	The Variational Functionals	63
4.4	Deriving the Finite Element Equations	68
4.5	Procedure of Computations to Obtain the Steady State	
	Solution	72

4.6 Procedure of Computations to Obtain the Time-Dependent Solution	74
---	----

CHAPTER 5 - THE EFFECT OF A SINGLE ROTATIONAL DISTURBANCE

ON THE LAMINAR BOUNDARY LAYER ON A FLAT PLATE ...	76
5.1 Introduction	76
5.2 Constructing the Finite Element Mesh	77
5.3 Choosing the Element Shape Function	77
5.4 Obtaining the Finite Element Equations	79
5.5 Steady State Solution	84
5.6 Calculation of Lift, Drag and Pitching Moment Coefficients	86
5.7 Effect of the Rotational Disturbance on the Laminar Layer Over the Plate	89
5.8 Discussion of the Method of Solution	91
5.9 Discussion of Results	93

CHAPTER 6 - THE RESPONSE OF THE VISCOUS LAYER OVER A FLAT

PLATE TO PSEUDO-TURBULENCE	99
6.1 Introduction	99
6.2 Description of the Considered Problem	101
6.3 The Unsteady Boundary Conditions	102
6.4 Method of Solution	105
6.5 Results and Discussion	106

CHAPTER 7 - CONCLUSION.....	109
7.1 General Conclusion	109
7.2 Recommendation for Future Studies	112
APPENDIX A - THE EQUATIONS OF MOTION OF A VISCOUS FLUID ...	114
APPENDIX B - DEDUCING THE FINITE ELEMENT EQUATIONS FOR A SIMPLE PROBLEM AND COMPARISON WITH FINITE- DIFFERENCES	116
APPENDIX C - AID FOR COMPUTATION AND COMPUTER FLOW CHARTS ..	112
APPENDIX D - HOWARTH'S SOLUTION FOR THE RETARDED FLOW OVER A FLAT PLATE	136
REFERENCES	140
VITA	191

LIST OF TABLES

Table	Description	page
D-1	Variation of local skin friction coefficient with distance from the leading edge of a flat plate (based on Howarth's solution)	139
1	Details of vortex model parameters	150

LIST OF FIGURES

Figure	Description	page
1	Finite-difference notations	151
2	Schematic diagram showing the flow field with the finite-difference mesh near the plate	151
3	Comparison between the velocity profiles at the entrance region of a channel by using the finite-difference method and the results obtained by Schlichting (58)	152
4	Comparison between the steady velocity profiles obtained by using the finite-difference method and the finite element method	153
5	Comparison between the local skin friction coefficient obtained by the finite element method and by the finite difference method and by using Blasius and Howarth's solutions	154
6	A four-sided flow region with a body of arbitrary cross-section inside	155
7	Schematic diagram showing the flow domain with the vortex approaching	156
8	The finite element mesh	157
9	Spatial variation of the velocity field at different times	158
10-a	Variation of velocity profiles 'u component' with time at a section $x^* = -0.92$	166
10-b	Variation of velocity profiles 'u component' with time at a section $x^* = 0.5$	167

11	Local skin friction coefficient on the two sides of the plate at different times	168
12	Variation of lift coefficient with time	179
13	Variation of the pitching moment coefficient about the leading edge with time	180
14	Variation of drag coefficients with time	181
15	Comparison between the velocity profiles at the entrance region of a channel by using the finite element method and the results obtained by Schlichting (54)	182
16	Variation of the pressure gradient with time at $x^* = 0.5$	183
17-a	Schematic diagram showing five boxes for the real vortices with the flat plate (PQ) mounted inside the flow domain (ABCD)	184
17-b	The finite element mesh inside the flow domain (ABCD)	184
18	Typical traces of velocity and vorticity variations with time	185
19	Variation of the fluctuating component of the velocity u' with time at some points in the flow domain	186
20	Variation of the v component of the velocity with time at some points of the flow field	187
21	Variation of the vorticity with time at some points in the flow field	188
22	Variation of plate drag coefficients with time	189
23	Variation of lift coefficient with time	190

NOMENCLATURE

a_1, a_2, a_3	constants in each finite element
(A)	square matrix defined in equation (5-10)
b_1, b_2, b_3	constants in each finite element
[B]	row matrix
c	cord of the flat plate
c_1, c_2, c_3	constants in each finite element
C_D	drag coefficient
C_L	lift coefficient
C_f	local skin friction coefficient: $C_f = \tau_0 / \frac{1}{2} \rho U_\infty^2$
C_m	pitching-moment coefficient
C_p	specific heat at constant pressure
e_i	denotes the finite element number (i)
(E)	square matrix defined in equation (5-17)
f	general variable
{F}	column matrix
{G}	column matrix
h	size of the finite-difference mesh
i, j	general integer variables
k	total number of elements inside the flow domain
L	total number of nodal points inside the flow domain
m	iteration number
n	a number indicates the time level
\underline{n}	a unit vector normal to the body surface

N_1, N_2, N_3 the element interpolation functions
 p pressure
 q velocity vector
 q_w a vector presents the velocity of the solid boundary
 Q a function related to u and v defined following to equation (1-7)^o
 $[Q]$ row matrix
 r_c the vortex viscous core radius
 R a residual defined in equation (2-11)
 Re Reynolds number
 $[R]$ row matrix
 t time
 T temperature of the fluid
 $[T]$ row matrix
 u component of the velocity in the x direction
 u' fluctuating component of the velocity in the x direction
 u_c convection velocity defined following to equation (2-17)
 u_{ref} reference velocity equal to the time mean of the u component of velocity in the turbulence model
 u_∞ the velocity of the undisturbed stream
 U free stream velocity
 \underline{U} velocity vector
 v component of the velocity in the y direction
 x, y cartesian coordinates
 x^* dimensionless distance from the leading edge: $x^* = x/c$

Δt time increment
 $\Delta x, \Delta y$ space increments in the x and y directions
 Γ vortex strength
 δ the boundary layer thickness
 Δ_i area of finite element number (i)
 θ a factor denotes an intermediate time level defined in section (4.3)
 τ_0 local shear stress on the surface of the plate
 μ dynamic viscosity
 ξ_0 the x coordinate of the initial position of the vortex center
 ξ_1, ξ_2, ξ_3 the finite element area coordinates defined in equation (B-4)
 ρ fluid density
 ∇^2 the Laplacian operator: $\nabla^2 = \frac{\partial^2}{\partial x^2} + \frac{\partial^2}{\partial y^2}$
 ϕ the velocity potential function
 η_0 the y coordinate of the initial position of the vortex center
 ω a relaxation factor defined in equation (2-12)
 Ω the flow domain
 ζ the vorticity: $\zeta = \nabla \times \underline{U}$
 X_1, X_2 variational functionals defined in equations (4-7) and (4-9)
 ψ the stream function defined following to equation (A-5)
 ν kinematic viscosity: $\nu = \mu/\rho$
 λ mean distance between vortices
 $\langle \rangle$ time mean value

The author of this thesis has granted The University of Western Ontario a non-exclusive license to reproduce and distribute copies of this thesis to users of Western Libraries. Copyright remains with the author.

Electronic theses and dissertations available in The University of Western Ontario's institutional repository (Scholarship@Western) are solely for the purpose of private study and research. They may not be copied or reproduced, except as permitted by copyright laws, without written authority of the copyright owner. Any commercial use or publication is strictly prohibited.

The original copyright license attesting to these terms and signed by the author of this thesis may be found in the original print version of the thesis, held by Western Libraries.

The thesis approval page signed by the examining committee may also be found in the original print version of the thesis held in Western Libraries.

Please contact Western Libraries for further information:

E-mail: libadmin@uwo.ca

Telephone: (519) 661-2111 Ext. 84796

Web site: <http://www.lib.uwo.ca/>

CHAPTER (1)

INTRODUCTION

1.1 General Introduction

Investigating the influence of free stream turbulence and other unsteady rotational flows on the laminar boundary layer growing on a body surface is an interesting and important problem.

It is mathematically interesting because of the nonlinear character of the governing equations of viscous fluid motion. This nonlinearity creates several difficulties, not only to obtain an analytical solution, but also to solve the equations numerically. Exact solutions of these equations, even without the complexities of unsteady disturbances in the free stream, exists only in a few elementary cases as, for example, the fully developed laminar flow in a pipe or a channel, Hiemenz stagnation flow and Couette flow.

The importance of the present study arises from the fact that most of the flows occurring in nature are turbulent. On the other hand most of the boundary layer studies carried out previously considered the flow, approaching the body to be idealised as steady uniform flow, accelerating flows, linear shear flows and in some cases the body or the main stream was assumed to be fluctuating in

a certain predetermined regular form.

The successful studies of simulating turbulence carried out recently by other authors as, for example, the work by Lilly (1), Base (2) and Ahmadi and Goldschmidt (3), enhanced the possibility of investigating the effect of free stream turbulence on the viscous boundary layers by using a mathematical model to represent the approaching flow. In the present work a single vortex and a turbulence model were used to simulate the outer flow conditions while the Navier-Stokes equations were solved near the solid body to predict the variation of the velocity field in the viscous layer with time.

This study may be of special interest in the field of aerodynamics and heat transfer. For example, it can be extended to investigate the response of aeroplane wing to the trailing vortices in the wake of another aircraft. In the field of heat transfer the variation of the velocity field in the viscous layer, due to free stream turbulence, may have an effect on the rate of heat transfer from a heated surface.

1.2 The Governing Equations

The governing equations of motion of an incompressible viscous fluid (Navier-Stokes equations) can be written as:

$$\left(\frac{\partial}{\partial t} + \underline{U} \cdot \nabla\right) \underline{U} = -\frac{1}{\rho} \nabla p + \nu \nabla^2 \underline{U} \quad (1-1)$$

where \underline{U} is the velocity vector,

p is the pressure,

t is the time,

and ν is the kinematic viscosity of the fluid which is assumed to be constant.

The continuity equation can be written as:

$$\nabla \cdot \underline{U} = 0 \quad (1-2)$$

In the case of two-dimensional flow in the (x,y) plane, the equation of continuity can be satisfied by introducing the stream function ψ such that,

$$u = \frac{\partial \psi}{\partial y}, \quad v = -\frac{\partial \psi}{\partial x} \quad (1-3)$$

where u and v are the velocity components in the x and y directions respectively.

Eliminating the pressure term from equation (1-1) (see Appendix (A)) and introducing the vorticity vector $\underline{\zeta}$ such that,

$$\underline{\zeta} = \nabla \times \underline{U} \quad (1-4)$$

the resulting equations can be written in two-dimensional form as:

$$\frac{\partial \zeta}{\partial t} + \frac{\partial \psi}{\partial y} \frac{\partial \zeta}{\partial x} - \frac{\partial \psi}{\partial x} \frac{\partial \zeta}{\partial y} = \nu \nabla^2 \zeta \quad (1-5)$$

where

$$-\zeta = \nabla^2 \psi, \quad (1-6)$$

$$\nabla^2 = \frac{\partial^2}{\partial x^2} + \frac{\partial^2}{\partial y^2},$$

and ζ is written as the component ζ_z in the vorticity vector $\underline{\zeta}$.

Equation (1-5) is called Helmholtz vorticity transport equation (two-dimensional form) and equation (1-6) is called the stream function equation.

A relationship between the pressure field and velocity field can be obtained from equation (1-1) (see Appendix (A)) and can be written in the two-dimensional form as;

$$\nabla^2 p = -\rho Q \quad (1-7)$$

where

$$Q = 2 \left(\frac{\partial u}{\partial y} \frac{\partial v}{\partial x} - \frac{\partial u}{\partial x} \frac{\partial v}{\partial y} \right)$$

Equation (1-7) can be used to obtain the pressure distribution from the known velocity distribution if the boundary conditions of the pressure are known.

1.3 Review of the Previous Work

In the past not many investigations have been made in the

study of the response of the laminar boundary layers to free stream turbulence by solving the time-dependent governing equations. To the author's knowledge the first investigation in this subject was carried out by Lighthill (4) who studied the response of laminar skin friction and heat transfer to harmonic fluctuations in the main stream velocity. The problem considered was to analyze mathematically the laminar boundary layer in two-dimensional flow about a cylindrical body when the velocity of the oncoming flow was fluctuating. The time-dependent boundary layer equations were solved and it was found that the maxima of the skin friction anticipated the maxima of the free stream velocity because the existing pressure gradient accelerated the slow flow near the wall sooner than the main stream itself. However the heat transfer fluctuations were found to lag behind their quasi-steady value, and also decreased in amplitude as the frequency increased. The case studied by Lighthill was limited to fluctuations of small magnitude relative to the main stream. Moreover, these fluctuations were restricted to be harmonic in magnitude and constant in direction.

Glauert (5) considered the problem of the two-dimensional laminar boundary layer on an infinite flat plate normal to an approaching stream for the case when the plate was making transverse oscillations in its own plane. The boundary layer equations were reduced to a single ordinary differential equation, containing the frequency as a parameter. The equation was solved and the solution

was found to satisfy the full Navier-Stokes equations. In the same work a study on the effect of oscillations on heat transfer from the plate showed that there was no effect at all on the temperature distribution and the rate of heat transfer. The oscillations of the flat plate in Glauerts' work was limited to be harmonic.

Ting (6) studied the problem of the boundary layer over a flat plate in the presence of shear flow. A similarity solution was obtained for large approaching vorticity while for moderate free stream vorticity the governing equation was replaced by an approximate one for which a similarity solution existed. The problem of shear flow past a flat plate was also studied by Mark (7), while an investigation for the pressure gradient induced by shear flow past a flat plate was reported by Glauert (8).

The effect of free stream turbulence on laminar skin friction and heat transfer was studied experimentally by Smith and Kuethé (9). Measurements were made on a flat plate and on circular cylinders located at various distances downstream of a turbulence generating grid placed normal to the flow in a wind tunnel. The results showed that the laminar heat transfer and skin friction on a flat plate at Reynolds number of 10^5 were increased by about 30% when the turbulence level at the leading edge was 6%. In the work by Smith and Kuethé the time variations of the skin friction and heat transfer were not investigated. Moreover, no analytical or

numerical treatments of the time-dependent governing equations were reported.

A study on the effect of turbulence intensity on the drag coefficient of an infinite cylinder in cross flow was presented in the work by Kestin (10). It was found that there was a critical range of Reynolds number for which the drag coefficient depended strongly on the turbulence intensity as well as on the Reynolds number. Outside this range the effect of turbulence intensity on the drag coefficient was found to be negligible.

Measurements of the response of the laminar boundary layer to free stream disturbances were carried out by Erens and Chasteau (11). These authors concentrated on the frequency analysis of the streamwise component of the laminar boundary layer velocity fluctuations at various points along the length of a flat plate. No measurements were reported for the variation of lift and drag due to the disturbed stream.

1.4 The Present Work

In the work presented in the thesis a method was first introduced and then applied to study the effect of free stream turbulence on the two-dimensional laminar boundary layer growing over a flat plate.

The investigation started by considering the plate to be located between two parallel sides of a channel with the leading edge a short distance downstream of the entrance to the channel. In order to develop the computer programs and method of solution the effect of a simple rotational disturbance, in the free stream approaching a flat plate, on the viscous layer over the plate was first studied. This disturbance was simulated by a modified Rankine vortex which was superimposed on the oncoming uniform stream. Although this problem does not have as much physical significance as the case of an aerofoil in a turbulent flow, it has important fundamental aspects, which could be extended to the study of the response of an aeroplane wing to discrete gusts or to the trailing vortices generated in the wake of another aircraft.

A numerical method, based on the use of the finite-difference technique, to solve the governing equations of viscous flow motion is introduced in Chapter (2). The method was stable when applied to obtain the steady state solution when the oncoming stream was uniform. However, it was not stable when applied to the study of the effect of a rotational disturbance on the laminar layer over a flat plate.

A finite element method of solution, based on the variational approach, was then introduced in Chapter (4) and applied in Chapter (5) to solve the physical problem of a single 'real'

vortex approaching and impinging on a flat plate. A new technique which will be called "the space-time delay technique", was also introduced and used to develop the time varying downstream boundary conditions. The finite element method, which was completely stable, was tested by applying it to a problem for which the analytical solution was known. The results showed a good agreement between the finite element and analytical solutions. Graphs were plotted to show the variation of the velocity field with time when the vortex was convected along by the incompressible free stream, impinging on the plate and then the disturbance generated moving downstream and allowing the flow field to return again to its original steady state. Results have been compiled for the variation of the pressure and shear stress along the plate with time and also the variation of lift, drag and pitching moment about the leading edge of the plate. The method of solution and results are discussed fully in Chapter (5).

In Chapter (6) the effect of free stream pseudo-turbulence on the laminar layer growing on a flat plate, together with the resulting time variations of pressure, viscous shear forces were studied. The approach was to use a relatively new computer simulation technique to generate pseudo-turbulence, which provided the outer boundary conditions to a finite element mesh set around the plate. In the pseudo-turbulence model, 'real' vortices, randomly distributed in space representing the turbulent eddy, were convected

along (without diffusion) in a uniform stream similarly as in Taylor's "frozen pattern" model of turbulence. Near the plate the variational approach was used to solve the stream function and vorticity transport equations. A complete discussion of the results is presented in Chapter (6) and conclusions in Chapter (7).

CHAPTER (2)

THE FINITE DIFFERENCE TECHNIQUE

2.1 Introduction

The analytical calculation, whether mathematically approximate or exact, of viscous flow problems particularly at high Reynolds numbers, except in a few cases, has been shown to be most complex, and in some cases the amount of work required for a solution to a particular problem ceases to be practicable. Due to the many difficulties associated with analytical solutions there was and still is an urgent need to develop alternative methods, particularly when the analytical methods fail to give a workable solution.

Two major types of numerical methods for solving differential equations have been established. The first is the use of the finite-difference methods in which the direct substitution of the derivatives in the governing equations by their finite-difference approximation will result in the difference analogue of the equations. The application of this analogue to each of the mesh points in the flow field will result in a system of difference equations which can be solved to obtain the required numerical solution. The second method is the use of the finite-element approximation which will be

discussed in detail in the following two Chapters.

In spite of the fact that the numerical methods will never lead to an exact solution, the success which has been achieved in solving different problems with a relatively high degree of accuracy, has greatly enhanced the importance and effectiveness of these methods as a powerful tool for solving general field problems. Developments in numerical procedures were encouraged by the invention and fast development of the electronic digital computers.

In this Chapter a review of some of the numerical methods, which are based on the use of the finite-difference approximation, for solving viscous flow problems is presented. A finite-difference scheme was used by the author for solving the two-dimensional time-dependent Navier-Stokes equations. The scheme was successful in reaching the steady state when studying the flow over a flat plate which was situated midway between the two parallel sides of a channel with the leading edge a short distance downstream from the entrance of the channel. However, the scheme was not successful when applied in the study of the effect of a rotational disturbance in the oncoming stream on the laminar boundary layer over the plate.

2.2 Review of the Finite-Difference Methods in Solving Viscous Flow Problems

The non-linearity in the governing equations of viscous flow motion makes them difficult to be solved not only analytically but also numerically. Although many trials have been made to numerically solve these equations in different flow situations, a unique successful method that can be used in studying all kinds of flow problems has not yet been found. To the author's knowledge, the first successful numerical solution of the complete equations of motion in two dimensions was obtained in 1928 by Thom (12) for the flow around a circular cylinder at a Reynolds number of 10. Later in 1938 Prandtl (13) used the step-by-step method for solving the steady, two-dimensional boundary layer flow equations. A review of the early work (up to 1955) on numerical solutions of the boundary layer equations is given by Rosenhead (14). In addition, recent reviews for the use of numerical methods in fluid dynamics are given by Blottner (15) and Roache (16).

During the last two decades an intensive investigation has been given to the numerical solution of the governing equations of viscous fluid motion. For example, Fromm and Harlow (17) studied numerically the problem of the development of a vortex street behind a rectangular cylinder, which was impulsively accelerated to constant speed in a channel of finite width. By transforming the two-dimensional

time-dependent Navier-Stokes equation to vorticity and stream function equations the pressure term was eliminated. The finite-difference analogue of the equations was obtained by using a forward time-centered space finite-difference scheme. The complete details of the numerical technique used is given by Fromm (18). This scheme was found to have a bounded instability at high values of Reynolds number and which was thought to be due to the non-linearity of the equations. A visual display technique for presenting the results was devised. This technique was analogous to a flow visualization experiment, in which a tracer is introduced into a fluid to make the flow visible.

Donovan (19) investigated the unsteady incompressible flow inside a two-dimensional square cavity. The fluid inside the cavity was initially at rest and then the upper surface of the cavity was jerked into motion in its own plane with a constant velocity. An alternative numerical technique for solving the two-dimensional time-dependent Navier-Stokes equations, together with the continuity equation was then used. In this technique the solution of the velocity field (u,v) at the end of the future time increment was carried out in two steps. The first step was to solve the Poisson's equation for the current pressure distribution at the grid points. The second step was to calculate the values of the velocity components u and v at the new time level by solving the x and y momentum equations and considering the pressure term to be known

from the first step. A forward time-centered space finite-difference scheme was used to obtain the difference analogue of the momentum equations. The start of the flow motion in a square cavity at $R_n = 100$ was studied and the velocity profiles obtained at large time were compared with previous studies which were for steady state conditions only, and a good agreement was achieved.

The "square cavity problem" has been the subject of many investigators. Mills (20) used an iterative scheme to solve the steady vorticity and stream function equations and Pan and Acrivos (21) studied the steady flow in square cavities while Chein (22) recently suggested a general finite-difference formulation for solving the Navier-Stokes equations and applied the method to study the time-dependent square cavity problem.

Thoman and Szewczyk (23) studied the time-dependent viscous flow over a circular cylinder for a range of Reynolds number from 1 to 3×10^5 . A finite-difference mesh was constructed such that cylindrical cells were employed near the cylinder and variable width rectangular cells were used in the remainder of the flow region. The authors gave more emphasis to the features of flow development when the flow was started impulsively from rest. The method was of explicit type and included a directional difference scheme for the non-linear terms which enhanced the stability of the solution at high values of Reynolds number.

The problem of calculating the initial flow past a cylinder in a viscous fluid was also investigated by Son and Hanratty (24) who tried to solve numerically the time-dependent equations of motion in order to extend the range of available data on steady flow around a cylinder to large values of Reynold's numbers. Dennis and Staniforth (25) later suggested a method in which the cylinder was mapped to a straight line by using a conformal transformation. This method could be used to solve the equations for higher values of Reynolds number. Jain and Rao (26) investigated the numerical solutions of the equations with particular emphasis on the existence of the limiting steady state of the Karman vortex street for different Reynolds number.

Wilkes and Churchill (27) developed a numerical technique for predicting the transient and steady state natural convection of a fluid contained in a long horizontal enclosure of rectangular cross-section with one vertical wall heated and the other cooled. The equations governing the conservation of mass, momentum and energy were transformed to the vorticity and energy transport equations together with the stream function equation. An implicit, alternating direction, finite-difference technique was employed to advance the fields of vorticity and temperature at the interior grid points across a time step Δt , while centered difference representations were given to all space derivatives. The natural con-

vection in a rectangular enclosure was also investigated by Rubel and Landis (28).

Phillips and Ackerberg (29) integrated numerically the unsteady boundary layer equations for the condition when there was regions of reverse flow. The problem considered was the unsteady flow over a semi-infinite flat plate which was parallel to the oncoming free stream. The fluid velocity outside the boundary layer was assumed to vary in magnitude but not in direction as a sinusoidal function of time. An asymptotic solution was assumed to be valid at the downstream end of the integration mesh. An implicit finite-difference scheme of second order accuracy was employed and a variable mesh size across the boundary layer was used. The results were compared with known numerical and asymptotic solutions and a good agreement was found.

Cebci and Smith (30) suggested a numerical scheme for solving the steady laminar and turbulent boundary layer equations for compressible and incompressible flows about two-dimensional and axisymmetric bodies. An implicit finite-difference method was used to solve the linearized momentum and energy equations after replacing the Reynolds stress ($\rho \overline{u'v'}$) in the momentum equation by an eddy viscosity term using Prandtl's mixing length theory. In the solution a non-uniform grid was used in the direction normal to the solid boundary, which permitted shorter space steps close to the

wall and longer space steps away from it. The reason for using a non-uniform grid was to increase the accuracy of computations near the solid boundary where the change in velocity was highest. The method was tested by being applied to cases for which analytical solutions were known. More applications of this method were later reported by Cebeci, Smith and Mosinskis (31).

A Crank-Nicolson finite-difference scheme with a variable grid was investigated by Blottner (32) and it was shown that the scheme was more efficient and more accurate for solving turbulent boundary layer equations than the previous methods used. The truncation error associated with the use of non-uniform grids in finite-difference equations was studied by de Rivas (33) who showed that although the finite-difference schemes that used uniform grids were the simplest and most accurate, the use of a suitable transformation function for stretching coordinates could be useful in decreasing the truncation error with non-uniform grid schemes.

To decrease the truncation error associated with the finite-difference approximation Hirsh (34) recently applied a higher order finite-difference scheme for solving fluid mechanics problems. In this technique three mesh points were necessary to obtain fourth order accuracy for both first and second derivatives. The difficulty with this technique was that at each time step tridiagonal matrix problems had to be solved to find the required

derivatives at the mesh points. Moreover the boundary values for these derivatives had to be known. The method was applied to study Howarth's retarded boundary layer flow and the time-dependent incompressible square cavity problem. Comparison between results obtained by using second and fourth order methods indicated that the accuracy achieved by the fourth order computations were significantly better.

Dwyer and McCroskey (35) summarized the many difficulties associated with the numerical solution of the three and four-dimensional boundary layer problems as 1) obtaining proper and consistent initial and boundary conditions for the equations; 2) developing a stable and unique numerical scheme to solve the equations and 3) calculating the flow up to the separation line. In the same work Dwyer and McCroskey developed an implicit finite-difference scheme which was used to integrate the three-dimensional time-dependent boundary layer equations. It was noted that it was best to use an implicit scheme when studying the case of a solid body in a fluid flow because of the stability problems that can occur with explicit schemes particularly near the leading edge of the body. The method was used to study oscillating flows over cylinders with both the wall and the inviscid flow oscillating and also to study the case of time-dependent flow over a rotating airfoil in forward flight.

Other work on the solution of the two and three-dimensional boundary layer equations by using the finite-difference approximation include studies by Singleton and Nash (36), Cooper and Reshotko (37) and Cebeci (38).

2.3 Vorticity-Stream Function Equations

Using the equation of continuity (1-2), the governing equations for a two-dimensional, incompressible flow (1-5) and (1-6) can be written in the form

$$\frac{\partial \zeta}{\partial t} + \frac{\partial(u\zeta)}{\partial x} + \frac{\partial(v\zeta)}{\partial y} = \nu \nabla^2 \zeta \quad (2-1)$$

where

$$-\zeta = \nabla^2 \psi,$$

$$\nabla^2 = \frac{\partial^2}{\partial x^2} + \frac{\partial^2}{\partial y^2}$$

and

$$u = \frac{\partial \psi}{\partial y}, \quad v = -\frac{\partial \psi}{\partial x} \quad (2-2)$$

Equation (2-1) is the two dimensional form of Helmholtz vorticity equation and the full derivation of this equation from the Navier-Stokes equations is given in Appendix (A).

2.4 The Finite-Difference Formulation

The numerical solution of these equations was based on using a forward time-centered space explicit finite-difference

scheme to integrate the vorticity transport equation. It was found however that in some parts of the flow field the explicit scheme was unstable. To eliminate this instability, the accuracy of the solution was improved by considering the solution obtained from the explicit scheme as a first approximation. An implicit scheme was then introduced and used to obtain more accurate results in parts of the domain at which the explicit scheme was unstable. A successive over-relaxation iterative technique was employed to solve the stream function equation. The explicit and implicit schemes are presented in this section and the full details of the solution procedure are given in section (2.9).

2.4.1 The First Scheme (Fully Explicit)

In this scheme the method used by Fromm (18) to write the difference approximation of the non-linear convective terms was employed. The individual terms of the vorticity equation (2-1) were replaced by the following finite-difference approximation:

$$\left[\frac{\partial \zeta}{\partial t} \right]_{ij}^k \approx \frac{1}{\Delta t} (\zeta_{ij}^{(k+1)} - \zeta_{ij}^k) \quad (2-3-a)$$

$$\left[\frac{\partial (u\zeta)}{\partial x} \right]_{ij}^k \approx \frac{1}{\Delta x} [(u\zeta)_{i+\frac{1}{2}j}^{(k)} - (u\zeta)_{i-\frac{1}{2}j}^{(k)}] \quad (2-3-b)$$

$$\left[\frac{\partial (v\zeta)}{\partial y} \right]_{ij}^k \approx \frac{1}{\Delta y} [(v\zeta)_{ij+\frac{1}{2}}^{(k)} - (v\zeta)_{ij-\frac{1}{2}}^{(k)}] \quad (2-3-c)$$

$$\left[\frac{\partial^2 \zeta}{\partial x^2} \right]_{ij}^k = \frac{1}{(\Delta x)^2} (\zeta_{i+1j} - 2\zeta_{ij} + \zeta_{i-1j})^{(k)} \quad (2-3-d)$$

$$\left[\frac{\partial^2 \zeta}{\partial y^2} \right]_{ij}^k = \frac{1}{(\Delta y)^2} (\zeta_{ij+1} - 2\zeta_{ij} + \zeta_{ij-1})^{(k)} \quad (2-3-e)$$

where the superscript k denotes the time level,

Δx is the space step in x direction,

Δy is the space step in y direction,

Δt is the time step,

and the notations used to label the grid points are given in Figure (1).

The different terms on the right hand side of equations (2-3) were calculated as follows:

$$u_{ij+\frac{1}{2}} = \frac{1}{\Delta y} (\psi_{ij+1} - \psi_{ij}) \quad (2-4-a)$$

$$v_{i+\frac{1}{2}j} = \frac{1}{\Delta x} (\psi_{ij} - \psi_{i+1j}) \quad (2-4-b)$$

$$u_{i+\frac{1}{2}j} = \frac{1}{4} (u_{i+1j+\frac{1}{2}} + u_{i+1j-\frac{1}{2}} + u_{ij-\frac{1}{2}} + u_{ij+\frac{1}{2}}) \quad (2-4-c)$$

$$v_{ij+\frac{1}{2}} = \frac{1}{4} (v_{i+\frac{1}{2}j+1} + v_{i-\frac{1}{2}j+1} + v_{i+\frac{1}{2}j} + v_{i-\frac{1}{2}j}) \quad (2-4-d)$$

$$\zeta_{i+\frac{1}{2}j} = \frac{1}{2} (\zeta_{ij} + \zeta_{i+1j}) \quad (2-4-e)$$

$$\zeta_{ij+\frac{1}{2}} = \frac{1}{2} (\zeta_{ij} + \zeta_{ij+1}) \quad (2-4-f)$$

Substituting from equations (2-3) in equation (2-1) the following equation was obtained,

$$\begin{aligned}
\zeta_{ij}^{(k+1)} = & \zeta_{ij}^{(k)} - \frac{\Delta t}{\Delta x} [(u\zeta)_{i+\frac{1}{2}j} - (u\zeta)_{i-\frac{1}{2}j}]^{(k)} \\
& + \frac{\Delta t}{\Delta y} [(v\zeta)_{ij+\frac{1}{2}} - (v\zeta)_{ij-\frac{1}{2}}]^{(k)} + \frac{v\Delta t}{(\Delta x)^2} [\zeta_{i+1j} \\
& - 2\zeta_{ij} + \zeta_{i-1j}]^{(k)} + \frac{v\Delta t}{(\Delta y)^2} [\zeta_{ij+1} - 2\zeta_{ij} + \\
& \zeta_{ij-1}]^{(k)} \quad (2-5)
\end{aligned}$$

Applying equation (2-5) to each of the mesh points the values of the vorticity ζ at the $(k+1)$ time level can be predicted, assuming that the velocity field is completely known at the k time level.

2.4.2 The Second Scheme (Fully-implicit)

An implicit finite-difference scheme was employed in an attempt to eliminate the stability problems created at some parts of the flow field when using the explicit scheme mentioned previously. It was recommended by Dwyer and McCroskey (35) to use implicit schemes because of the stability problems that can occur with explicit schemes when solving the flow field near the leading edge of a solid body. The following finite-difference approximations were used to replace the individual terms of equation (2-1) when applied to a typical field point (ij) :

$$\left[\frac{\partial \zeta}{\partial t} \right]_{ij} \approx \frac{1}{\Delta t} (\zeta_{ij}^{(k+1)} - \zeta_{ij}^{(k)}) \quad (2-6-a)$$

$$\left[\frac{\partial(u\zeta)}{\partial x} \right]_{ij} \approx \frac{1}{\Delta x} [(u\zeta)_{i+\frac{1}{2}j} - (u\zeta)_{i-\frac{1}{2}j}]^{(k+1)} \quad (2-6-b)$$

$$\left[\frac{\partial(v\zeta)}{\partial y} \right]_{ij} \approx \frac{1}{\Delta y} [(v\zeta)_{ij+\frac{1}{2}} - (v\zeta)_{ij-\frac{1}{2}}]^{(k+1)} \quad (2-6-c)$$

$$\left[\frac{\partial^2 \zeta}{\partial x^2} \right]_{ij} \approx \frac{1}{(\Delta x)^2} (\zeta_{i+1j} - 2\zeta_{ij} + \zeta_{i-1j})^{(k+1)} \quad (2-6-d)$$

$$\left[\frac{\partial^2 \zeta}{\partial y^2} \right]_{ij} \approx \frac{1}{(\Delta y)^2} (\zeta_{ij+1} - 2\zeta_{ij} + \zeta_{ij-1})^{(k+1)} \quad (2-6-e)$$

The values of $(u\zeta)_{i+\frac{1}{2}j}$, $(u\zeta)_{i-\frac{1}{2}j}$, $(v\zeta)_{ij+\frac{1}{2}}$ and $(v\zeta)_{ij-\frac{1}{2}}$ in the above equations were obtained at each mesh point by using equation (2-4). Substituting from equations (2-6) in equation (2-1) the following equation was then obtained:

$$\begin{aligned} & \zeta_{ij}^{(k+1)} \left[1 + \frac{\Delta t}{2\Delta x} (u_{i+\frac{1}{2}j} - u_{i-\frac{1}{2}j}) + \frac{\Delta t}{2\Delta y} (v_{ij+\frac{1}{2}} - v_{ij-\frac{1}{2}}) + \right. \\ & \left. 2v\Delta t \left(\frac{1}{(\Delta x)^2} + \frac{1}{(\Delta y)^2} \right) \right] + \zeta_{ij+1}^{(k+1)} \left[\frac{\Delta t}{\Delta y} \left(\frac{1}{2} v_{ij+\frac{1}{2}} - \frac{v}{\Delta y} \right) \right] - \\ & \zeta_{i-1j}^{(k+1)} \left[\frac{\Delta t}{\Delta x} \left(\frac{1}{2} u_{i-\frac{1}{2}j} + \frac{u}{\Delta x} \right) \right] - \zeta_{ij-1}^{(k+1)} \left[\frac{\Delta t}{\Delta y} \left(\frac{1}{2} v_{ij-\frac{1}{2}} + \frac{v}{\Delta y} \right) \right] + \\ & \zeta_{i+1j}^{(k+1)} \left[\frac{\Delta t}{\Delta x} \left(\frac{1}{2} u_{i+\frac{1}{2}j} - \frac{u}{\Delta x} \right) \right] = \zeta_{ij}^{(k)} \quad (2-7) \end{aligned}$$

The application of equation (2-7) at each of the mesh points result in a system of linear algebraic equations which can be written in a matrix form as:

$$(A) \{\zeta\}^{k+1} = \{F\} \quad (2-8)$$

where (A) is a square matrix and {F} and {\zeta} are column matrices.

The solution of (2-8) gives the distribution of the vorticity ζ at the $(k+1)$ time level.

2.5 Solution of the Stream Function Equation

Using central differences the finite-difference analogue of equation (2-2) can be written at a typical point (ij) as:

$$-\zeta_{ij} = \frac{1}{(\Delta x)^2} (\psi_{i+1j} - 2\psi_{ij} + \psi_{i-1j}) + \frac{1}{(\Delta y)^2} (\psi_{ij+1} - 2\psi_{ij} + \psi_{ij-1}) \quad (2-9)$$

Equation (2-9) defines a system of difference equations which can be solved by using a direct or iterative method. The unextrapolated Liebmann iterative technique (see reference (39)) for solving equation (2-9) can be written as:

$$\psi_{ij}^{(m+1)} \left[\frac{2}{(\Delta x)^2} + \frac{2}{(\Delta y)^2} \right] = \zeta_{ij} + \frac{1}{(\Delta x)^2} (\psi_{i+1j}^{(m)} + \psi_{i-1j}^{(m+1)}) + \frac{1}{(\Delta y)^2} (\psi_{ij+1}^{(m)} + \psi_{ij-1}^{(m+1)}) \quad (2-10)$$

where the superscript m denotes the iteration number. Equation (2-10) can be written in the condensed form,

$$\psi_{ij}^{(m+1)} = \psi_{ij}^{(m)} + R_{ij}^{(m)} \quad (2-11)$$

$$\text{where } R_{ij}^{(m)} = \frac{(\Delta x)^2 (\Delta y)^2}{2[(\Delta x)^2 + (\Delta y)^2]} \left[\tau_{ij} + \frac{1}{(\Delta x)^2} (\psi_{i+1j}^{(m)} + \psi_{i-1j}^{(m)}) + \frac{1}{(\Delta y)^2} (\psi_{ij+1}^{(m)} + \psi_{ij-1}^{(m)}) \right] - \psi_{ij}^{(m)}$$

The convergence of the iteration procedure (2-11) can be accelerated by using a relaxation factor ω such that

$$\psi_{ij}^{(m+1)} = \psi_{ij}^{(m)} + \omega R_{ij}^{(m)} \quad (2-12)$$

The value of ω which resulted in the minimum number of iterations in this solution was 1.7. The iterative method mentioned in equation (2-12) is the so called successive over-relaxation method.

2.6 The Effect of a Two-Dimensional Rotational Disturbance on the Laminar Boundary Layer Over a Flat Plate

To illustrate the method of solution proposed in sections (2.4) and (2.5) the problem of the effect of a two-dimensional rotational disturbance and then of pseudo free stream turbulence on the laminar boundary layer on a flat plate is now considered. In this example the plate was situated midway between two parallel sides of a channel with the leading edge a short distance downstream of the entrance of the channel as shown in Figure (2).

The investigation started by studying the response of the velocity field to the rotational disturbance. This disturbance

was mathematically simulated by a modified Rankine vortex which was superimposed on a free stream of uniform velocity. The vortex was initially set away from the plate such that its influence on the flow pattern at the entrance of the flow field was almost negligible. The vortex was then convected (without diffusion) towards the entrance of the flow field along the centerline of the channel. The single modified Rankine vortex was particularly chosen to simulate the rotational disturbance because it was the main element in a vortex model that was used to simulate pseudo free stream turbulence later in the thesis. A full discussion of this model is given in Chapter (6).

The main purpose of this study is not to investigate the flow pattern in the immediate neighbourhood of the leading and trailing edges of the flat plate. The difficulty in conducting such kind of study by using a numerical technique arises from the fact that discontinuity of the variables occurs at these points. To overcome this difficulty, for the purpose of the numerical solution, each of the leading and trailing edges was situated between two nodal points in the finite-difference mesh, as shown in Figure (2), and were not selected as mesh points. The same technique for the treatment of the trailing edge was used by Plotkin and Flugge-Lotz (40) to extend Blasius solution for the case of a semi-infinite flat plate to that of a finite plate with the associated wake flow.

Further their solution also succeeded to approach the Goldstein wake solution far downstream of the trailing edge. In the same paper it was stated that the solution obtained was valid upstream and downstream of the trailing edge, but not in its immediate neighbourhood.

2.7 Boundary Conditions for the Vorticity and Stream Function

In most of the numerical studies carried out previously to solve steady and unsteady viscous flow problems, especially those of flow over a solid body, the boundary conditions were made to satisfy certain assumptions which were approximations to what was happening in the real physical problem as, for example, the work by Fromm and Harlow (17), Cheng (41) and Smith and Brebbia (42).

Most of the boundary conditions used in the past were either Dirichlet conditions (specified function value) or the Neumann conditions (specified normal gradient). In the present work the Dirichlet type boundary conditions were used. The boundary conditions that can be used in a numerical scheme to simulate the real boundary conditions depends on the physical problem under consideration. The emphasis in this work was to study the problem of a time-dependent flow over a flat plate which was assumed to be situated midway between two semi-infinite parallel

sides of a channel as shown in Figure (2). The determination of the boundary conditions on the four sides of the flow field and on the flat plate were as follows:

2.7.1 The Upstream Boundary

More than one method have been found in the literature to specify the upstream boundary when dealing with the problem of flow over a solid body. In most of the work done previously the upstream boundary conditions were completely independent on the conditions inside the flow field, for example, the work by Pao and Daugherty (43) and Kawaguti (44). In some other cases, for example, the work by Thoman and Szewczyk (45), the upstream boundary conditions depended on the conditions inside the flow domain by assuming that $v = -\frac{\partial \psi}{\partial x} = 0$ at that boundary.

In this study the upstream boundary conditions were assumed to be completely specified and independent of the conditions inside the flow field whether a steady or an unsteady flow problems were being considered. This assumption was based on the work carried out by Kinney and Paolino (46) who studied the flow near the leading edge of a flat plate moving through a stationary incompressible viscous fluid. In their work it was concluded that the flow disturbance ahead of the plate due to the leading edge

was quite noticeable and the non-uniformity of the flow upstream of the leading edge extended to $x = -50$ (where x was made dimensionless with the plate velocity U and the kinematic viscosity of the fluid ν). This factor was taken into consideration when setting up the problem described in this chapter and a distance, between the leading edge of the plate and the upstream side of the field, equivalent to $x = -90$ was considered.

The distribution of ψ and ζ on the upstream boundary were calculated from the assumed u and v distributions at that boundary by using the relations

$$\psi = \int_0^y u(y) dy \quad (2-13)$$

and

$$\zeta = \frac{\partial v}{\partial x} - \frac{\partial u}{\partial y} \quad (2-14)$$

where ψ was assumed to be zero at $y = 0$. In the study carried out in this chapter a vortex model (see section 2.8) was also used to generate the time-dependent upstream boundary conditions.

2.7.2 The Boundary Conditions at the Two Sides of the Flow Field

The u and v velocity components will have zero value along the upper and lower stationary boundaries. Since $v = -\frac{\partial \psi}{\partial x} = 0$ on the two boundaries, then the value of ψ will be constant with x .

The constant ψ values on the upper and lower sides of the field were determined from the known upstream conditions.

To calculate the vorticity on the two boundaries, the Taylor series expansion of the stream function ψ near a typical point 0 (see Figure (2)) on the solid boundary was written as:

$$\psi_1 = \psi_0 + h \left(\frac{\partial \psi}{\partial y} \right)_0 + \frac{h^2}{2!} \left(\frac{\partial^2 \psi}{\partial y^2} \right)_0 + \frac{h^3}{3!} \left(\frac{\partial^3 \psi}{\partial y^3} \right)_0 + \dots \quad (2-15)$$

Writing $\frac{\partial \psi}{\partial y} = 0$ for the fixed boundary and knowing that $\frac{\partial \psi}{\partial x} = \frac{\partial^2 \psi}{\partial x^2} = 0$ on the two boundaries, then by using equation (2-15) the following equation was obtained,

$$\zeta_0 = - \frac{2}{h^2} (\psi_1 - \psi_0) + O(h) \quad (2-16)$$

Since the discretization error in equation (2-16) depends on h , a finer finite-difference mesh will result in small discretization error.

2.7.3 The Boundary Conditions on the Flat Plate

On the flat plate, no slip condition apply and therefore ψ was constant along the length of the plate. To find this constant ψ value the condition $\frac{\partial \psi}{\partial x} = 0$ was applied at the leading edge which was situated between two mesh points as shown in Figure (2). The calculations of the vorticity ζ on the upper and lower sides of the plate was obtained by using equation (2-16).

2.7.4 The Downstream Boundary Conditions

The convergence and stability of a numerical solution of a time dependent viscous flow problem depends strongly on the downstream boundary conditions. Roache (16) stated that from previous experience when solving flow problems numerically that catastrophic instabilities may be propagated upstream from the outflow boundary and cause the solution to go numerically unstable. Many trials were made previously to find reasonable boundary conditions to be used for the downstream side of fluid flow problems. In the work by Allen and Southwell (47), Michael (48) and Son and Hanratty (24) a potential flow solution was used to simulate the downstream conditions. Katsanis (49) used uniform flow with $u = \text{constant}$ and $v = 0$ at the upstream and downstream boundaries, whereas Friedman (50), Lee and Fung (51) and Cheng (41) used the Poiseuille flow solution at the outflow. A less restrictive type of downstream conditions was used by Paris and Whitaker (52) where $v = 0$ and $\frac{\partial \zeta}{\partial x} = 0$ were assumed at the outflow of a two-dimensional channel. A survey of the boundary conditions used previously with fluid flow problems is well presented in the book by Roache (16).

In the present work a new technique, which will be called the 'space-time delay technique', was introduced and used to develop the downstream boundary conditions. This technique was

based on relating the velocities at the downstream side with the velocities at an adjacent section Δx apart at a time delay Δt , where Δx was a small distance and with the proviso that $u > 0$. This idea was used before in studying the laminar boundary layer flow over an impulsively started flat plate by Hall (53). The relationship between the velocity components at the two adjacent sections can be written as:

$$u(x + \Delta x, y, t) = u(x, y, t - \frac{\Delta x}{u_c}) \quad (2-17)$$

Similar expressions were used for the v and ζ components. The convection velocity u_c was assumed to be the mean value of the velocities at the two grid points so that,

$$u_c = u(x + \frac{\Delta x}{2}, y, t - \Delta t)$$

This technique was tested by applying it to the analysis of the flow in the entrance region of a channel and details are given in section (2.9.5).

2.8 Mathematical Model of a Two-Dimensional Rotational Disturbance

A mathematical model was used to simulate the two-dimensional rotational disturbance and from which the free stream conditions (ψ, ζ) can be developed at a given time. For the purpose of this study the two-dimensional rotational disturbance was simu-

lated by a single modified Rankine vortex superimposed on a uniform stream. A number of vortices could have been used, however one vortex only was considered in this example to simplify the analysis of the results. The velocity field in this case can be written as:

$$u = U_{\infty} - \frac{\Gamma}{\pi} \frac{y - \eta_0}{r_c^2 + (x - \xi_0 - u_c t)^2 + (y - \eta_0)^2} \quad (2-18)$$

$$v = \frac{\Gamma}{\pi} \frac{x - \xi_0 - u_c t}{r_c^2 + (x - \xi_0 - u_c t)^2 + (y - \eta_0)^2} \quad (2-19)$$

where ξ_0, η_0 is the initial position of the vortex center,
 r_c is the viscous core radius,
 Γ is the vortex strength,
 and u_c is the convection velocity.

In terms of the stream function and vorticity the conditions at the entrance to the flow field were calculated at a given time t from the relations,

$$\psi = u_{\infty} y - \frac{\Gamma}{2\pi} \log_e \left(\frac{r_c^2 + (x - \xi_0 - u_c t)^2 + (y - \eta_0)^2}{r_c^2 + (x - \xi_0 - u_c t)^2 + \eta_0^2} \right) \quad (2-20)$$

$$\zeta = \frac{\Gamma}{\pi} \frac{2r_c^2}{[r_c^2 + (x - \xi_0 - u_c t)^2 + (y - \eta_0)^2]^2} \quad (2-21)$$

where ψ was considered to have a zero value at the lower side of the field ($y = 0$). Equations (2-20) and (2-21) were then used to

generate the variables ψ , ζ which represents the rotational disturbance.

2.9 Procedure of Solution

To illustrate the procedure of solution and later, to be used as an initial condition in a more complicated unsteady flow problem, the simple case of a steady uniform flow, with no vortex present, approaching a flat plate as defined in section (2.6) was considered.

The solution started by considering a fluid stream of uniform velocity (without any disturbances) approaching the flow region. To obtain the steady state solution for the velocity field, potential flow was assumed initially to exist everywhere in the flow domain and this was used as the starting conditions in studying the time dependent flow approaching steady state. At this point in the solution a viscous fluid flow was assumed to exist and hence no-slip conditions were imposed on the solid boundaries. The explicit finite-difference scheme given in section (2.4.1) was then used to calculate the distribution of the vorticity ζ at the future time level. Due to the instability of the solution which was originated at the upstream side of the plate, the implicit scheme was employed at that part of the field to

improve the accuracy of the results. The steady state solution was then used as an initial condition in a subsequent example to study the effect of a two-dimensional rotational disturbance on the laminar boundary layer over the flat plate.

2.9.1 Procedure of Computations When Using the Explicit Scheme

The procedure of computations when using the explicit finite-difference scheme, given in section (2.4.1), to advance the solution of the stream function ψ and vorticity ζ through a time increment Δt was as follows:

1. The stream function ψ and the vorticity ζ were assumed to be known at time t (at the start of calculations $t = 0$).
2. Equation (2-5) was applied in order to predict the values of ζ at each of the mesh points at time $t + \Delta t$.
3. Knowing the boundary values of ψ at $(t + \Delta t)$ and the distribution of ζ at $(t + \Delta t)$ from step (2) the relaxation method presented in section (2.5) was then used to obtain the corresponding ψ distribution at time $(t + \Delta t)$.

2.9.2 Procedure of Computations When Using the Implicit Scheme

The procedure of computations when using the implicit finite-difference scheme given in section (2.4.2) was as follows:

1. The stream function ψ and vorticity ζ were assumed to be known at the k time level ($t = k \cdot \Delta t$).
2. Assume as a first approximation that ψ^{k+1} and ζ^{k+1} were the same as ψ^k and ζ^k (where the superscript k denotes the time level).
3. Using the nearest available approximation for ψ^{k+1} and equation (2-16) it was possible to get an estimate for ζ^{k+1} at the solid boundaries.
4. Equation (2-7) was applied to all points inside the flow region and the elements of the matrices (A) and $\{F\}$ in equation (2-8) were calculated.
5. The matrix equation (2-8) was solved to determine a better approximation for ζ^{k+1} inside the field.
6. Knowing the values of ψ^{k+1} on the boundaries and ζ^{k+1} from step (5), the relaxation method given in section (2.5) was then used to solve for a better approximation for ψ^{k+1} .
7. Comparing ψ^{k+1} and ζ^{k+1} with the previous approximation and if the convergence has been achieved go to step (8), otherwise return to step (3) and repeat.
8. Stop.

2.9.3 Procedure of Calculations to Obtain the Steady Velocity Field Around a Flat Plate in Uniform Flow

The procedure of calculations to obtain the steady velocity field when the oncoming stream approaching the plate was uniform was as follows:

1. Consider the potential flow solution to exist everywhere in the flow field at the start of the calculations ($t = k \cdot \Delta t = 0$).
2. Keep the conditions at the upstream boundary unchanged ($v = \zeta = 0$, $u = U$).
3. Calculate the values of the vorticity ζ at the solid boundaries by using equation (2-16).
4. Use the space-time delay technique given in section (2.4.4) to generate the values of ψ^{k+1} and ζ^{k+1} at the downstream side of the flow field.
5. Determine the distribution of the vorticity ζ^{k+1} and stream function ψ^{k+1} by using the explicit scheme procedure given in section (2.9.1).
6. Apply the implicit scheme procedure given in section (2.9.2) to improve the calculations at the upstream side of the plate. The values of ψ^{k+1} and ζ^{k+1} obtained from step (5) can be used

as a first approximation for the implicit solution (i.e. in step (3) of section (2.9.2)).

7. Compare the values of ψ^{k+1} and ζ^{k+1} with that of ψ^k and ζ^k .

If the convergence has been achieved go to step (9), otherwise go to step (8).

8. Put $k = k+1$ and go to step (4).

9. Stop.

2.9.4 Procedure of Calculations When Studying the Effect of the Rotational Disturbance on the Laminar Layer Over the Plate

The steps of the calculations carried out when studying the response of the laminar layer over a flat plate to a two-dimensional rotational disturbance were as follows:

1. The steady state solution obtained from section (2.9.3) was considered as an initial condition ($t = k \cdot \Delta t = 0$).
2. Use the mathematical model given in section (2.8) to generate the upstream conditions (ψ, ζ) at $t = (k+1) \cdot \Delta t$.
3. Use the space-time delay technique given in section (2.4.4) to generate the values of ψ^{k+1} and ζ^{k+1} at the downstream side of the flow field.

4. Solve for the vorticity ζ^{k+1} and stream function ψ^{k+1} by using the explicit scheme given in section (2.9.1).
5. Apply the implicit scheme procedure given in section (2.9.2) to improve the calculations at the upstream side of the plate. The values of ψ^{k+1} and ζ^{k+1} obtained from step (4) can be used as a first approximation (i.e. in step (3) of section (2.9.2)).
6. If $t < t_{\max}$, where t_{\max} is the time limit, put $t = t + \Delta t$ and $k = k + 1$ and go to step (2), otherwise go to step (7).
7. Stop.

2.9.5 A Test Problem

The numerical technique previously presented in this chapter was tested by applying it to the problem of laminar flow development in the entrance region of a straight channel with flat parallel walls. This problem was solved by Schlichting (54) who used the method of series expansion to solve the steady laminar boundary layer equations. The velocity profiles obtained from the method described in this chapter together with those predicted by Schlichting were plotted in Figure (3). The difference between the axial velocity components obtained from the two solutions was found to be within 4%.

2.10 Discussion of the Method of Solution and Results

The finite-difference method presented in this chapter was first used to obtain the steady velocity field for the case of the flow over a flat plate which was situated between two parallel sides of a straight channel, as described in section (2.6), when the approaching stream was uniform. The stability of the solution depended significantly on the space increment in the x and y directions (Δx , Δy), the time increment Δt and the Reynolds number R_e ($R_e = \frac{U_\infty c}{\nu}$, where c was the length of the plate). In the solution, where $\Delta x = \Delta y = 0.167$, $\Delta t = 0.053$ and $R_e = 600$ (Δx , Δy and Δt were made dimensionless by using U_∞ and c), it was found that one or two iterations were sufficient for the convergence of the implicit solution. The steady state velocity profiles, obtained from the present method, were plotted in Figure (4).

The results were tested by comparing the variation of the skin friction drag coefficient c_f along the length of the plate, which was obtained from the present solution, with that obtained by Blasius (54) and Howarth (55). The Blasius solution was based on using the mean value of the velocity at the edge of the boundary layer over the plate as u_∞ . However in Howarth's solution the variation of the velocity at the edge of the boundary layer with the distance x, where x was measured from the leading edge, was assumed to be a linear variation. Figure (5) shows that the devia-

tion between the skin friction coefficient obtained from the present method and that of Blasius and Howarth's solutions was considerable. Moreover the skin friction coefficient c_f obtained from the present method was almost constant along the length of the plate. It was concluded that the severe variation of the velocity component u with the normal distance y in the immediate neighbourhood of the plate, particularly near the leading edge, tended to increase the truncation error in the finite-difference scheme.

The next part of the investigation was to study the effect of the rotational disturbance on the laminar layer over the plate as described in section (2.6). At the start of the solution the vortex was located at $x = -5$ (where x was measured from the leading edge of the plate) where its influence on the flow pattern at the entrance to the field was negligible. The solution procedure given in section (2.9.4) was then applied and the vortex was convected with the stream towards the plate. Approximately at $t = 5.4$ the convergence of the solution was not achieved and the results were not accurate from this time henceforth.

In the following chapters a finite element method of solution, based on the variational approach, is introduced by the author in an attempt to achieve a convergent and stable solution for the flow problem introduced previously in the thesis where a rotational disturbance approaches and impinges on a flat plate and affects the viscous boundary layer over the plate.

CHAPTER (3)

LITERATURE SURVEY OF THE USE OF THE FINITE ELEMENT METHOD IN SOLVING FLUID FLOW PROBLEMS

3.1 Introduction

In the past two decades the finite-difference methods have been used for obtaining numerical solutions to some complicated fluid flow problems. These problems include potential flow solutions, slow viscous flows and unsteady compressible and incompressible fluid flows. In some cases the finite-difference methods proved to be inadequate, especially with problems that had complex geometry or those involving 'ill posed' boundary conditions. The introduction of the finite element methods enabled solutions to be obtained to some of the problems in which the finite-difference methods failed. The finite element methods offers great flexibility in the construction of the finite element mesh and this flexibility can help in dealing with complex geometry problems. Moreover the size of the elements in the finite element mesh can be varied such that small elements can be used in areas of rapid dependent variable change and large elements when variations are less severe.

The main difference between the two methods is that the finite-difference approximation is used to derive the difference

equations from the governing differential equations directly whereas in the finite element method the difference equations can be derived by using the variational formulation of the governing equations. It has been found that the difference equations derived by the two methods are identical when using a simple regular mesh together with a linear interpolation function and a simple problem illustrating this comparison is presented in Appendix (B). In some cases the finite element method can provide an approximate solution of the same order of accuracy as the finite difference method, but at less expense in terms of computer cpu time. The accuracy of the solution of any of the two methods depends on the mesh size and the order of approximation in the solution. Problems of stability and convergence can occur with either method.

3.2 Review of Some Finite Element Applications in Solving Flow Problems

Several investigations have been made recently (58-67) to find numerical solutions for the governing equations of motion of fluid flow by using the finite element technique. In all of these trials the method was simply a process of numerical approximation to the continuum problem in which the unknown functions were usually replaced by an approximate set of functions together with a finite set of unknown parameters which described the value of the function at some discrete points in the flow field.

In the following some important works, on the application of the finite element technique to solve fluid flow problems, are reviewed.

3.2.1 Incompressible Inviscid Flow Problems

In 1971 de Vries and Norrie (56) applied the finite element method to solve field problems governed by Laplace equation, and in particular, to potential flow problems. The governing equations in the case of a two-dimensional, incompressible, irrotational flow were,

$$\nabla^2 \psi = 0 \quad , \quad \nabla^2 \phi = 0 \quad (3-1)$$

and

$$u = \frac{\partial \psi}{\partial y} = \frac{\partial \phi}{\partial x} \quad , \quad v = -\frac{\partial \psi}{\partial x} = \frac{\partial \phi}{\partial y} \quad (3-2)$$

where ψ was the stream function,
 ϕ was the velocity potential function,
 and u, v were the x and y velocity components.

The boundary condition at the solid boundary was

$$\underline{q} \cdot \underline{n} = \underline{q}_w \cdot \underline{n} \quad (3-3)$$

where \underline{n} was the unit vector normal to the surface,
 \underline{q} was the velocity vector
 \underline{q}_w was the vector that represented the velocity
 of the solid boundary.

The potential flow problem was then reduced to the solution of Laplace equation subjected to Dirichlet boundary conditions, Neumann conditions, or mixed boundary conditions. The variational functionals of the equations were obtained and then minimized to determine an approximate solution of the unknown dependent variables ψ and ϕ . The first example studied by de Vries and Norrie was to consider the two-dimensional, incompressible, irrotational flow over four irregular shaped bodies placed between two parallel walls while the approaching stream had a uniform velocity. The method of solution was also applied in the study of the flow over an aerofoil set at an angle of attack to the incident stream.

Vooren and Labrujere (57) studied the case of the incompressible inviscid flow over an aerofoil in a non-uniform stream. The governing equation was written as:

$$\nabla^2 \psi = - \zeta(\psi) \quad (3-4)$$

where the vorticity $\zeta(\psi)$ was constant along the stream lines which coincided with the pathlines in the case of steady flow. The solution, which was of the iterative type, started by assuming a particular vorticity distribution everywhere inside the flow field. The differential equation (3-4) was then reduced to Poisson's equation which was solved by using a variational finite element technique to obtain the distribution of the stream function ψ .

In each iteration the vorticity $\zeta(\psi)$ was estimated from the values obtained in the preceding step. The solution continued until the calculated values of ψ and ζ converged to the assumed ones. Another application of the finite element method to solve potential flow problems was given by Doctors (58).

3.2.2 Slow Creeping Flows

Atkinson et al. (59, 60) developed a numerical method for solving the Navier-Stokes equations for the class of creeping flows (low Reynolds number flows) by using the variational approach. In steady creeping flows the inertia forces are very small compared with the viscous forces, and the equations of motion in the case of two-dimensional flow can be written as:

$$\nabla^4 \psi = 0 \quad (3-5)$$

where ψ is the stream function and

$$\nabla^4 = \frac{\partial^4}{\partial x^4} + 2 \frac{\partial^4}{\partial x^2 \partial y^2} + \frac{\partial^4}{\partial y^4}$$

A variational principle was used to construct the finite element solution of the axis-symmetric flow in cylindrical coordinates and planar flow in rectangular coordinates. The solutions for the case of the flow in the entrance region of a channel and the flow around a sphere were compared with other analytical and numerical solutions and good agreements were achieved.

Thompson and Hâque (61) developed a higher order finite element method for the analysis of the creeping flow of an incompressible material. The governing equations of motion were written with the pressure and velocity as dependent variables. A candle slowly bending under its own weight was used as an illustrative example for the application of the method.

More applications of the finite element method to study the viscous creeping flow problems are described by Yamada et al. (62), Lyness et al. (63) and Zienkiewicz and Godbole (64).

3.2.3 The Two-Dimensional Steady Flow of a Viscous Fluid

Cheng (41) suggested a finite element method to be used for solving the Navier-Stokes equations for any arbitrary region of interest. An unsteady flow approach was used to eliminate the difficulties associated with the non-linearity of the governing equations. The two-dimensional time-dependent Navier-Stokes equations were expressed in terms of the vorticity transport equation and the stream function equation. These equations were solved numerically by using the finite element technique. The variational approach was used to derive the finite element form of the equations. The exact variational functional of the stream function equation was known and a pseudo-variational functional was used for the vorticity transport equation. The method for solving the

development with time of an unsteady flow approaching steady state, which was previously suggested by Crocco (65), was used. The non-linearity in the vorticity equation was overcome by evaluating the non-linear terms using values at the previous time step. The equations considered were,

$$\nabla^2 \psi = -\zeta \quad (3-6)$$

$$\frac{\partial \zeta}{\partial t} + \frac{\partial(\zeta, \psi)}{\partial(x, y)} = R_e^{-1} \nabla^2 \zeta \quad (3-7)$$

where ζ was the vorticity and $u = \frac{\partial \psi}{\partial y}$, $v = -\frac{\partial \psi}{\partial x}$.

The method was applied to study the planar two-dimensional flow inside a channel with a constriction. A non-slip boundary condition was applied at the walls and Poiseuille type flow was assumed at the entrance into, and exit from the channel far from the constriction. The procedure of the numerical solution was to start by assuming initial values for the vorticity ζ everywhere in the flow field and then to solve equation (3-6) to obtain the ψ distribution by minimizing the corresponding functional. The next step was to solve for the vorticity ζ at the future time level by minimizing the functional of equation (3-7). It should be noted that the time derivative of the vorticity was substituted by its forward finite-difference approximation. The computations were carried out to values of Reynolds numbers for which a separation eddy was established downstream of the constriction. The results were com-

pared with those obtained by Lee and Fung (51) and it was found that they were comparable.

Olson (66) applied the finite element method to solve the steady two-dimensional and axis-symmetric flow problems. By introducing the stream function and eliminating pressure the steady two-dimensional Navier-Stokes equations reduced to

$$\nu \nabla^4 \psi + \frac{\partial \psi}{\partial x} \frac{\partial (\nabla^2 \psi)}{\partial y} - \frac{\partial \psi}{\partial y} \frac{\partial (\nabla^2 \psi)}{\partial x} = 0 \quad (3-8)$$

A functional was obtained for each of the two-dimensional and axis-symmetric cases. A high precision, 18 degrees of freedom triangular element, was used. A fifth degree polynomial was used as an interpolation function for ψ and following the standard finite element derivation, a set of non-linear algebraic equations for the generalized coordinates was obtained. These non-linear equations were then solved by using the Newton-Raphson iterative scheme. The method of solution was verified by applying it to the solution of the circulatory flow in a square cavity and the flow over a circular cylinder. Good results were obtained in both examples.

The finite element method has also been applied to solve the steady equations of fluid motion including the work by Tong (67), Gartling et al. (68), Kawahara et al. (69), Guymon (70), Baker (71, 72), Bilgen and Too (73) and Hood and Taylor (74).

3.2.4 The Two-Dimensional Unsteady Flow of a Viscous Fluid

Taylor and Hood (75) suggested a numerical method for solving the time-dependent Navier-Stokes equations by using the finite element technique. Two alternative formulations of the equations were presented, the first was in terms of the dependent variables, velocity and pressure and the second was in terms of the stream function and vorticity. The major part of their work was devoted to a formulation involving the velocity and pressure as dependent variables. The method of weighted residuals, in particular the Galerkin method, was used to derive the finite element form of the Navier-Stokes equations. In the case of two-dimensional flow, three equations were compiled at each node, two from the momentum equations and one from the continuity equation. The unknowns associated with each nodal point were u , v and p . These equations, which were directly coupled, were assembled into a single matrix problem and solved by using an iterative method.

In the same work by Taylor and Hood it was stated that the determination of realistic boundary conditions at the inlet and exit from a contained flow problem is an extremely difficult task. It was also stated that if the velocities at these points were unknown, then it would be reasonable to assume the value of the stress at the entrance and exit of the field or to assume a

value for the normal derivatives of the velocity components.

The second method suggested by Taylor and Hood was to use the stream function and vorticity as variables. The Galerkin method was used as with the previous case to derive the finite element form of the governing equations (3-6) and (3-7). An iterative method was used to obtain self-consistent stream function and vorticity fields. The approach depended on whether the steady or transient solution was required.

For the steady state case the term $\frac{\partial \zeta}{\partial t}$ in equation (3-7) will be zero. In the solution by Taylor and Hood it was first necessary to assume a velocity profile at the entrance to and exit from the flow region. The solution procedure was to guess an initial vorticity distribution and then to solve equation (3-6) for ψ . The vorticity at the boundary points was then calculated and equation (3-7) was solved for ζ . The stream function-vorticity cycle was repeated until convergence was achieved.

In the case when the transient solution was required the value of the vorticity at the next time step was obtained from equation (3-7) by using a forward difference time stepping scheme and then using an iterative procedure to obtain the stream function and vorticity fields. This method was applied to the tran-

sight problem of the development of Couette flow and the results were compared with the known analytical solution and a good agreement was found. The method was also applied to other cases for which there were no analytical solutions.

Bratanow et al. (76) applied the finite element method in the analysis of the unsteady incompressible flow around an oscillating obstacle of arbitrary shape. The equations of motion considered were the Helmholtz vorticity equation (3-7) together with the stream function equation (3-6). The pressure distribution for a given velocity field was obtained independently from the equation,

$$\nabla^2 p = -\rho Q \quad (3-9)$$

where

$$Q = 2 \left(\frac{\partial u}{\partial y} \frac{\partial v}{\partial x} - \frac{\partial u}{\partial x} \frac{\partial v}{\partial y} \right)$$

At a particular time step a direct variational functional existed for equations (3-6) and (3-9), however because of the non-linear convective terms in equation (3-7) the variational functional could not be obtained. To overcome this difficulty the non-linear terms were linearized by using a Taylor series expansion of the velocities in terms of vorticity as follows:

$$u(t+\Delta t) = u(t) + \left(\frac{\partial u}{\partial \zeta} \right)_t d\zeta + \frac{1}{2!} \left(\frac{\partial^2 u}{\partial \zeta^2} \right)_t (d\zeta)^2 + \dots \quad (3-10)$$

The boundary conditions for the stream function, vorticity and pressure were described at the four boundaries of a rectangular flow region by defining the free stream conditions. The conditions on the solid boundary were made to satisfy the no-slip condition and the pressure gradient normal to the obstacle surface was assumed to be zero. Further details of this study can be seen in references (77, 78). The application of the method to the analysis of the three-dimensional unsteady viscous flow around oscillating wings is described in reference (79), while other applications in unsteady aerodynamics can be seen in reference (80).

Smith and Brebbia (42) used the finite element technique for studying two-dimensional transient incompressible viscous flow. The problem considered was the vortex street development behind a rectangular obstruction in a channel of finite width. The governing equations were written in terms of the stream function and vorticity as variables and a variational (Galerkin type) statement was used to derive the finite element form of the equations. The solution strategy was similar to that of Bakers (71), however a simple Euler time integration scheme was used and a linear interpolation function was also considered. Due to the inherent instability of the explicit scheme, the time step was very small. Smith and Brebbia found their approach to be sufficiently accurate to describe the overall flow configuration for Reynolds numbers up to 100.

Kawahara et al. (81) have developed a finite element method for studying the steady and unsteady flow of an incompressible viscous fluid. The non-linear equations arising from the finite element analysis in the steady flow problem were solved by using the Newton-Raphson method. Steady flows of temperature dependent free convection were also discretized and analyzed by using the Galerkin finite element method. The method was applied to study the two-dimensional steady and unsteady incompressible flow of a viscous fluid through a channel bounded by rigid walls, one of which had a sharp corner. The method was also used to study the free convection, in a two-dimensional rectangular reservoir, with different boundary conditions for the temperature.

More applications of the finite element method for solving the unsteady Navier-Stokes equations were carried out by Ikenouchi and Kimura (82), Aral (83), Lieber et al. (84) and Argyris and Mareczek (85).

3.2.5 Steady Two-Dimensional Flow of a Viscous Fluid With Temperature Variation

Tay and Davis (86) applied the finite element method to study the convective heat transfer between two parallel planes. The problem considered was that of a fluid of constant properties

flowing in a steady laminar motion between two infinite stationary parallel planes with no internal heat generation and the viscous dissipation was neglected. The fluid temperature at the entrance of the test section was assumed to be uniform and different conditions were considered for the temperature variation along the two surfaces. A parabolic velocity distribution was assumed to exist everywhere in the test section. Moreover the temperature distribution at the exit of the test section was assumed to be fully developed. According to these simplifications the energy equation reduced to,

$$\rho C_p u \frac{\partial T}{\partial x} = K \left(\frac{\partial^2 T}{\partial x^2} + \frac{\partial^2 T}{\partial y^2} \right) \quad (3-11)$$

where K was the thermal conductivity of the fluid,
 C_p was the specific heat at constant pressure,
 and ρ, T were respectively the density and temperature
 of the fluid.

The quasi-variational functional used in this study was,

$$I(T) = \int_A \left[\rho C_p u \frac{\partial T}{\partial x} T + \frac{K}{2} \left\{ \left(\frac{\partial T}{\partial x} \right)^2 + \left(\frac{\partial T}{\partial y} \right)^2 \right\} \right] dA + \int_S (\underline{q} \cdot \underline{n}) T ds$$

where A the area of the flow domain
 \underline{n} a unit vector normal to the surface
 \underline{q} the heat flux
 S the surface surrounding the flow domain.

The obtained solution was compared with theoretical solutions obtained by other authors and a good agreement was achieved.

Skiba et al. (87) applied the finite element method to find a solution for a class of two-dimensional viscous fluid flow problems in which the Boussinesq approximations were assumed so that the effect of temperature variation was negligible except on the body force term. The solution was based on an approximate variational principle in the sense that one or more terms in the governing equation were approximated. These principles were previously developed by other authors, for the continuity, momentum and energy equations. The continuity requirements were satisfied by introducing the stream function ψ which reduced the problem to the extremization of two coupled functionals of the momentum and energy equations. The solution started by assuming initial values for the stream function (ψ) and then calculating the values of the temperature (T) by extremizing the energy functional. Using these values of ψ and T in the momentum equation new values of ψ could then be obtained. Several iterations were performed to attain consistent ψ and T fields. The natural convection in low aspect ratio rectangular cavities was studied and a solution was obtained. This solution was compared with other analytical and experimental solutions and an agreement was achieved.

CHAPTER (4)

FINITE ELEMENT FORMULATION AND METHOD OF SOLUTION

4.1 Introduction to the Finite Element Approach

The basic idea of using the finite element method, when using it to solve field problems, is to divide the solution domain into a finite number of subdomains or elements. These elements may be one, two, or three-dimensional according to the problem under investigation. The shape of element to be used can be one of many different forms, for example, in the case of a two-dimensional domain the element may be triangle, rectangle, quadrilateral or curved. The degrees of freedom of an element depend on the number of nodes in that element and the number of variables associated with each node. In a triangular shape element the nodes are situated at the vertices of the triangle. Often the nodal variables or the parameters assigned to an element are called the degrees of freedom of that element. Once the type of element has been decided and the finite element mesh has been constructed, the behavior of the unknown field variable over each element can be approximated by continuous functions expressed in terms of the nodal values of the field variable and sometimes the nodal values of its derivatives up to a certain order. The approximate repre-

resentation of a two-dimensional field variable $\phi(x,y)$ within an element 'e' can be written in terms of the element unknown parameters ϕ_j as,

$$\phi^{(e)}(x,y) = \sum_{j=1}^m N_j(x,y)\phi_j \quad (4-1)$$

where m is the number of unknown parameters and $N_j(x,y)$, $j=1, \dots, m$ are the element shape functions.

The element shape functions cannot be chosen arbitrarily because these functions have to satisfy the continuity requirements on the element and at its interfaces to ensure the convergence criteria of the method. More details concerning types of elements shape functions are given in references (88, 89).

One of the main advantages of the finite element method is the variety of ways in which one can derive the finite element form of the governing equations of a problem. There are basically three different approaches:

1. The Variational Approach

In this approach a physical problem, governed by a set of differential equations, may be equivalently expressed as an extremum problem by the methods of calculus of variations. For

example, if one considers the simple problem of potential flow governed by Laplace's equation

$$\frac{\partial^2 \phi}{\partial x^2} + \frac{\partial^2 \phi}{\partial y^2} = 0 \quad (4-2)$$

where ϕ is the velocity potential function then this problem may be solved by extremizing the following integral or functional as it is called,

$$I(\phi) = \iint_{\Omega} \frac{1}{2} \left[\left(\frac{\partial \phi}{\partial x} \right)^2 + \left(\frac{\partial \phi}{\partial y} \right)^2 \right] dx dy \quad (4-3)$$

with respect to the unknown function ϕ .

In general it can be shown by using variational methods (in particular, Euler's theorem) that the extremization of the general functional $I(\phi)$ where

$$I[\phi(x,y)] = \iint_{\Omega} f(x,y;\phi, \frac{\partial \phi}{\partial x}, \frac{\partial \phi}{\partial y}) dx dy \quad (4-4)$$

will result in the following differential equation

$$\frac{\partial f}{\partial \phi} - \frac{\partial}{\partial x} \left[\frac{\partial f}{\partial (\frac{\partial \phi}{\partial x})} \right] - \frac{\partial}{\partial y} \left[\frac{\partial f}{\partial (\frac{\partial \phi}{\partial y})} \right] = 0 \quad (4-5)$$

Using the same theorem it follows that the extremization of the functional $I(\phi)$ in equation (4-3) is a necessary condition for the satisfaction of equation (4-2).

Physical problems of the Laplace's and Poisson's equations have already been solved numerically by the finite element method. An excellent description of the numerical procedure for these and other problems is given in references (88) and (89).

2. The Weighted Residuals Approach

In this approach two steps have to be carried out. The first step is to assume a general behavior of the dependent field variable in such a way that it can approximately satisfy the given differential equation and the associated boundary conditions. The substitution of this approximation into the differential equation results in some errors called the residuals. These residuals are required to vanish in some average sense over the entire solution domain. The next operation is to solve the equations resulting from the first step to find the approximate solution. The advantage of this approach is that it makes it possible to extend the finite element method to problems where no variational functional is available or known.

3. The Direct Method

This method can be used only for relatively simple problems. The procedure is to apply the governing equations to each

individual element which results in a number of algebraic equations. The set of equations arising from the different elements can be arranged in a matrix form and solved to obtain the required solution.

The details of the three different approaches including many applications are given in references (88), (89) and (90).

4.2 The Governing Equations of Viscous Flow

The governing equations of motion for the general transient case of two-dimensional flow of an incompressible viscous fluid can be written either in terms of the velocity and pressure as dependent variables (the Navier-Stokes equations) or in terms of the stream function and vorticity (the Helmholtz vorticity equation). Considering the second case the equations are,

$$\frac{\partial \zeta}{\partial t} + \frac{\partial \psi}{\partial y} \frac{\partial \zeta}{\partial x} - \frac{\partial \psi}{\partial x} \frac{\partial \zeta}{\partial y} = \nu \left(\frac{\partial^2 \zeta}{\partial x^2} + \frac{\partial^2 \zeta}{\partial y^2} \right) \quad (4-6)$$

$$-\zeta = \frac{\partial^2 \psi}{\partial x^2} + \frac{\partial^2 \psi}{\partial y^2} \quad (4-7)$$

where ζ is the vorticity and ψ is the stream function. The pressure distribution for any given velocity field can be obtained from the equation,

$$\frac{\partial^2 p}{\partial x^2} + \frac{\partial^2 p}{\partial y^2} = \rho Q(x, y) \quad (4-8)$$

where
$$Q(x,y) = 2 \left(\frac{\partial u}{\partial x} \frac{\partial v}{\partial y} - \frac{\partial u}{\partial y} \frac{\partial v}{\partial x} \right)$$

and
$$u = \frac{\partial \psi}{\partial y}, \quad v = - \frac{\partial \psi}{\partial x}.$$

4.3 The Variational Functionals

In the present study the variational approach was used to derive the finite element form of the governing equations of motion. The exact variational functional of the stream function equation (4-7) is known and exactly the same as Poisson's equation, which was discussed in detail in reference (88), however the exact variational functional of the vorticity equation (4-6) does not exist because of the presence of the non-linear convective terms. A proof for the non-existence of a variational functional for the vorticity equation is presented in reference (91). A limited number of quasi-variational functionals were tried previously as, for example, the study by Cheng (41) to obtain the steady state solution of the Navier-Stokes equations and the study by Bratanow et al. (92) to obtain time-dependent solutions for the flow over stationary and moving bodies.

In the study by Cheng (41), the velocity components u and v were approximated by their values at the previous time step. From the author's point of view, this approximation is reasonable so long as the steady state solution is required. No studies have

been made to apply the method to a time-dependent problem. In the steady state analysis carried out by Cheng the method could only be used up to values of Reynolds numbers for which a separation eddy was established in the flow. Furthermore the assumption of a Poiseuille velocity distribution at the exit of the flow field simplified the solution of the problem.

In the work of Bratanow and Ecer (92) it was assumed that the vorticity field was not sensitive to incremental changes in velocity. The velocity components u and v were approximated by using the Taylor series expansion of velocities in terms of vorticity as given in equation (3-10). It is the opinion of the author that these approximations and assumptions add some restrictions to the general use of the method. In a previous work by Bratanow et al. (76) it was assumed that the boundary conditions for the stream function, vorticity and pressure, which were completely defined from the freestream conditions, were unchanged during the numerical integration of the vorticity transport equation. Since the problem considered by Bratanow was the time-dependent flow around an oscillating obstacle, the above assumptions for the boundary conditions seems to be in contradiction with the physical situation of the problem since flow disturbances would propagate downstream.

In the present method the vorticity transport equation together with the stream function equation are integrated by using finite elements for space approximations and a weighted average method in the direction of time.

Consider ψ_n and ζ_n to represent the stream function and vorticity at the n time level ($t = n\Delta t$) and ψ_{n+1} , ζ_{n+1} to represent the same variables at the $(n+1)$ time level where Δt is the time increment. Consider also $\psi_{n+\theta}$, $\zeta_{n+\theta}$ to represent the stream function and vorticity at an intermediate level between the n and $(n+1)$ levels such that $t = (n+\theta)\Delta t$ and $0 < \theta < 1$. Applying the vorticity equation at the $(n+\theta)$ level and writing the subscript θ to represent that level, then one obtains,

$$\left(\frac{\partial \zeta}{\partial t}\right)_\theta + \frac{\partial \psi_\theta}{\partial y} \frac{\partial \zeta_\theta}{\partial x} - \frac{\partial \psi_\theta}{\partial x} \frac{\partial \zeta_\theta}{\partial y} = \nu \nabla^2 \zeta_\theta \quad (4-9)$$

where

$$\nabla^2 = \frac{\partial^2}{\partial x^2} + \frac{\partial^2}{\partial y^2}$$

This approach will result in a fully explicit solution when $\theta = 0$ and a fully implicit solution when $\theta = 1$. The stability of the numerical method therefore depends on the selection of the value of θ .

Since the finite element method will only be used for space approximations, the term $-\left(\frac{\partial \zeta}{\partial t}\right)_\theta$ will be considered as invari-

ant when deriving the variational functional of equation (4-9).

The non-linear terms in the same equation will be approximated by using linear interpolation between the n and $(n+1)$ time levels as follows:

$$\frac{\partial \psi_{\theta}}{\partial x} = \theta \frac{\partial \psi_{n+1}}{\partial x} + (1-\theta) \frac{\partial \psi_n}{\partial x} \quad (4-10-a)$$

$$\frac{\partial \zeta_{\theta}}{\partial x} = \theta \frac{\partial \zeta_{n+1}}{\partial x} + (1-\theta) \frac{\partial \zeta_n}{\partial x} \quad (4-10-b)$$

The terms $\frac{\partial \psi_{\theta}}{\partial y}$, $\frac{\partial \zeta_{\theta}}{\partial y}$ can be obtained in a similar way.

The truncation error associated with the calculations of the spacial derivatives on the left hand sides of equations (4-10-a and b) can be estimated as follows:

Consider a general variable $f(x,y,t)$ and consider a specific point in space (x_1, y_1) at which this variable is $f(x_1, y_1, t)$ or simply f_t . Using Taylor series expansion then;

$$f_t = f_{\theta} - \theta \Delta t \left(\frac{\partial f}{\partial t} \right)_{\theta} + \frac{(\theta \Delta t)^2}{2!} \left(\frac{\partial^2 f}{\partial t^2} \right)_{\theta} - \dots \quad (4-11)$$

$$f_{t+\Delta t} = f_{\theta} + (1-\theta) \Delta t \left(\frac{\partial f}{\partial t} \right)_{\theta} + \frac{[(1-\theta) \Delta t]^2}{2!} \left(\frac{\partial^2 f}{\partial t^2} \right)_{\theta} + \dots$$

where the subscript θ represents the time $(t+\theta \Delta t)$. Multiplying the first equation by $(1-\theta)$ and the second by θ and adding the two equations then,

$$f_{\theta} = (1-\theta)f_t + \theta f_{t+\Delta t} + O[(\Delta t)^2] \quad (4-12)$$

From the above equation it was shown that the truncation error was of second order of the time increment Δt which should be small and of such a value that the solution converges. From a comparison, presented in Appendix B, it was shown that the truncation error associated with the finite element method was of the same order of magnitude as the finite difference method when using a simple regular mesh and linear interpolation function. It was concluded that the finer the finite element mesh the less the truncation error.

The variational functional of equation (4-9), after calculating approximate values for the non-linear terms, was

$$\begin{aligned} \chi_1(\zeta_{\theta}) = \iint_{\Omega} \left\{ \left[\left(\frac{\partial \zeta_{\theta}}{\partial t} \right)_{\theta} + \frac{\partial \psi_{\theta}^*}{\partial y} \frac{\partial \zeta_{\theta}^*}{\partial x} - \frac{\partial \psi_{\theta}^*}{\partial x} \frac{\partial \zeta_{\theta}^*}{\partial y} \right] \zeta_{\theta} + \right. \\ \left. \frac{\nu}{2} \left[\left(\frac{\partial \zeta_{\theta}}{\partial x} \right)^2 + \left(\frac{\partial \zeta_{\theta}}{\partial y} \right)^2 \right] \right\} dx dy \quad (4-13) \end{aligned}$$

where Ω was the solution domain and the superscript * denotes that the values were approximated by using equations (4-10).

Applying the stream function equation (4-7) at the $(n+1)$ time level, then

$$\nabla^2 \psi_{n+1} = -\zeta_{n+1} \quad (4-14)$$

The variational functional of this equation is exactly the same as Poisson's equation (see reference 88) and can be written as:

$$X_2(\psi_{n+1}) = \iint_{\Omega} \left[\left(\frac{\partial \psi_{n+1}}{\partial x} \right)^2 + \left(\frac{\partial \psi_{n+1}}{\partial y} \right)^2 \right] - \psi_{n+1} \zeta_{n+1} dx dy \quad (4-15)$$

In the rest of this chapter the method of deriving the finite element equations is considered and then the procedure of solution for both steady and unsteady flow problems is presented.

4.4 Deriving the Finite Element Equations

In deriving the finite element equations from the known variational functional, the first step was to find a suitable approximate representation for the variation of the field variable over each element. According to the choice of the element shape function the continuity of the variable and its derivatives to a certain order can be achieved. Although it is not a rule to use one shape function to represent the variation of different variables, however, for the simplicity of this analysis, the same element shape function was used to give an approximate representation for the variation of the stream function ψ and the vorticity ζ within each element. Using equation (4-1) the approximation of ψ and ζ over the element e_i can be written as:

$$\psi(e_i) = \sum_{j=1}^m N_j(x,y) \psi_j \quad (4-16-a)$$

$$\zeta^{(e_i)} = \sum_{j=1}^m N_j(x,y) \zeta_j \quad (4-16-b)$$

The variational functional given in equation (4-13) can be written in terms of the element parameters as:

$$\begin{aligned} X_1(\zeta_\theta) = & \sum_{i=1}^k \iint_{e_i} \left\{ \frac{\partial}{\partial t}([N]^{(i)} \{\zeta_\theta\}^{(i)}) + \frac{\partial}{\partial y}([N]^{(i)} \{\psi_\theta^*\}^{(i)}) \right. \\ & \left. \frac{\partial}{\partial x}([N]^{(i)} \{\zeta_\theta^*\}^{(i)}) - \frac{\partial}{\partial x}([N]^{(i)} \{\psi_\theta^*\}^{(i)}) \cdot \frac{\partial}{\partial y}([N]^{(i)} \{\zeta_\theta^*\}^{(i)}) \right] \\ & [N]^{(i)} \{\zeta_\theta\}^{(i)} + \frac{v}{2} \left[\left(\frac{\partial}{\partial x} [N]^{(i)} \{\zeta_\theta\}^{(i)} \right)^2 + \left(\frac{\partial}{\partial y} [N]^{(i)} \{\zeta_\theta\}^{(i)} \right)^2 \right] \\ & \left. \right\} dx dy \quad (4-17) \end{aligned}$$

where $[N]^{(i)}$ represented a row matrix and each of its elements was one of the shape functions of the element 'e_i', $\{\zeta_\theta\}^{(i)}$ represented a column matrix of the nodal values of the vorticity in the element 'e_i', $\{\psi_\theta^*\}^{(i)}$ represented a column matrix of the nodal values of the stream function in the same element and k was the total number of elements inside the solution domain.

Using a weighted average time marching scheme the time derivative of the vorticity was approximated by

$$\left(\frac{\partial \zeta}{\partial t} \right)_\theta = \frac{1}{\Delta t} (\zeta_{n+1} - \zeta_n) \quad (4-18)$$

Substituting equation (4-18) into equation (4-17) and writing

$\frac{\partial [N]^{(i)}}{\partial x}$ as $[N_x]^{(i)}$ and $\frac{\partial [N]^{(i)}}{\partial y}$ as $[N_y]^{(i)}$, then the functional $\chi_1(\zeta_\theta)$ could be written as;

$$\begin{aligned} \chi_1(\zeta_\theta) = & \sum_{i=1}^k \iint e_i \left\{ \left[\frac{1}{\Delta t} [N]^{(i)} \{ \zeta_{n+1} \}^{(i)} - \frac{1}{\Delta t} [N]^{(i)} \{ \zeta_n \}^{(i)} + \right. \right. \\ & [N_y]^{(i)} \{ \psi_\theta^* \}^{(i)} \cdot [N_x]^{(i)} \{ \zeta_\theta^* \}^{(i)} - [N_x]^{(i)} \{ \psi_\theta^* \}^{(i)} \\ & \left. \left. [N_y]^{(i)} \{ \zeta_\theta^* \}^{(i)} \right] [N]^{(i)} \{ \zeta_\theta \}^{(i)} + \frac{\nu}{2} \left[([N_x]^{(i)} \{ \zeta_\theta \}^{(i)})^2 + \right. \right. \\ & \left. \left. ([N_y]^{(i)} \{ \zeta_\theta \}^{(i)})^2 \right] \right\} dx dy \quad (4-19) \end{aligned}$$

The extremization of the functional (4-19) with respect to each of the nodal values of ζ_θ was a necessary condition to satisfy the vorticity equation. Considering a typical nodal point j in the solution domain and extremizing the functional $\chi_1(\zeta_\theta)$ with respect to the nodal vorticity $\zeta_{\theta j}$, the following equation was obtained

$$\begin{aligned} & \sum_{i=1}^k \iint e_i \left\{ \left[\frac{1}{\Delta t} [N]^{(i)} \{ \zeta_{n+1} \}^{(i)} - \frac{1}{\Delta t} [N]^{(i)} \{ \zeta_n \}^{(i)} + [N_y]^{(i)} \{ \psi_\theta^* \}^{(i)} \right. \right. \\ & \left. \left. [N_x]^{(i)} \{ \zeta_\theta^* \}^{(i)} - [N_x]^{(i)} \{ \psi_\theta^* \}^{(i)} \cdot [N_y]^{(i)} \{ \zeta_\theta^* \}^{(i)} \right] [N]^{(i)} \right. \\ & \left. \frac{\partial}{\partial \zeta_{\theta j}} \{ \zeta_\theta \}^{(i)} + \frac{\nu}{2} \left[2 [N_x]^{(i)} \{ \zeta_\theta \}^{(i)} \cdot [N_x]^{(i)} \frac{\partial}{\partial \zeta_{\theta j}} \{ \zeta_\theta \}^{(i)} + \right. \right. \\ & \left. \left. 2 [N_y]^{(i)} \{ \zeta_\theta \}^{(i)} \cdot [N_y]^{(i)} \frac{\partial}{\partial \zeta_{\theta j}} \{ \zeta_\theta \}^{(i)} \right] \right\} dx dy = 0, \quad j = 1, L \end{aligned} \quad (4-20)$$

where L was the number of nodal points inside the solution domain. Equation (4-20) represents a set of linear algebraic equations and

upon writing

$$\zeta_{\theta} = \theta \zeta_{n+1} + (1-\theta) \zeta_n \quad (4-21)$$

the only unknowns in these equations were ζ_{n+1} at the L interior points, provided that the values of ψ_{θ}^* and ζ_{θ}^* are known. The final form of equations (4-20) can be written as:

$$(A) \{ \zeta_{n+1} \} = \{ F \} \quad (4-22)$$

The finite element equations given in (4-22) are linear algebraic equations which can be solved to find the nodal values of the vorticity at the $(n+1)$ time level.

The next step was to derive the finite element equations corresponding to the stream function equation (4-14). Using the previous notations the variational functional given in equation (4-15) can be written in terms of the element parameters as:

$$\chi_2(\psi_{n+1}) = \sum_{i=1}^k \iint_{e_i} \left\{ \frac{1}{2} \left([N_x]^{(i)} \{ \psi_{n+1} \}^{(i)} \right)^2 + \left([N_y]^{(i)} \{ \psi_{n+1} \}^{(i)} \right)^2 \right\} - [N]^{(i)} \{ \psi_{n+1} \}^{(i)} \cdot [N]^{(i)} \{ \zeta_{n+1} \}^{(i)} \} dx dy \quad (4-23)$$

Extremizing this functional with respect to each of the nodal values of the stream function at the L interior points, the following equation was obtained

$$\sum_{i=1}^k \iint e_i \left[[N_x]^{(i)} \{\psi_{n+1}\}^{(i)} [N_x]^{(i)} \frac{\partial}{\partial \psi_{n+1j}} \{\psi_{n+1}\}^{(i)} + \right. \\ \left. [N_y]^{(i)} \{\psi_{n+1}\}^{(i)} [N_y]^{(i)} \frac{\partial}{\partial \psi_{n+1j}} \{\psi_{n+1}\}^{(i)} - \right. \\ \left. [N]^{(i)} \frac{\partial}{\partial \psi_{n+1j}} \{\psi_{n+1}\}^{(i)} \cdot [N]^{(i)} \{\zeta_{n+1}\}^{(i)} \right] dx dy = 0, j = 1, L \quad (4-24)$$

where j was a typical point inside the solution domain. Again equation (4-24) represented a set of linear algebraic equations which were written finally in the simple form,

$$(E) \{\psi_{n+1}\} = \{G\} \quad (4-25)$$

The set of equations (4-25) can be solved by using a direct or iterative method to find the stream function field which was consistent with the given vorticity field.

4.5 Procedure of Computations to Obtain the Steady State Solution

Consider the four sided region (ABCD) shown in Figure (6) with a body of arbitrary cross-section within the solution domain. The steady upstream boundary conditions (ψ, ζ) can be calculated from the assumed steady velocity profile at the inlet to the flow field AB as given in section (2.7.1). The free stream conditions can be used to define the boundary conditions at the two sides of the flow field AD and BC, providing that those sides are a large

distance away from the solid body such that the boundary layer on the body does not affect the freestream. In the case when the two sides of the field are stationary the boundary conditions on those sides can be defined in a way similar to that presented in section (2.7.2). The conditions at the downstream boundary CD can be obtained by using the space-time delimitation technique given in section (2.7.4), or it can be made to satisfy certain assumed conditions which should be consistent and compatible with the physical situation of the considered problem. To start the solution a relaxation method may be used where a reasonable distribution for the vorticity everywhere inside the flow field is assumed.

The functional given in equation (4-23) can then be minimized and the resulting set of equations (4-25) can be solved to find the stream function distribution associated with the assumed vorticity field. These values of the stream function and vorticity will be considered as the solution at the start of the calculations (ψ_n, ζ_n where $n = 0$). An iterative procedure can be used to find the solution at the next time step. This procedure starts by assuming the values of ψ_{n+1} and ζ_{n+1} (the closer to the solution the initial assumption the less number of iterations will be necessary). A reasonable guess is to consider ψ_{n+1} and ζ_{n+1} to be exactly the same as ψ_n and ζ_n respectively. An approximation for the convective terms can be obtained by using equations (4-10-

a and b). Substituting these approximate values in the functional (4-19) and minimizing this functional with respect to the values of the vorticity at each nodal point will result in a set of algebraic equations (4-22) which can be solved to find a second approximation for the vorticity field at the $(n+1)$ time level. A second approximation for the stream function can be obtained by solving equations (4-25) as mentioned before. The values of the vorticity at the solid boundaries at the $(n+1)$ time level can be calculated after each iteration by using equation (2-16). The iterative procedure stops when the difference between two successive iterations is within a certain limiting value. In the computer program the solution for a steady flow problem will continue to determine ψ_{n+2}, ζ_{n+2} at the next time level and so on until convergence is achieved. The computer flow chart for obtaining the steady state solution is shown in Appendix (C).

4.6 Procedure of Computations to Obtain a Time-Dependent Solution

The time-dependent solution for the case of unsteady flow approaching the field can be obtained by using the following procedure. The steady state solution obtained from section (4.5) can be used to define the conditions (ψ, ζ) everywhere in the flow field at the start of the calculations. The unsteady boundary conditions at the upstream and the two sides of the flow field are assumed to be predetermined and can be generated from a given mathematical model.

The downstream conditions can be determined by using the space-time delay technique presented in section (2.7.4). The rest of the solution procedure is similar to the previous steady state case. The computer flow chart to obtain the time dependent solution is shown in Appendix (C) and an example on the application of the method is given in the following chapter.

CHAPTER (5)

THE EFFECT OF A SINGLE ROTATIONAL DISTURBANCE ON THE LAMINAR BOUNDARY LAYER ON A FLAT PLATE

5.1 Introduction

In this chapter the effect of a two-dimensional rotational disturbance on the laminar boundary layer growing over a flat plate was investigated using the vorticity-stream function method of solution described fully in Chapter (4). The free stream disturbance in this example was simulated by a single vortex and the laminar boundary layer was developed on a thin flat plate at zero incidence to the undisturbed stream.

The investigation started by considering the rotational disturbance to be simulated by a modified Rankine vortex in the oncoming free stream approaching the flat plate. The limitation to one vortex simplified the analysis of the results, however it does not imply a limitation to the method of solution as will be shown in Chapter (6). The considered flow field was the entrance region of a channel with a flat plate of finite length situated midway between the two straight parallel sides of the channel as shown in Figure (7). The effect of the vortex on the time variation of the velocity field, the drag coefficient on the upper and lower sides of the plate

and the lift and pitching moment coefficients were also investigated. The following steps were carried out in this investigation.

5.2 Constructing the Finite Element Mesh

The three node flat triangular element is the simplest two-dimensional element, and it has the distinction of being the first used and now the most often used basic finite element. The reason for this is that an assemblage of triangles can always be made to represent a two-dimensional domain of any shape. The finite element mesh used in this problem is shown in Figure (8). This mesh was constructed in such a way that small elements were used near the walls where a large variation of the velocity across the boundary layer was expected and also small elements near the flat plate aided in calculating the shear stress distribution and the drag force more accurately. A finer mesh was also constructed near the downstream side of the flow region in order to generate the downstream conditions at any time step by using the space-time delay technique presented in section (2.7.4).

5.3 Choosing the Element Shape Function

The element shape function is usually chosen to satisfy certain continuity requirements of the field variable and its deri-

vatives at the element interfaces joining the nodal points. In this study the continuity of the field variable at the element interfaces was only considered. The shape function used was a linear interpolation function and was written as:

$$\phi = \sum_{k=1}^3 \xi_k \phi_k \quad (5-1)$$

where ξ_k was the area coordinate defined as:

$$\xi_j = \frac{1}{2\Delta_i} (a_j + b_j x + c_j y) \quad j = 1, 3$$

and ϕ_i was the value of the field variable at the nodal point i .

For further details see Appendix (B).

Using this linear function the finite element approximations for the variation of the stream function ψ and vorticity ζ over each element were written as:

$$\psi^{(e_i)} = [B]^{(i)} \{\psi\}^{(i)} \quad (5-2-a)$$

$$\zeta^{(e_i)} = [B]^{(i)} \{\zeta\}^{(i)} \quad (5-2-b)$$

where

$$[B]^{(i)} = [\xi_1 \ \xi_2 \ \xi_3]^{(i)}$$

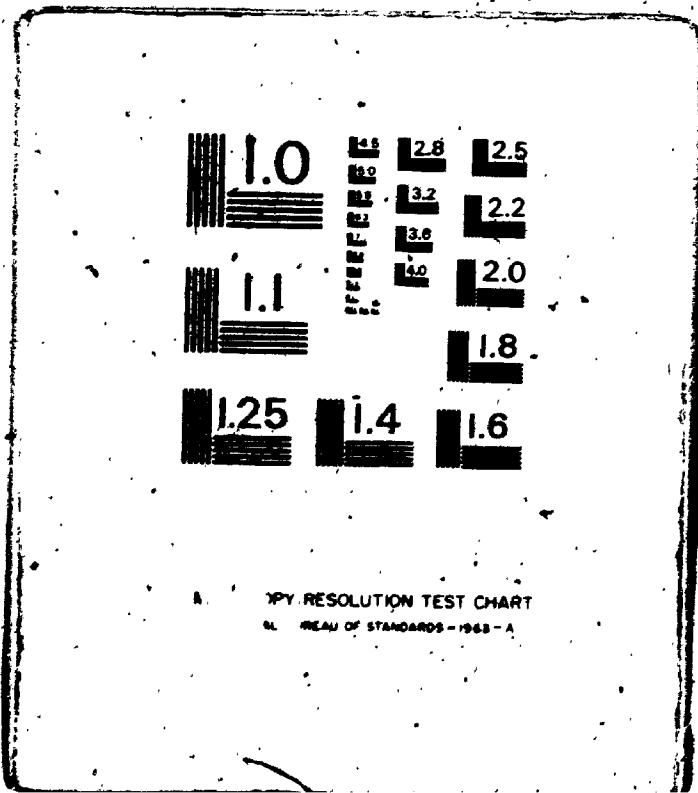
$$\{\psi\}^{(i)} = \begin{bmatrix} \psi_1 \\ \psi_2 \\ \psi_3 \end{bmatrix}^{(i)} \quad \{\zeta\}^{(i)} = \begin{bmatrix} \zeta_1 \\ \zeta_2 \\ \zeta_3 \end{bmatrix}^{(i)}$$

and the superscript (i) denoted the number of the element.

2

OF/DE

3



5.4 Obtaining the Finite Element Equations

The variational functional of the vorticity equation was written in terms of the element parameters by substituting equations (5-2-a and b) into equation (4-19) as follows:

$$\begin{aligned} \chi_{1i}(\zeta_{\theta}) = & \sum_{i=1}^k \iint_{e_i} \left\{ \left[\frac{1}{\Delta t} [B]^{(i)} \{\zeta_{n+1}\}^{(i)} - \frac{1}{\Delta t} [B]^{(i)} \{\zeta_n\}^{(i)} + \right. \right. \\ & [B_y]^{(i)} \{\psi_{\theta}^*\}^{(i)} [B_x]^{(i)} \{\zeta_{\theta}^*\}^{(i)} - [B_x]^{(i)} \{\psi_{\theta}^*\}^{(i)} \\ & [B_y]^{(i)} \{\zeta_{\theta}^*\}^{(i)} [B]^{(i)} \{\zeta_{\theta}\}^{(i)} + \frac{\nu}{2} \left. \left. \left([B_x]^{(i)} \{\zeta_{\theta}\}^{(i)} \right)^2 + \right. \right. \\ & \left. \left. \left([B_y]^{(i)} \{\psi_{\theta}^*\}^{(i)} \right)^2 \right\} dx dy \end{aligned} \quad (5-3)$$

where $[B_x]^{(i)} = \frac{\partial}{\partial x} [B]^{(i)} = \frac{1}{2\Delta_i} [b_1 \ b_2 \ b_3]^{(i)}$

and $[B_y]^{(i)} = \frac{\partial}{\partial y} [B]^{(i)} = \frac{1}{2\Delta_i} [c_1 \ c_2 \ c_3]^{(i)}$

Equation (5-3) can be written simply as:

$$\chi_{1i}(\zeta_{\theta}) = \sum_{i=1}^k \chi_{1i}(\zeta_{\theta}) \quad (5-4)$$

where χ_{1i} was the double integral over the element 'e_i' written in equation (5-3).

It should be noted that the derivative of $\chi_{1i}(\zeta_{\theta})$ with respect to the vorticity at a typical point j will have a non-zero value only if j is one of the nodes of the element 'e_i'. Therefore

when minimizing the functional $\chi_1(\zeta_\theta)$ with respect to each of the nodal values of the variable $\zeta_{\theta j}$, the summation over the elements that contain the point j as one of its nodes may only be considered, and

$$\frac{\partial \chi_1(\zeta_\theta)}{\partial \zeta_{\theta j}} = \sum_{i=1}^k \frac{\partial \chi_{1i}(\zeta_\theta)}{\partial \zeta_{\theta j}} = \sum_{i=1}^{k_1} \frac{\partial \chi_{1i}(\zeta_\theta)}{\partial \zeta_{\theta j}} \quad (5-5)$$

where k_1 is the number of elements that have the node j as one of its nodes.

Suppose that the element 'e_i' contains the node j then the derivative $\partial \chi_{1i}(\zeta_\theta) / \partial \zeta_{\theta j}$ can be obtained as follows:

$$\begin{aligned} \frac{\partial \chi_{1i}(\zeta_\theta)}{\partial \zeta_{\theta j}} &= \frac{1}{\Delta t} \iint_{e_i} \xi_j \left[[B]^{(i)} \{ \zeta_{n+1} \}^{(i)} - [B]^{(i)} \{ \zeta_n \}^{(i)} \right] dx dy + \\ &\iint_{e_i} \xi_j \left[[B_y]^{(i)} \{ \psi_\theta^* \}^{(i)} [B_x]^{(i)} \{ \zeta_\theta^* \}^{(i)} - [B_x]^{(i)} \{ \psi_\theta^* \}^{(i)} \right. \\ &\left. [B_y]^{(i)} \{ \zeta_\theta^* \}^{(i)} \right] dx dy + \frac{v}{2\Delta_i} \iint_{e_i} \left[[B_x]^{(i)} \{ \zeta_\theta \}^{(i)} b_j + \right. \\ &\left. [B_y]^{(i)} \{ \zeta_\theta \}^{(i)} c_j \right] dx dy \quad (5-6) \end{aligned}$$

Substituting from equation (5-2) in equation (5-6) and rearranging then,

$$\begin{aligned}
\frac{\partial \chi_{1i}(\zeta_\theta)}{\partial \zeta_{\theta j}} &= \left[\frac{1}{\Delta t} \iint_{e_i} \xi_j [\xi_1 \xi_2 \xi_3]^{(i)} dx dy + \frac{v\theta}{4\Delta_i} \{b_j [b_1 b_2 b_3]^{(i)} + \right. \\
&\quad \left. c_j [c_1 c_2 c_3]^{(i)} \} \right] / \{\zeta_{n+1}\}^{(i)} - \left[\frac{1}{\Delta t} \iint_{e_i} \xi_j [\xi_1 \xi_2 \xi_3]^{(i)} \right. \\
&\quad \left. \otimes dx dy - \frac{1-\theta}{4\Delta_i} \{b_j [b_1 b_2 b_3]^{(i)} + c_j [c_1 c_2 c_3]^{(i)} \} \right] \{\zeta_n\}^{(i)} - \\
&\quad \frac{1}{12 \Delta_i} [[b_1 b_2 b_3]^{(i)} \{\psi_\theta^*\}^{(i)} [c_1 c_2 c_3]^{(i)} - \\
&\quad [c_1 c_2 c_3]^{(i)} \{\psi_\theta^*\}^{(i)} [b_1 b_2 b_3]^{(i)}] \{\zeta_\theta^*\}^{(i)} \quad (5-7)
\end{aligned}$$

Calculating the approximate values of ψ_θ^* and ζ_θ^* from the known values ψ_n and ζ_n and the values of ψ_{n+1} and ζ_{n+1} obtained from the previous iteration by using linear interpolation, equation (5-7)

can then be written as:

$$\frac{\partial \chi_{1i}(\zeta_\theta)}{\partial \zeta_{\theta j}} = [T]^{(i)} \{\zeta_{n+1}\}^{(i)} - [Q]^{(i)} \{\zeta_n\}^{(i)} - [R]^{(i)} \{\zeta_\theta^*\}^{(i)} \quad (5-8)$$

Substituting this equation into equation (5-5) and equating

$\partial \chi_1(\zeta_\theta) / \partial \zeta_{\theta j}$ to zero, the following equation was then obtained,

$$\begin{aligned}
\frac{\partial \chi_1(\zeta_\theta)}{\partial \zeta_{\theta j}} &= \sum_{i=1}^{k_1} [[T]^{(i)} \{\zeta_{n+1}\}^{(i)} - [Q]^{(i)} \{\zeta_n\}^{(i)} - \\
&\quad [R]^{(i)} \{\zeta_\theta^*\}^{(i)}] = 0 \quad j = 1, L \quad (5-9)
\end{aligned}$$

where L was the number of internal points and ζ_n , ζ_θ^* were known.

Equations (5-9) represent a set of linear algebraic equations which may be written finally in the form

$$(A) \{\zeta_{n+1}\} = \{F\} \quad (5-10)$$

where (A) was a square matrix of dimension (L,L) and the right hand side {F} was a column vector the elements of which were calculated according to initial assumed values for ζ_{n+1} , ψ_{n+1} . It should be noted that the square matrix (A) does not depend on the field variables ψ and ζ but depends completely on the construction of the finite element mesh, the chosen element shape function, the factor θ and the time increment Δt .

The variational functional of the stream function equation can be obtained by substituting from equation (5-2) into equation (4-22) as follows:

$$\chi_2(\psi_{n+1}) = \sum_{i=1}^k \iint_{e_i} \{ \frac{1}{2} [([B_x]^{(i)} \{\psi_{n+1}\}^{(i)})^2 + ([B_y]^{(i)} \{\psi_{n+1}\}^{(i)})^2] - [B]^{(i)} \{\psi_{n+1}\}^{(i)} [B]^{(i)} \{\zeta_{n+1}\}^{(i)} \} dx dy \quad (5-11)$$

This equation may be written as,

$$\chi_2(\psi_{n+1}) = \sum_{i=1}^k \chi_{2i}(\psi_{n+1}) \quad (5-12)$$

The extremization of the functional $\chi_2(\psi_{n+1})$ is a necessary condition to satisfy the stream function equation (4-14). The derivative

of $\chi_2(\psi_{n+1})$ with respect to the stream function at a typical point j can be written as:

$$\begin{aligned} \frac{\partial \chi_2(\psi_{n+1})}{\partial \psi_{n+1j}} &= \sum_{i=1}^k \frac{\partial \chi_{2i}(\psi_{n+1})}{\partial \psi_{n+1j}} \\ &= \sum_{i=1}^{k_1} \frac{\partial \chi_{2i}(\psi_{n+1})}{\partial \psi_{n+1j}} = 0, \quad j = 1, L \end{aligned} \quad (5-13)$$

where k_1 is the number of the elements that contain the point j as one of its nodes.

Suppose that 'e_i' is one of the elements that has the node j as one of its nodes then,

$$\begin{aligned} \frac{\partial \chi_{2i}(\psi_{n+1})}{\partial \psi_{n+1j}} &= \iint_{e_i} \frac{1}{4\Delta_i^2} [[b_1 \ b_2 \ b_3] b_j + \\ &\quad [c_1 \ c_2 \ c_3] c_j] \{\psi_{n+1}\}^{(i)} dx dy - \\ &\quad \iint_{e_i} \xi_j [\xi_1 \ \xi_2 \ \xi_3] \{\tau_{n+1}\}^{(i)} dx dy \end{aligned} \quad (5-14)$$

This equation may be written simply as,

$$\frac{\partial \chi_{2i}(\psi_{n+1})}{\partial \psi_{n+1j}} = [P]^{(i)} \{\psi_{n+1}\}^{(i)} - [S]^{(i)} \{\tau_{n+1}\}^{(i)} \quad (5-15)$$

and substituting in equation (5-13) one obtains,

$$\frac{\partial \chi_2(\psi_{n+1})}{\partial \psi_{n+1j}} = \sum_{i=1}^{k_1} [[P]^{(i)} \{\psi_{n+1}\}^{(i)} - [S]^{(i)} \{\tau_{n+1}\}^{(i)}] = 0, \quad j = 1, L \quad (5-16)$$

Equation (5-16) represents a set of linear algebraic equation, which can be written simply as:

$$(E) \{\psi_{n+1}\} = \{G\} \quad (5-17)$$

where (E) was a square matrix of dimension (L,L) which was also independent of the field variables ψ , ζ and depended only on the finite element mesh and the element shape function. The right hand side {G} was calculated for a given vorticity distribution by using equations (5-14), (5-15) and (5-16).

5.5 Steady State Solution

The steady state solution, without any freestream disturbance present, was first obtained and then used as an initial condition in the study of the time dependent flow. To obtain the steady solution the procedure of computations mentioned previously in section (4.5) was used. The potential flow solution was assumed to exist initially everywhere in the solution domain, which was the same case as if the two boundaries of the field and the flat plate had jerked into motion from rest with a constant speed. The subsequent solution was for a viscous fluid. The upstream flow was assumed to be of uniform velocity while the downstream boundary conditions were obtained at a given time step by using the space-time delay technique mentioned previously in section (2.7.4).

The steady state velocity distribution at different sections in the flow field can be seen in Figure (4) where the solution was also compared with that obtained by using the finite difference method presented previously in Chapter (2). As a check for the results the skin friction coefficient, obtained by using the present method and the finite-difference method, are plotted in Figure (5). On the same graph the coefficient of skin friction calculated from Blasius solution (54) and also from Howarth solution (see Appendix (D)) were plotted. The Blasius solution was based on approximating the freestream constant velocity by the mean value of the velocity at the edge of the boundary layer growing over the flat plate. The only difference between Blasius and Howarth's solutions was that the latter took into consideration the change in the freestream velocity at the edge of the boundary layer.

In spite of the fact that the two flow regimes had slightly different velocity distributions at the edge of the boundary layer the comparison between the author's present solution and Blasius solution can be made on the basis that the core region of the flow at the upstream side of the flat plate had almost a uniform velocity distribution. The deviation in the skin friction coefficient between the two solutions was due to the following reasons,

1. In the considered problem a uniform freestream velocity did not exist and it can be seen from Figure (4) that the maximum velo-

city in the upper (or lower) side of the plate increased downstream.

2. The boundary layer approximations on which Blasius solution was based were not valid near the leading edge.

A comparison between the finite element solution and Howarth's solution showed that the coefficient of skin friction obtained from the two methods were very close over most of the length of the plate except near the leading edge.

Another comparison between the finite element and finite-difference solutions in the same plot showed that the finite element method had the distinction of being more accurate near the solid boundaries which will imply more accurate estimates for the drag force on the flat plate (or any streamlined body).

5.6 Calculations of Lift, Drag and Pitching Moment Coefficients

The shear stress τ at the upper and lower surfaces of the infinitely thin flat plate can be calculated from

$$\tau_u = \mu \left(\frac{\partial u}{\partial y} \right)_{y=+0}$$

(5-18)

$$\tau_l = -\mu \left(\frac{\partial u}{\partial y} \right)_{y=-0}$$

where μ was the dynamic viscosity and the subscript u and l denoted the upper and lower surfaces respectively.

Since $\zeta = \frac{\partial v}{\partial x} - \frac{\partial u}{\partial y}$ and therefore

$$\zeta_u = \left(-\frac{\partial u}{\partial y}\right)_{y=+0}, \quad \zeta_l = \left(-\frac{\partial u}{\partial y}\right)_{y=-0} \quad (5-19)$$

the value of the shear stress was expressed in terms of the vorticity at the plate surface as,

$$\begin{aligned} \tau_u &= -\mu \zeta_u \\ \tau_l &= \mu \zeta_l \end{aligned} \quad (5-20)$$

and the local skin friction coefficient was written as,

$$C_{fu} = \frac{-\mu \zeta_u}{\frac{1}{2}\rho U_\infty^2}, \quad C_{fl} = \frac{\mu \zeta_l}{\frac{1}{2}\rho U_\infty^2} \quad (5-21)$$

The resulting drag coefficients were calculated from

$$\begin{aligned} C_{Du} &= -\mu \int_0^c \zeta_u dx / (\frac{1}{2}\rho U_\infty^2 c) \\ C_{Dl} &= \mu \int_0^c \zeta_l dx / (\frac{1}{2}\rho U_\infty^2 c) \\ C_{DT} &= \mu \int_0^c (\zeta_l - \zeta_u) dx / (\rho U_\infty^2 c) \end{aligned} \quad (5-22)$$

where C_D was the drag coefficient and the subscript T denoted the total value.

Since the lift was due to the pressure difference between the top and bottom surfaces of the plate, it was necessary to determine this pressure difference as a function of position.

The x component of the Navier-Stokes equation can be written as,

$$\frac{\partial u}{\partial t} + u \frac{\partial u}{\partial x} + v \frac{\partial u}{\partial y} = -\frac{1}{\rho} \frac{\partial p}{\partial x} + \nu \left(\frac{\partial^2 u}{\partial x^2} + \frac{\partial^2 u}{\partial y^2} \right) \quad (5-23)$$

At the plate surface the u and v velocity components and the x space and time derivatives of u, v were zero so that equation (5-23) reduced to

$$\left(\frac{\partial p}{\partial x} \right)_{y=0} = \mu \left(\frac{\partial^2 u}{\partial y^2} \right)_{y=0} = \mu \left[\frac{\partial}{\partial y} \left(\frac{\partial u}{\partial y} \right) \right]_{y=0} \quad (5-24)$$

Using the definition of the vorticity at the plate surface given in equation (5-19), it was possible to express the pressure gradient in terms of the vorticity gradient as,

$$\left(\frac{\partial p}{\partial x} \right)_{y=0} = -\mu \left(\frac{\partial \zeta}{\partial y} \right)_{y=0}$$

By assuming that the pressure at the upper and lower surfaces of the plate was unique at the leading edge, the difference in pressure between the lower and upper surfaces at a point on the plate (x,0) was obtained from

$$\Delta p = -\mu \left[\int_0^x \left(\frac{\partial \zeta}{\partial y} \right)_l dx - \int_0^x \left(\frac{\partial \zeta}{\partial y} \right)_u dx \right]$$

Knowing the pressure difference Δp between the two surfaces as a function of distance x , the lift coefficient C_L and pitching moment coefficient about the leading edge C_m was then obtained from the following relationships;

$$C_L = \int_0^c \Delta p \, dx / (\frac{1}{2} \rho U_\infty^2 c) \quad (5-25)$$

$$C_m = \int_0^c \Delta p \, x \, dx / (\frac{1}{2} \rho U_\infty^2 c^2) \quad (5-26)$$

where c was the length of the plate.

The integrations in equations (5-24), (5-25) and (5-26) were carried out by using Simpson's one third rule which gives an exact solution when the polynomial that can be fitted to the data points is up to a third order.

5.7 Effect of the Rotational Disturbance on the Laminar Layer Over the Plate

The response of the laminar boundary layer over the plate to a two-dimensional rotational disturbance was investigated. The steady state solution obtained in section (5.5) was assumed to exist initially everywhere in the flow field. The mathematical model presented in section (2.8), where the flow disturbance was considered to be in the form of a 'real' vortex was used to simulate the freestream disturbance. The center of the modified Rankine

vortex was assumed to be initially located far upstream of the plate such that its influence on the flow pattern at the entrance of the flow field was negligible. The velocity distribution in a section passing through the vortex center can be seen in Figure (7). The solution procedure for solving a time-dependent problem mentioned previously in section (4.6) was used. The upstream boundary conditions were developed by using equations (2-20) and (2-21). The time-dependent downstream conditions were obtained by using the space-time delay technique presented in section (2.7.4). The solution was continued until the vortex entered the field, impinged on the plate and then the disturbance generated moved downstream allowing the flow region to return again to its original steady state. Details of the solution procedure can be seen in Appendix (C).

The velocity profiles at different sections in the flow field were plotted at different time intervals and can be seen in Figures (9-a to p). Figures (10-a and b) were also plotted to show the variation of the velocity profiles with time at two particular sections. The variation of the local skin friction coefficient on the upper and lower sides of the flat plate at different times can also be seen in Figures (11-a to v). From these curves it can be seen that the computer program solution predicted that separation of flow occurred at different parts in the flow region at different times. This will be discussed in more detail in section (5.9).

The drag coefficient (C_{Dc}), lift coefficient (C_L), and the pitching moment coefficient about the leading edge (C_m) were calculated from the known vorticity field at any particular time level by using equations (5-22), (5-25) and (5-26) respectively. The variation of C_L and C_m with time are shown in Figures (12) and (13) respectively while the time variation of C_{Dc} , C_{Du} and C_{DT} are shown in Figure (14).

5.8. Discussion of the Method of Solution.

One of the main advantages for using the finite element method for solving flow problems is that the shear stress on the body can be calculated with a relatively high degree of accuracy. The more fine the mesh near the body the more accurate the shear stress distribution and subsequently the more accurate the calculated drag force. Other advantages of the finite element method presented in this work was that the two matrices (A) and (E) in equations (5-10) and (5-17) had the following favourable characteristics:

1. The matrices did not depend on the values of the stream function ψ or the vorticity ζ but depended only on the time increment Δt , the chosen element shape function, the factor θ and the construction of the finite element mesh.

2. The two matrices were diagonally dominant which made it easy to solve the matrix problem by an iterative or direct method.
3. By assigning optimum numbers to the nodal points, the resulting matrices (A) and (E) were banded and this helped in reducing the required computer storage and computation time. This was achieved by minimizing the difference between the number of nodal points in each finite element.

The Crouts' reduction method for solving a set of linear algebraic equations, which is based on the Gauss elimination technique, was used to obtain the augmented matrices of (A) and (E). This operation was applied once to each of the (A) and (E) matrices and the resulting augmented matrices (A') and (E') were then stored on the computer disc. The required computations for solving equations (5-10) and (5-17) were then limited to the calculation of the right hand sides {F} and {G} and then using the stored augmented matrices (A') and (E') to obtain the solution.

Three iterations were required to obtain a solution accurate to at least three decimal places for both ψ and ζ in the case where no flow separation occurred. When separation took place the number of iterations was observed to be increased from three to as much as eight to obtain the same accuracy. The stability of the solution depended on the time increment Δt as well as the factor θ .

The method presented in this Chapter was tested by applying it to study the problem of flow development in the entrance region of a two-dimensional channel. A comparison between the velocity profiles obtained from the present method and those obtained by Schlichting (54) can be seen in Figure (15).

5.9 Discussion of Results

According to the comparison carried out in section (5.5) it has been shown that in the steady state solution the distribution of the local skin friction coefficient obtained from the finite element method was close to Howarth's solution for most of the length of the plate. For example at the center of the plate the error was 5%. The deviation between the two solutions near the leading edge was due to the fact that the boundary layer approximations were not valid within this region.

In the time dependent solution, when the freestream was disturbed, the separation of flow occurred at different parts in the flow field. In order to simplify the discussion, the flow field was divided into six regions as shown in Figure (7). Separation of flow first started to occur upstream of the plate and on the lower side of region (2). The reason for this was that, when the vortex approached the flow field it tended to decrease the velo-

city of flow at the entrance of region (2) and to increase it at the entrance of region (1). Due to this decrease in velocity the condition at region (2) became as follows:

1. A deceleration of the flow existed at the entrance.
2. The core region downstream of the entrance could not respond quickly to this change in velocity because of the inertia effect.

Therefore a decrease in the flow velocity in the viscous region near the lower wall could be expected. The decrease caused the separation of flow.

As the vortex approached the flat plate its effect on the velocity distributions at the entrance of regions (3) and (4) increased. The increase of the velocity at the entrance of region (3) tended to increase the shear stress and subsequently the skin friction coefficient on the upper side of the plate. On the other hand the decrease of velocity at the entrance of region (4) tended to decrease the shear stress on the lower side of the plate as shown in Figures (11-2a to v). Again, the retardation of flow at the entrance of region (4) caused the flow to separate due to the reasons mentioned previously, however in this case the separation occurred on the lower plate surface and the lower boundary wall.

When the vortex moved further downstream and its effect decreased at the entrance of regions (3) and (4), the flow started to recover speed again at the entrance of (4) while slowing down at the entrance of (3). This effect tended to decrease the shear stress on the upper-side of the plate while increasing it on the lower side. Separation occurred next at the upper side of region (5) for two reasons. First because the flow was retarded at the entrance of region (3). Second because the accelerated flow coming from the lower side of the plate tended to increase the velocity of flow at the lower part of region (5). At the same time it was observed that the shear stress on the lower side of the plate was larger than that on the upper side. The reason for this was that during the time at which the flow was accelerating on the lower side it was being retarded on the upper one. This can be clarified by considering the boundary layer equations for the case of accelerating (or retarding) free stream as follows. From the Navier-Stokes equations, with Prandtl's approximations,

$$\frac{\partial u}{\partial t} + u \frac{\partial u}{\partial x} + v \frac{\partial u}{\partial y} = -\frac{1}{\rho} \frac{\partial p}{\partial x} + \nu \frac{\partial^2 u}{\partial y^2} \quad (5-27)$$

with the boundary conditions,

$$\text{at } y = 0 \quad u = v = 0 \quad \text{and at } y = \delta \quad u = U \quad v = 0$$

where

δ is the boundary layer thickness,

and

U is the freestream velocity

then:
$$\frac{\partial U}{\partial t} + U \frac{\partial U}{\partial x} = - \frac{1}{\rho} \frac{\partial P}{\partial x} \quad (5-28)$$

Equation (5-28) indicates that the term $\frac{\partial P}{\partial x}$ depends on both $\frac{\partial U}{\partial t}$ and $U \frac{\partial U}{\partial x}$. If $\frac{\partial U}{\partial t}$ is negative (i.e. the flow is retarding) such that $(\frac{\partial U}{\partial t} + U \frac{\partial U}{\partial x})$ is negative definite then by equation (5-28) the pressure will increase downstream. This increase of pressure tends to decrease the shear stress at the wall and also may tend to cause flow separation in some cases.

The lift coefficient (in the case when the vortex had negative strength-'clockwise' rotation) was of positive sign when the vortex was approaching the plate. For this flow incidence, one would intuitively expect negative lift on the plate. The reason for this reverse was that the negative vortex created higher velocities on the upper side of the plate than on the lower side. This effect caused suction on the upper side and increased the pressure on the lower one and both effects tended to create a positive lift. This can be understood by considering the boundary layer equation (5-28) in the following way. When the vortex was approaching the plate the terms $\frac{\partial U}{\partial t}$ and $U \frac{\partial U}{\partial x}$ had increasing positive definite values on the upper side which implied by equation (5-28) that the pressure gradient $\frac{\partial P}{\partial x}$ had a decreasing negative definite value. On the lower side, when the vortex was approaching the plate, the term $\frac{\partial U}{\partial t}$ had a decreasing negative value which tended to increase the value of $\frac{\partial P}{\partial x}$ on that side. The variation of the pressure gradient $\frac{\partial P}{\partial x}$ with time, obtained from

the finite element solution, at a point at the middle of the plate ($x^* = x/c = \frac{1}{2}$) was plotted in Figure (16). Since the pressure gradient was decreasing on the upper side and increasing on the lower one (when the vortex was approaching the plate) a higher pressure on the lower side would be expected and resulting in an increase of the lift coefficient as shown in Figure (12).

When the vortex impinged on the plate and started to move downstream (approximately at $t = 1.6$ secs) the velocity on the upper side of the plate was decelerating while accelerating on the lower side. Accordingly a negative value for $\frac{\partial U}{\partial t}$ was created on the upper side and a positive value on the lower one. By equation (5-28) it can be seen that the pressure gradient would decrease on the lower side and increase on the upper side. The same response was obtained from the computer program as shown in Figure (16). At the same time the pressure started to decrease on the lower side and to increase on the upper side and this tended to decrease the lift coefficient C_L and to have a negative lift when the vortex was being shed downstream as obtained from the solution and shown in Figure (12).

Figures (12) and (14) shows that the variation of the total drag coefficient with time was much less than that of the lift coefficient. The reason was that any increase of the velocity on one side of the plate was accompanied by a decrease of the velocity

on the other side. This effect tended to increase the drag on one side and decrease it on the other side such that the mean value did not change considerably. On the other hand a pressure decrease on one side of the plate was accompanied by a pressure increase on the other side and both effects tended to create a normal force towards the low pressure side.

CHAPTER (6)

THE RESPONSE OF THE VISCOUS LAYER OVER A FLAT PLATE TO PSEUDO-TURBULENCE

6.1 Introduction

Recently more interest has been given to the studies of simulating unsteady flows, such as turbulence, using the digital computer; the so called computer simulation experiments. The success that has been achieved in these studies enhanced the possibility of investigating the effect of pseudo free stream turbulence on the viscous boundary layer over a body surface by using a mathematical model to simulate the approaching turbulent flow.

One of these studies is the work by Lilly (1) who developed a numerical simulation technique for two-dimensional turbulence. In his approach Lilly considered an incompressible turbulent velocity field to be idealized as a random vector field governed in time and two-dimensional space by the Navier-Stokes equations.

Base (2) developed a method that can be used for simulating pseudo-turbulence of different statistical characteristics

and to obtain a continuous velocity time history at each point in the flow field. The approach was to assume that the free stream turbulence consisted of a discrete random distribution of moving 'real' vortices and by using a suitable vortex function, the flow was rotational and the continuity equation was implicitly satisfied. It was found that by changing the rotational core size of the individual 'real' vortices and also by changing the mean distance between them the statistical characteristics of the pseudo-turbulence was changed. Another contribution in the numerical solution of two-dimensional turbulence is found in the work by Ahmadi and Goldschmidt (3).

In this chapter a computer simulated model of pseudo-turbulence, based on the work by Base (2, 93) was used to generate the outer boundary conditions for the flow over a flat plate at a Reynolds number of 600 (based on the time mean value of the approaching flow velocity and the chord of the plate). The continuity and momentum conservation equations were solved near the plate by using the variational-finite element method of solution presented in Chapter (4). Results were obtained for the time variation of lift and drag forces on the plate and these results were expressed in coefficient form. The variation of the velocity components and vorticity at different points in the flow field with time were also plotted.

6.2 Description of Considered Problem

The problem considered was that of a thin flat plate set at zero incidence to an initially uniform flow. A finite element mesh was set around the plate as shown in Figure (17-b). Upstream and out of influence of the plate, finite groups of randomly positioned moving vortices to represent the oncoming eddy structure were set up on the computer and allowed to move with the free stream towards the flat plate. To illustrate the method of solution, Figure (17-a) shows five boxes for the real vortices, with the center box subdivided into an additional three boxes near the centreline, with the plate (PQ) mounted as shown.

With an increase of time, the vortices assembled randomly in box number 1 were convected towards the plate until the first four boxes were filled with vortices. With further increase of time and with no further increase in the number of vortices being added to the model, the program was so scaled that within a given time period the vortices moved one box length downstream. At this particular time period approximately one quarter of the total number of vortices furthest downstream, that by now had little influence at the outer boundary points of the finite element mesh stencil (ABCD), were removed and replaced by the same number of similar vortices with new random positions and new signs upstream

of the plate where again the vortices had little influence on the conditions at the boundaries of the finite element mesh stencil (ABCD).

The vortex model then continued and the process repeated again so that a continuously running program was achieved. By this means, therefore, the vortex model provided a continuous velocity field at the outer grid points along the boundaries AB, BC and CD of the finite element mesh.

The effect of the pseudo-turbulence therefore entered the flow field in the form of time-dependent boundary conditions. The unsteady flow and vorticity were convected and diffused within the mesh stencil and finally modified the flow field over the flat plate.

6.3 The Unsteady Boundary Conditions

In this section pseudo-turbulence flow models are discussed which provided boundary conditions upstream of the plate and at adjacent sides of the finite element mesh, as shown in Figure (17-a).

The approach to model the turbulent flow in this chapter follows the method described in references (2, 93). In the model

to determine the boundary conditions, 'real' vortices representing the pseudo-turbulent eddy were convected along in a uniform stream, similarly as in Taylor's "frozen pattern" model of turbulence. This was similar to what has been observed in 'grid turbulence' where the disturbance (or eddy) can be convected downstream unchanged for a considerable distance and decays very slowly. Only the continuity equation was satisfied with this model which ensured that it was kinematically possible. At a fixed point in space the stream function value, the velocity components and vorticity varied with time but the eddy pattern did not change as it was convected downstream.

The continuity equation was satisfied by suitable choice of vortex function. The method provided a continuous pseudo-turbulent velocity time history at each point on the finite element mesh boundaries as shown in Figure (19). In the model of pseudo-turbulence developed by Base (2) it was constrained to satisfy the continuity equation as follows.

The tacit assumption was that the velocity at any field point (\underline{x}) was given by the sum of the contributions from the real vortex expressions. The velocity (u_i) therefore at a boundary point (\underline{x}_i) was given by

$$u_i = \sum_{m=1}^N (u_i)_m \quad (6-1)$$

where \underline{x}_i was the position vector of the boundary point (i).

u_i , $i = 1, 2$ were the velocity components in the x and y direction,

and $(u_i)_m$ was the contribution to the velocity at the point (\underline{x}_i) due to the m^{th} vortex and N was the total number of vortices representing the model. It could also be shown, from equation (6-1) that the spacial derivative at the point (\underline{x}_i) was also equal to the sum of the derivative contributions from the complete array of vortices so that,

$$\frac{\partial u_i}{\partial x_i} = \sum_{m=1}^N \left(\frac{\partial u_i}{\partial x_i} \right)_m, \quad i = 1, 2 \quad (6-2)$$

Since a condition for the vortex generating function was that the continuity equation be satisfied so that,

$$\left(\frac{\partial u_i}{\partial x_i} \right)_m = 0 \quad (6-3)$$

then by substituting equation (6-3) into (6-2) then:

$$\frac{\partial u_i}{\partial x_i} = 0 \quad (6-4)$$

The continuity equation was therefore satisfied implicitly throughout the whole vortex model. The velocity field for an individual two-dimensional vortex was obtained by using a stream function expression with the following form;

$$\psi = \frac{\Gamma_1}{2\pi} \log_e [r_c^2 + (x - \xi_0 - u_c t)^2 + (y - \eta_0)^2] \quad (6-5)$$

where (x, y) was a field point, (ξ_0, η_0) the initial random position of a vortex in space, Γ_1 the circulation constant, r_c the vortex core radius, u_c the convection velocity which in this case was constant and 't' the time. The vorticity field for the same vortex can be obtained from the relation $\zeta = \nabla^2 \psi$ and can be written finally as:

$$\zeta = - \frac{\Gamma_1}{\pi} \frac{2r_c^2}{[r_c^2 + (x - \xi_0 - u_c t)^2 + (y - \eta_0)^2]^2} \quad (6-6)$$

where ζ is the vorticity at the point (x, y) .

6.4 Method of Solution

The equations governing the motion of the two-dimensional viscous fluid flow were expressed in the form of the stream function and vorticity form (see section 4.2). The numerical solution of the considered problem started by calculating the boundary conditions for the stream function and vorticity from the pseudo-turbulence model at time $t = t_0$. With boundary conditions temporarily fixed at $t = t_0$ the steady state solution was then obtained by using the method presented in section (4.5). This steady state solution was considered as an initial condition for the unsteady flow problem. The conditions at the upstream boundary (BC) and side boundaries

(AB) and (CD) of the flow field (ABCD, see Figure 17-a) were then generated at each time step from the pseudo-turbulence model and assumed to be independent of the conditions inside the flow field. The conditions at the downstream boundary (AD) were obtained by using the space-time delay technique presented in section (2.7.4). The rest of the solution procedure was almost similar to that given in section (4.6). The only difference was that in the problem considered in this chapter the conditions at the two sides of the flow field were completely specified by the vortex model.

6.5 Results and Discussion

In this example a vortex model, with data given in table (1), was used to simulate the free stream turbulence as outlined in section (6-3). Typical variations with time of the velocity components (u' , v) and vorticity (ζ) are shown in Figure (18) where u' was the fluctuating velocity in the x direction such that $u' = (u - u_{ref})$ and u_{ref} was the mean value of u component of velocity in the pseudo-turbulence model. Figures (19, 20 and 21) show the complete flow domain with the time varying velocities (u' , v) and vorticity (ζ) values at some of the boundary points. On the same figures the variation of the variables (u' , v and ζ), which were obtained from the finite element solution at a point downstream from the plate, were also plotted. The variation of the vorticity (ζ) at this point

(see Figure 21) was considerably higher than that at any other boundary point and this was to be expected in the wake region of the plate. The variation of u' at the same point (see Figure 19) shows that it has a negative value over most of the sample time and this was expected because of the momentum deficit that occurred due to the drag force on the plate.

Figure (22) shows the variation of the drag coefficients of the plate with time. Although the variation of the drag coefficient on each individual side of the plate was considerable, the total drag coefficient was found to have small variation with time. A comparison between the total drag coefficient obtained from the solution and the one obtained from Blasius solution, based on steady laminar flow with $u_{\infty} = u_{ref}$, showed that the two coefficients were close over most of the sample time as can be seen in Figure (22). This should not be considered as a general conclusion for the case of a turbulent flow approaching a flat plate because flows with other statistical descriptions and higher Reynolds numbers were not studied in the thesis. The variation of the lift coefficient C_L with time is shown in Figure (23) and illustrate how with this method of solution an actual time variation of the forces on the plate can be achieved.

In the considered problem the outer boundary conditions

of the finite element mesh set around the plate, were unsteady, continuous and stochastic. The variational-finite element approach was extremely stable and the effect on the method of solution of sudden changes of the flow velocity and direction with time at a point was simply an increase in the number of iterations in the solution to predict a close approximation for the non-linear terms in the flow equations.

CHAPTER (7)

CONCLUSION

7.1. General Conclusion

The main object of this thesis was to investigate the influence of a two-dimensional rotational disturbance and free stream pseudo-turbulence on the laminar boundary layer growing on a body surface.

The governing equations of the two-dimensional, time-dependent, incompressible, viscous flow were written in the form of the Helmholtz vorticity transport equation and the stream function equation. A variational-finite element method for solving these equations was developed by the author. This method was of iterative type to overcome the difficulties that arose due to the nonlinearity of the equations. A new technique "the space-time delay technique" was also introduced to generate the time-varying downstream boundary conditions. The method of solution was tested by applying it to the problem of the laminar flow development in the entrance region of a straight channel with flat parallel walls. The results for this test problem were compared with the analytical solution obtained by Schlichting (54) and a good agreement was achieved.

The first problem considered was that of a flat plate which was situated midway between two parallel sides of a straight channel with the leading edge a short distance downstream from the entrance of the channel. The steady state solution, when the approaching stream was steady and uniform, was first obtained and this was later used as an initial condition when studying the time-dependent flow problem. The steady velocity profiles were plotted together with the variation of the local skin friction coefficient over the plate and compared with the available results of a problem approximately similar to the considered one. Howarth's solution for accelerated flow over a flat plate was used for comparison and a good agreement was found with the finite element solution.

The variational-finite element method introduced in the thesis was applied to study the effect of a two-dimensional rotational disturbance in the approaching stream on the laminar boundary layer over the flat plate. In this example the rotational disturbance was simulated by a modified Rankine vortex which was set initially far from the plate such that its influence on the flow pattern at the entrance to the flow field was almost negligible. The vortex was then convected along with the free stream until it entered the flow domain, impinged on the plate and then the disturbance generated convected downstream allowing the flow field to return again to its original steady state. Results have been com-

piled for variation of lift, drag and pitching moment about the leading edge of the plate. The method of solution was extremely stable even when separation occurred at several parts in the flow field. A complete discussion of the method and full analysis of the results were presented in Chapter (5), and showed that the results were fairly consistent with the physical situation of the considered problem.

A more complicated flow regime was then studied when the effect of free stream pseudo-turbulence on the laminar boundary layer growing over a flat plate at a Reynolds number of 600 (based on the time mean of the free stream velocity and the length of the plate) was investigated. A computer simulation technique to generate pseudo-turbulence, based on the work by Base (2, 93) was used to generate the outer boundary conditions to a finite element mesh set around the plate. Near the plate the variational approach was used to solve the stream function and vorticity transport equations. The results obtained in this particular example showed that the vorticity at a point downstream of the plate was considerably higher than that at any other boundary point due, not only to the convected vorticity, but also due to that generated on the plate. The variation of the fluctuating component of the axial velocity u' at the same point showed that it had a negative value over most of the sample time and this was expected because of the momentum deficit that occurred due to the drag force on the plate. It may be noted

that in this case the fluctuating velocity u' was with respect to the upstream mean velocity value and not the local mean value. Results were also obtained for the variation of lift and drag coefficients over the plate. In this example although the variation of the drag coefficient with time on each of the upper and lower sides of the plate was considerable, the total drag coefficient was found to vary only slightly about its mean value. The time mean of the total drag coefficient was found to be close to the value calculated from Blasius solution which was based on a uniform approaching stream having a constant velocity equal to the time mean of the velocity of the turbulent stream. This should not be considered as a general conclusion for such kind of flow because flows with other statistical descriptions at different values of Reynolds numbers were not studied in the thesis. A complete discussion of the results was presented in Chapter (6).

7.2 Recommendations for Future Studies

As a recommendation for future work in this research area the following points may be considered.

1. Studying the effect of the variation of Reynolds number on the laminar boundary layer response to free stream turbulence.

2. Changing the turbulence statistical characteristics and finding its effect on the variation of lift and drag forces.
3. Studying the case of a vortex approaching an aerofoil at different angles of attack and investigating its effect on the lift, drag and pitching moment coefficients (as a simulation for an aeroplane wing approaching the trailing vortices of another aircraft).
4. Investigating the effect of free stream turbulence on the rate of heat transfer from heated bodies by considering the solution of the energy conservation equation simultaneously with the present solution for the momentum conservation equations.

APPENDIX (A)

THE EQUATIONS OF MOTION OF A VISCOUS FLUID-

The equations of motion in the case of a three-dimensional, unsteady flow of an incompressible viscous fluid (Navier-Stokes equation) can be written in vector form as:

$$\left(\frac{\partial}{\partial t} + \underline{U} \cdot \underline{\nabla}\right) \underline{U} = -\frac{1}{\rho} \underline{\nabla} p + \nu \nabla^2 \underline{U} \quad (\text{A-1})$$

and the continuity equation as,

$$\underline{\nabla} \cdot \underline{U} = 0 \quad (\text{A-2})$$

Taking the vector curl of equation (A-1) and noting that,

$$(\underline{U} \cdot \underline{\nabla}) \underline{U} = \underline{\nabla} U^2 - \underline{U} \times (\underline{\nabla} \times \underline{U})$$

the following equation can be obtained

$$\left(\frac{\partial}{\partial t} + (\underline{U} \cdot \underline{\nabla})\right) \underline{\zeta} = (\underline{\zeta} \cdot \underline{\nabla}) \underline{U} + \nu \nabla^2 \underline{\zeta} \quad (\text{A-3})$$

where $\underline{\zeta}$ is the vorticity vector defined by

$$\underline{\zeta} = \underline{\nabla} \times \underline{U} \quad (\text{A-4})$$

In the case of two-dimensional flow only one component of the vorticity (ζ_3) exists which is perpendicular to the plane of motion such that

$$\zeta_3 = \frac{\partial v}{\partial x} - \frac{\partial u}{\partial y} \quad (\text{A-5})$$

In this case the stream function ψ may be introduced such that

$$u = \frac{\partial \psi}{\partial y}, \quad v = -\frac{\partial \psi}{\partial x}$$

and equations (A-3) and (A-4) can be written as,

$$\frac{\partial \zeta}{\partial t} + \frac{\partial (u\zeta)}{\partial x} + \frac{\partial (v\zeta)}{\partial y} = \nu \nabla^2 \zeta \quad (\text{A-6})$$

$$\text{and} \quad -\zeta = \nabla^2 \psi \quad (\text{A-7})$$

$$\text{where} \quad \nabla^2 = \frac{\partial^2}{\partial x^2} + \frac{\partial^2}{\partial y^2} \quad \text{and} \quad \zeta = \zeta_3$$

Equations (A-6) and (A-7) are known as the vorticity transport (Helmholtz) and stream function equations respectively.

An expression for the pressure can be obtained by taking the divergence of the two sides of equation (A-1) and by using the continuity equation (A-2). The following equation was obtained,

$$\underline{\nabla} \cdot (\underline{U} \cdot \underline{\nabla}) \underline{U} = -\frac{1}{\rho} \nabla^2 p \quad (\text{A-8})$$

which can be written in two-dimensional, cartesian coordinates as,

$$\frac{\partial^2 p}{\partial x^2} + \frac{\partial^2 p}{\partial y^2} = -\rho Q \quad (\text{A-9})$$

$$\text{where} \quad Q = 2 \left(\frac{\partial u}{\partial y} \frac{\partial v}{\partial x} - \frac{\partial u}{\partial x} \frac{\partial v}{\partial y} \right)$$

APPENDIX (B)

DEDUCING THE FINITE ELEMENT EQUATIONS FOR A SIMPLE PROBLEM AND COMPARISON WITH FINITE-DIFFERENCE

In this Appendix the equations arising from using the finite element method of solution for a simple regular mesh and linear interpolation function are shown to be exactly the same as when the conventional finite-difference approach is used.

Considered, for example, the variation of the variable ϕ in the x-y plane to be satisfied by Laplace's equation

$$\frac{\partial^2 \phi}{\partial x^2} + \frac{\partial^2 \phi}{\partial y^2} = 0 \quad (B-1)$$

and consider the value of ϕ to be defined along the boundaries AB, BC, CD and DA of the simple finite element mesh shown in figure (B-1).

The variational principle of equation (B-1) (see reference 88) can be written as,

$$I(\phi) = \iint_{\Omega} \frac{1}{2} \left\{ \left(\frac{\partial \phi}{\partial x} \right)^2 + \left(\frac{\partial \phi}{\partial y} \right)^2 \right\} dx dy \quad (B-2)$$

where Ω is the solution domain.

The integration over Ω in equation (B-2) can be obtained as the summation of integrations over the individual finite elements and then the functional $I(\phi)$ can be written as,

$$I(\phi) = \sum_{i=1}^N \iint_{e_i} \frac{1}{2} \left\{ \left(\frac{\partial \phi}{\partial x} \right)^2 + \left(\frac{\partial \phi}{\partial y} \right)^2 \right\} dx dy \quad (B-3)$$

where e_i denotes the element number (i)

and N is the total number of elements in the solution domain.

The area coordinates ξ_1 , ξ_2 and ξ_3 of the finite element ABC shown in figure (B-2) are defined as,

$$\xi_1 = \frac{\text{Area of triangle BCD}}{\text{Area of triangle ABC}}$$

$$\xi_2 = \frac{\text{Area of triangle ACD}}{\text{Area of triangle ABC}}$$

$$\xi_3 = \frac{\text{Area of triangle ABD}}{\text{Area of triangle ABC}}$$

therefore

$$\xi_1 = \frac{\begin{vmatrix} 1 & 1 & 1 \\ x & x_2 & x_3 \\ y & y_2 & y_3 \end{vmatrix}}{\begin{vmatrix} 1 & 1 & 1 \\ x_1 & x_2 & x_3 \\ y_1 & y_2 & y_3 \end{vmatrix}}$$

or
$$\xi_1 = \frac{1}{2\Delta} (a_1 + b_1 x + c_1 y)$$

similarly
$$\xi_2 = \frac{1}{2\Delta} (a_2 + b_2 x + c_2 y) \quad (\text{B-4})$$

$$\xi_3 = \frac{1}{2\Delta} (a_3 + b_3 x + c_3 y)$$

where Δ is the area of triangle ABC,

and

$$a_1 = x_2 y_3 - x_3 y_2$$

$$b_1 = y_2 - y_3$$

$$c_1 = x_3 - x_2$$

The other coefficients are obtained by cyclically permuting the subscripts.

Using a linear interpolation function to give an approximate representation for the variation of the variable ϕ within each element e_i then

$$\phi^{e_i} = \{ \xi_1 \phi_1 + \xi_2 \phi_2 + \xi_3 \phi_3 \}_i \quad (\text{B-5})$$

where 1, 2 and 3 are the local numbers of the nodes in the finite element e_i ,

ϕ_1 , ϕ_2 and ϕ_3 are the nodal values of ϕ in the element e_i ,

and ξ_1 , ξ_2 and ξ_3 are the area coordinates of the same element.

Substituting from equation (B-5) in equation (B-3) and then minimizing the functional $I(\phi)$ with respect to the nodal value of ϕ at each of the interior points in the finite element mesh (Figure (1)) then,

$$\begin{aligned} \frac{\partial I(\phi)}{\partial \phi_M} &= \sum_{i=1}^K \iint_{e_i} \left\{ \left(\frac{\partial \phi}{\partial x} \right)_i \frac{b_L}{2\Delta_i} + \left(\frac{\partial \phi}{\partial y} \right)_i \frac{c_L}{2\Delta_i} \right\} dx dy \\ &= 0, \quad M = 1, 4 \end{aligned} \quad (B-6)$$

where K is the number of the elements that have the point M as one of its nodes,

L is the local number of the nodal point M inside the finite element e_i and has the range 1, 2 or 3,

and M is one of the nodal points inside the solution domain.

For example, suppose one considers the nodal point 3 in Figure (B-1). In this case, $M = 3$, $K = 6$ and $L = 3$ for element number 10 and $L = 2$ for element number 11 and so on.

Using equations (B-4) and (B-5) together with equation (B-6) then,

$$\begin{aligned} \frac{\partial I(\phi)}{\partial \phi_M} &= \sum_{i=1}^K \iint_{e_i} \frac{1}{4\Delta_i^2} \left\{ (b_1 \phi_1 + b_2 \phi_2 + b_3 \phi_3)_i \frac{b_L}{2\Delta_i} + (c_1 \phi_1 + c_2 \phi_2 + \right. \\ &\left. c_3 \phi_3)_i \frac{c_L}{2\Delta_i} \right\} dx dy = 0, \quad M = 1, 4 \end{aligned} \quad (B-7)$$

Considering the mesh size in Figure (B-1) to be unity and then applying equation (B-7) to each of the interior nodal points the following equations can be obtained,

$$M = 1 \rightarrow 4\phi_1 - \phi_2 - \phi_4 - \phi_6 - \phi_{16} = 0$$

$$M = 2 \rightarrow -\phi_1 + 4\phi_2 - \phi_3 - \phi_7 - \phi_9 = 0$$

(B-8)

$$M = 3 \rightarrow -\phi_2 + 4\phi_3 - \phi_4 - \phi_{10} - \phi_{12} = 0$$

$$M = 4 \rightarrow -\phi_1 - \phi_3 + 4\phi_4 - \phi_{13} - \phi_{15} = 0$$

The equations (B-8) obtained by the finite element formulation are therefore exactly the same as the difference-equations that arises when using the same mesh size and central finite-differences at the points 1, 2, 3 and 4 respectively. However, it may be noted that the finite element method is not restricted to regular mesh shapes as is the finite-difference method.

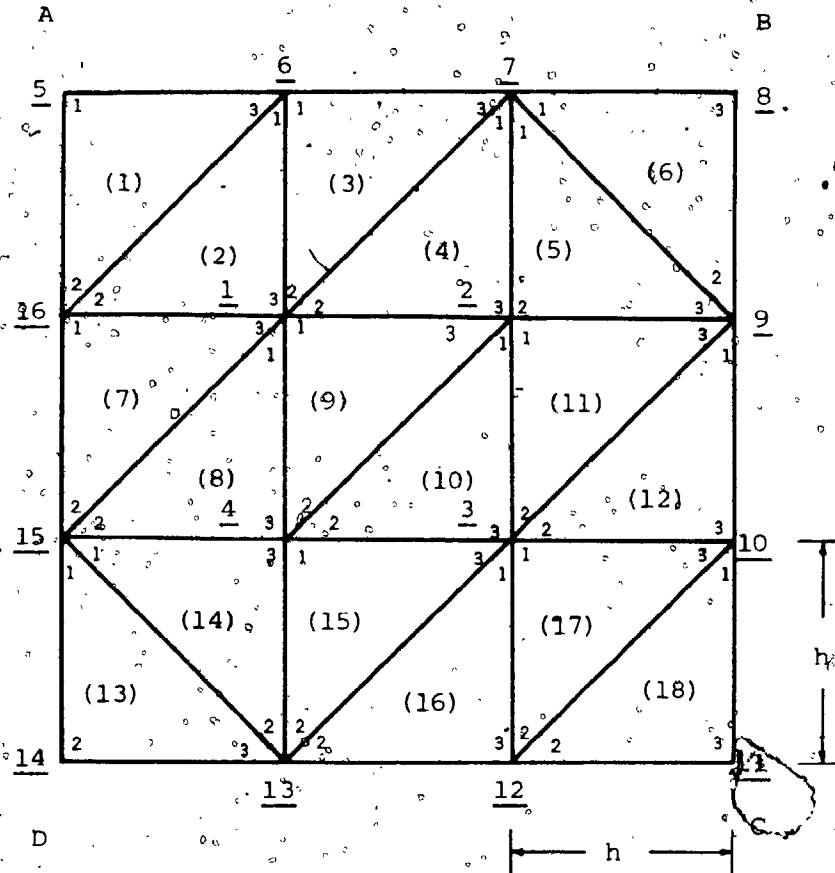


Fig. (B-1) A simple finite element mesh

- Legend - Number in parentheses denote the number of each finite element ($n = 1 \rightarrow N$).
- The underlined numbers denote the global number of each of the nodal points (M).
 - Small numbers denote the local number of the nodal point inside each element (L).

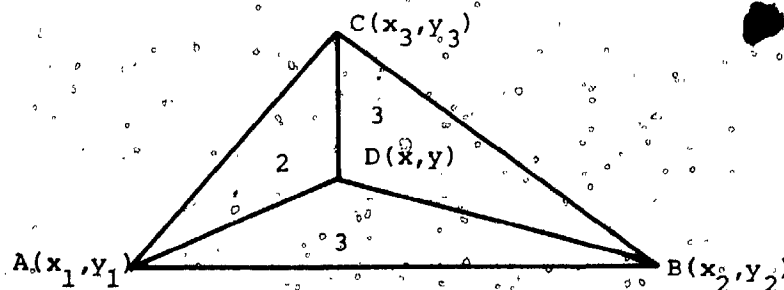


Fig. (B-2) A typical finite element

APPENDIX (C)

AIDS FOR COMPUTATION AND COMPUTER

FLOW CHARTS

In this Appendix some details of computations, together with the computer flow charts for the problems considered in Chapters (5) and (6) are presented.

The first problem considered in Chapter (5) was to obtain the steady state solution for the flow over a flat plate when the oncoming stream was uniform. The solution was obtained by solving the stream function and vorticity equation with the procedure given in Chapter (4). The application of equations (5-9) and (5-16) at each nodal point inside the finite element mesh resulted in one equation for the vorticity and another equation for the stream function. In the derivation of these equations the following expression (see reference (89)) was frequently used to carry out the integration of the area coordinates over each element

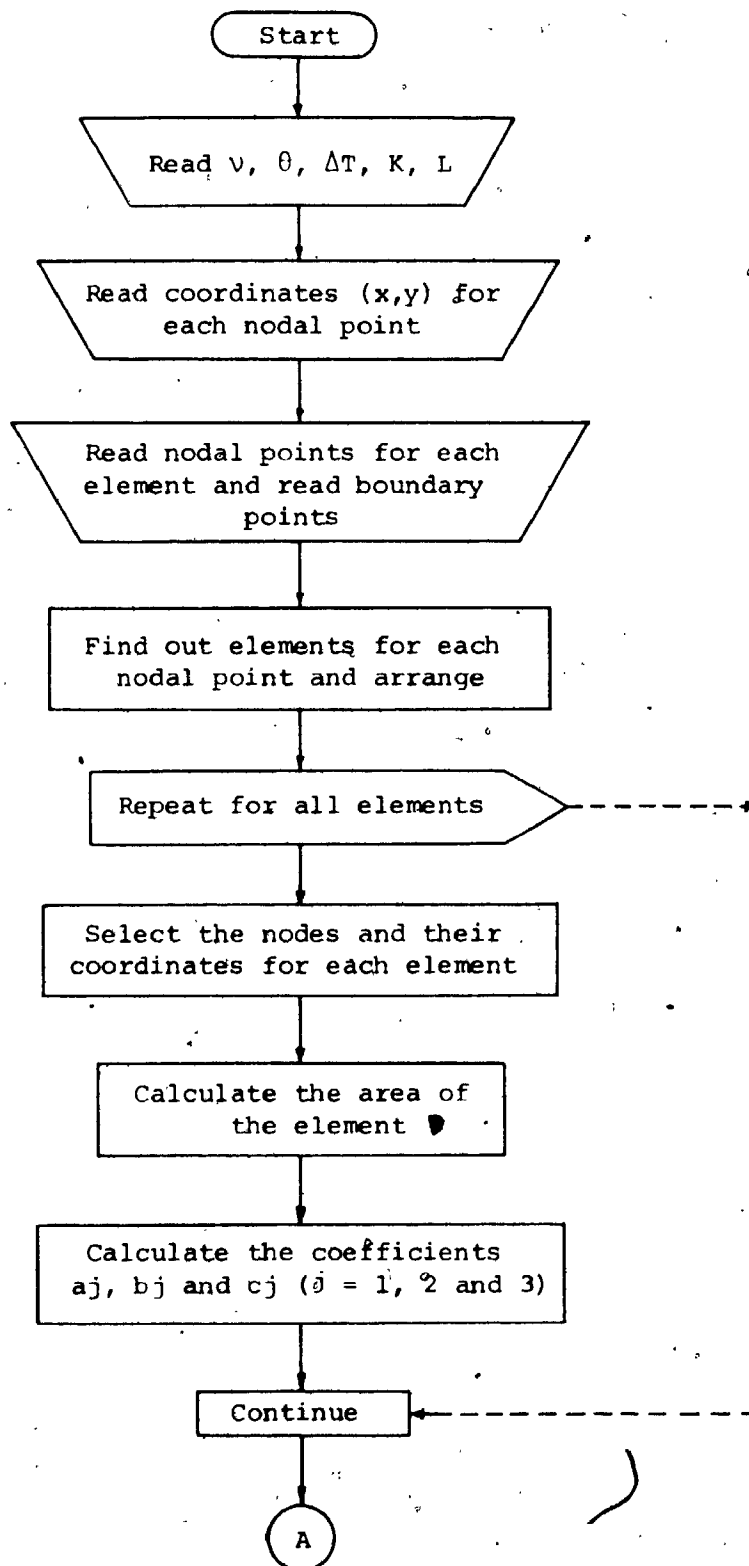
$$\iint_{e_i} \xi_1^p \xi_2^q \xi_3^r dx dy = 2\Delta_i \frac{p! q! r!}{(p+q+r+2)!} \quad (C-1)$$

The equations resulting at each nodal point were assembled in the matrix forms given in equations (5-10) for the vorticity and (5-17) for the stream function. It was found that the location of the coef-

coefficients in the two square coefficient matrices (A) and (E) in equations (5-10) and (5-17) depended on the method used for labeling the nodal points in the finite element mesh. In this problem the nodal points were labeled in such a way that the difference between the number of any two points in one element was minimum, except for the boundary points where the boundary conditions were assumed to be completely specified. By using this method the resulting square matrices (A) and (E) were banded (non zero elements only near the principle diagonal). The actual storage used in the computer for each of these matrices was (257 x 23) instead of (257x257) (i.e. about 8.9% of the computer storage required for the original matrix) since the zero elements away from the band were eliminated. To solve the matrix problems given in equations (5-10) and (5-17) a special routine was written to apply the Crouts' reduction method to the bands stored. This method has the advantage of allowing the resulting augmented matrix to occupy the same space that the original matrix was in (i.e. no more storage was required for the solution). Furthermore by restricting the calculations to the bands of (A) and (E) the time of computation for solving the set of equations was 2% of the original solution time when using the conventional Crouts' method. Since (A) and (E) are independent of the flow variables (u, v, ψ , ζ) the Crouts' reduction method was applied only once and the resulting augmented matrices (A') and (E') were then stored. The overall computation procedure is shown in Figures (C-1), (C-2) and (C-3). Figure (C-1) shows the computer flow chart for the pro-

gram used for arranging data and deducing (A) and (E) and for obtaining (A') and (E'). The computational procedure to obtain the steady state solution is shown in figure (C-2) whereas the procedure to obtain the time dependent solution for the problem considered in Chapter (5) is given in Figure (C-3). The solution procedure for the problem given in Chapter (6) is almost the same as that shown in Figure (C-3) except that the boundary conditions at the upstream and at the two sides of the flow domain were generated at each time step by using the pseudo-turbulence model which was based on the work by Base (2).

Fig. (C-1): Computational procedure for arranging data and
for the assembly of the constant matrices (A)
and (E) of equations (5-10) and (5-17).



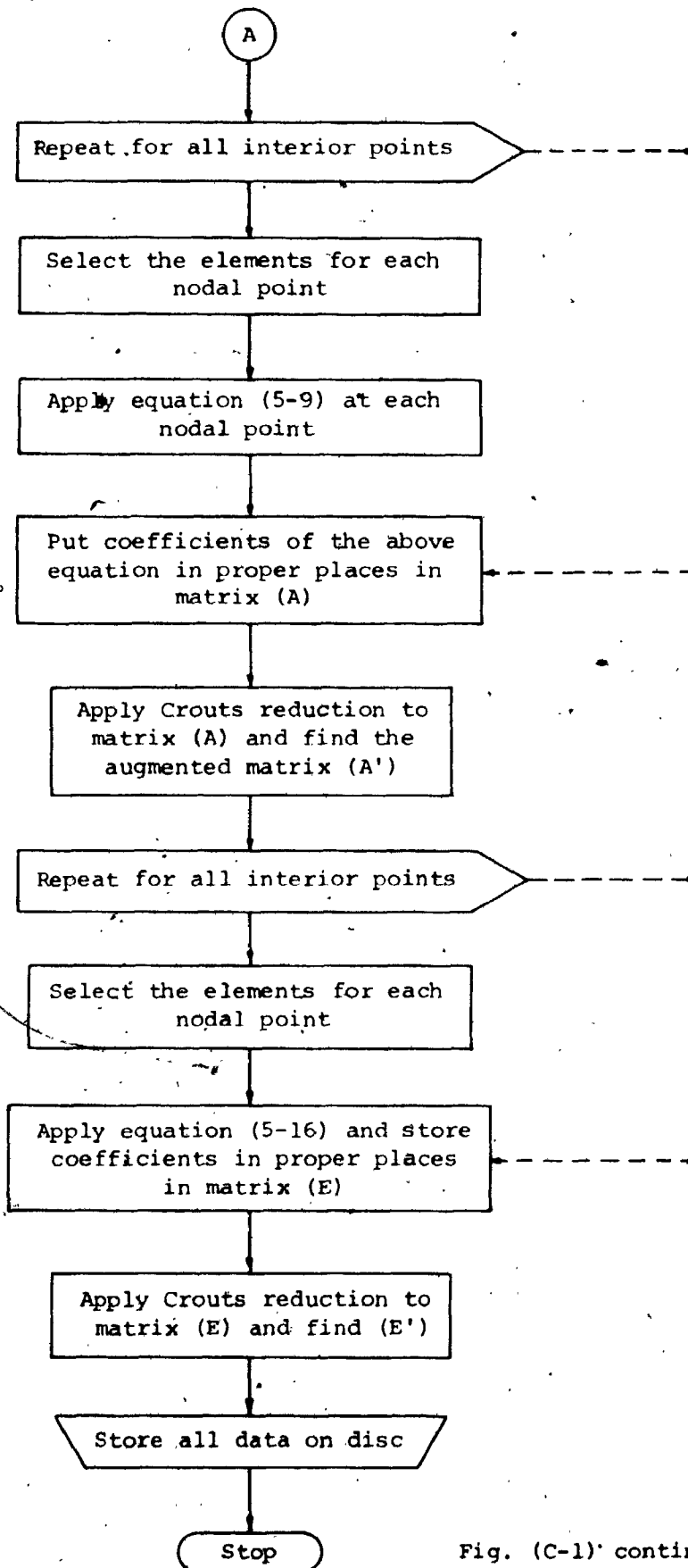
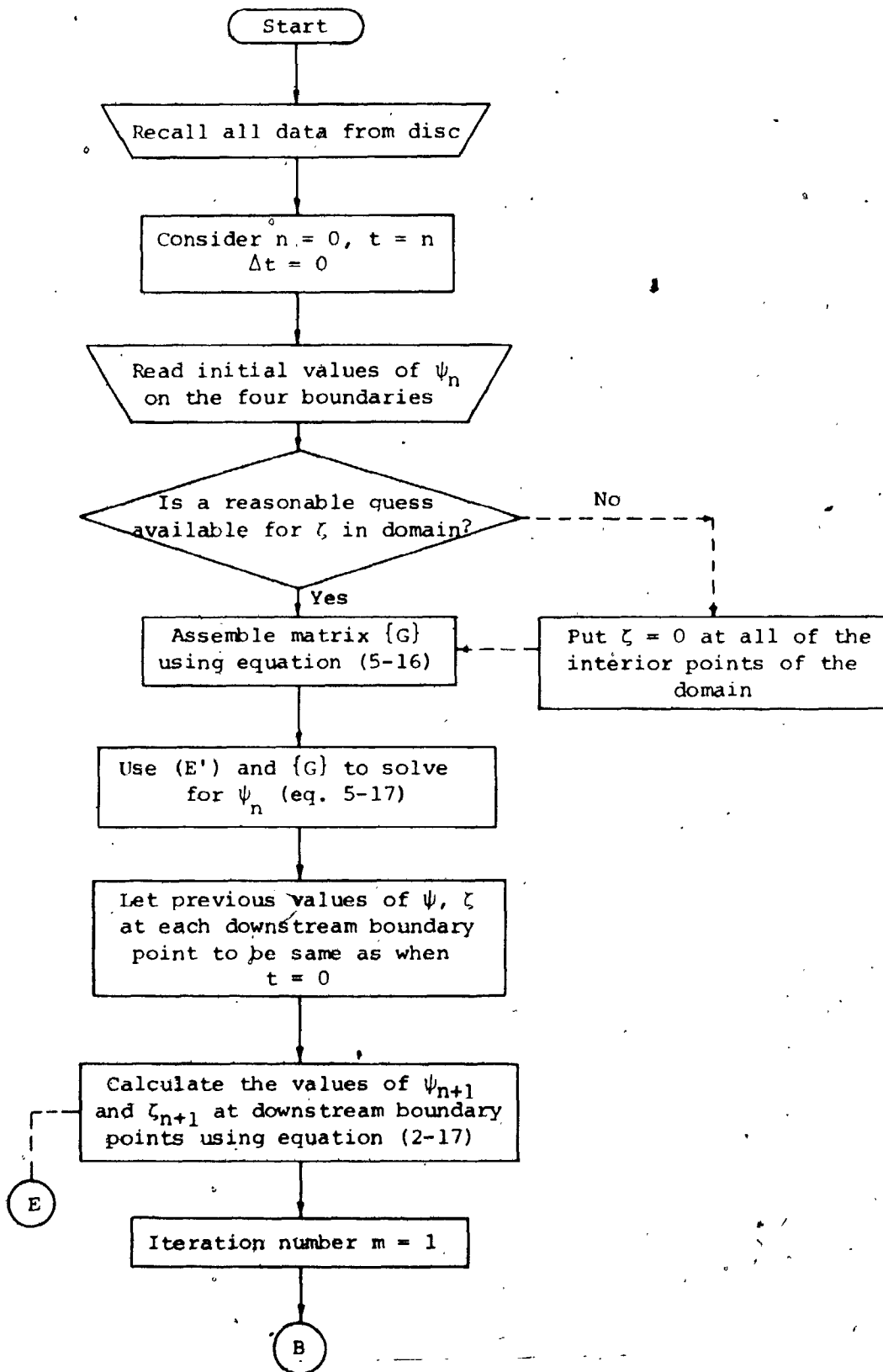


Fig. (C-1) continued

Fig. (C-2): Computational procedure to obtain the steady state pollution for the problem stated in Chapter (5) - the steady flow over a flat plate.



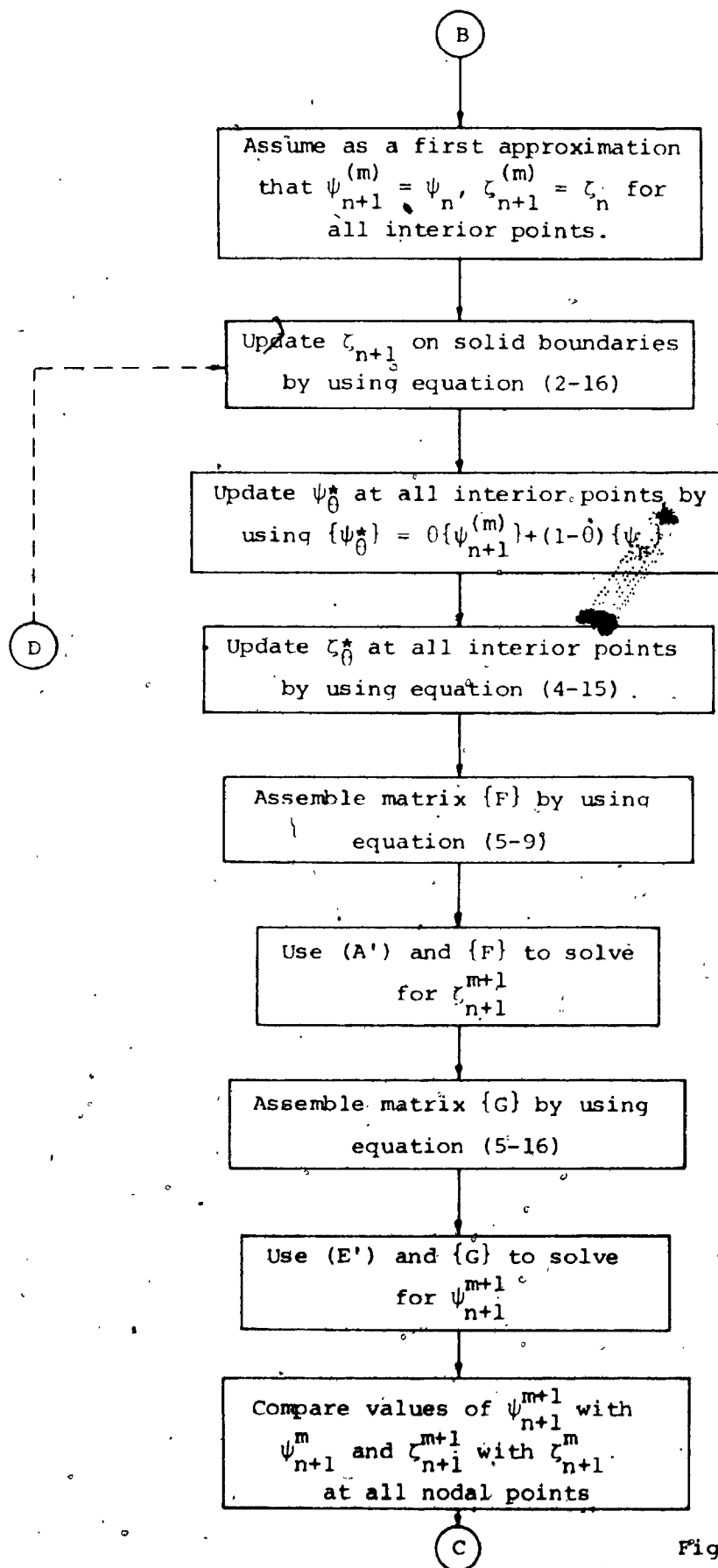


Fig. (C-2) continued

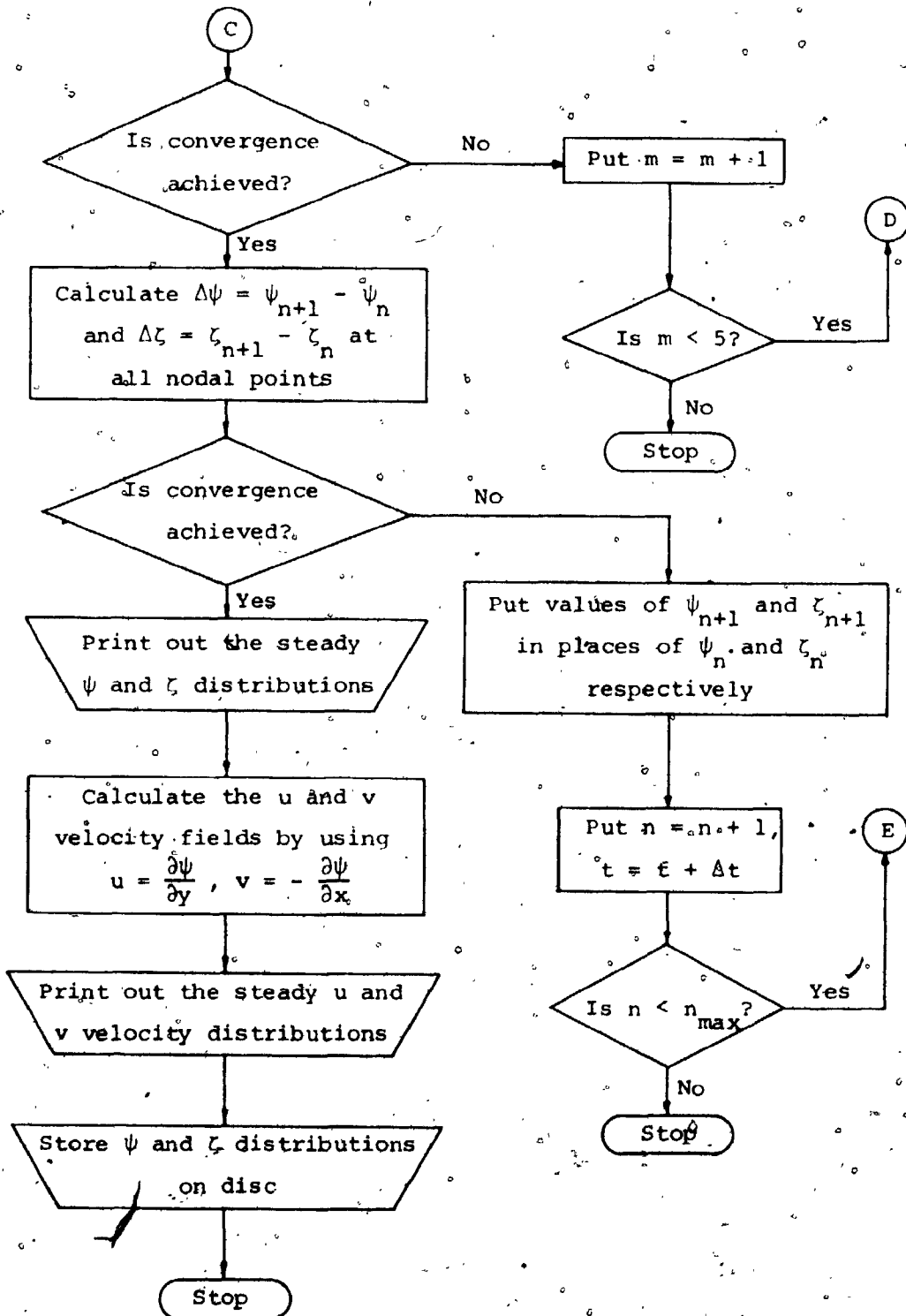


Fig. (C-2) continued

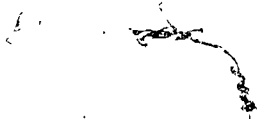
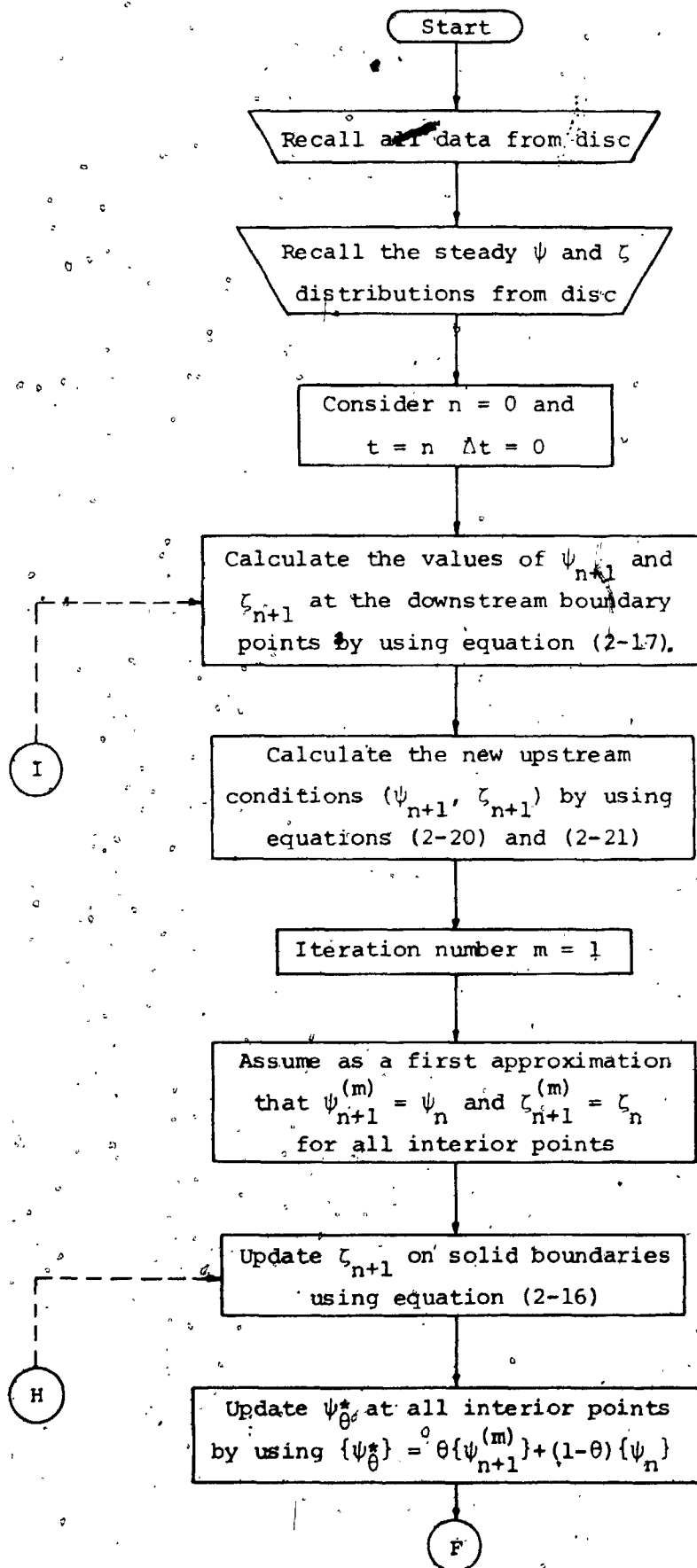


Fig. (C-3): Computational procedure for obtaining the time dependent solution for the problem stated in Chapter (5) - The unsteady flow over a flat plate due to a single rotational disturbance.



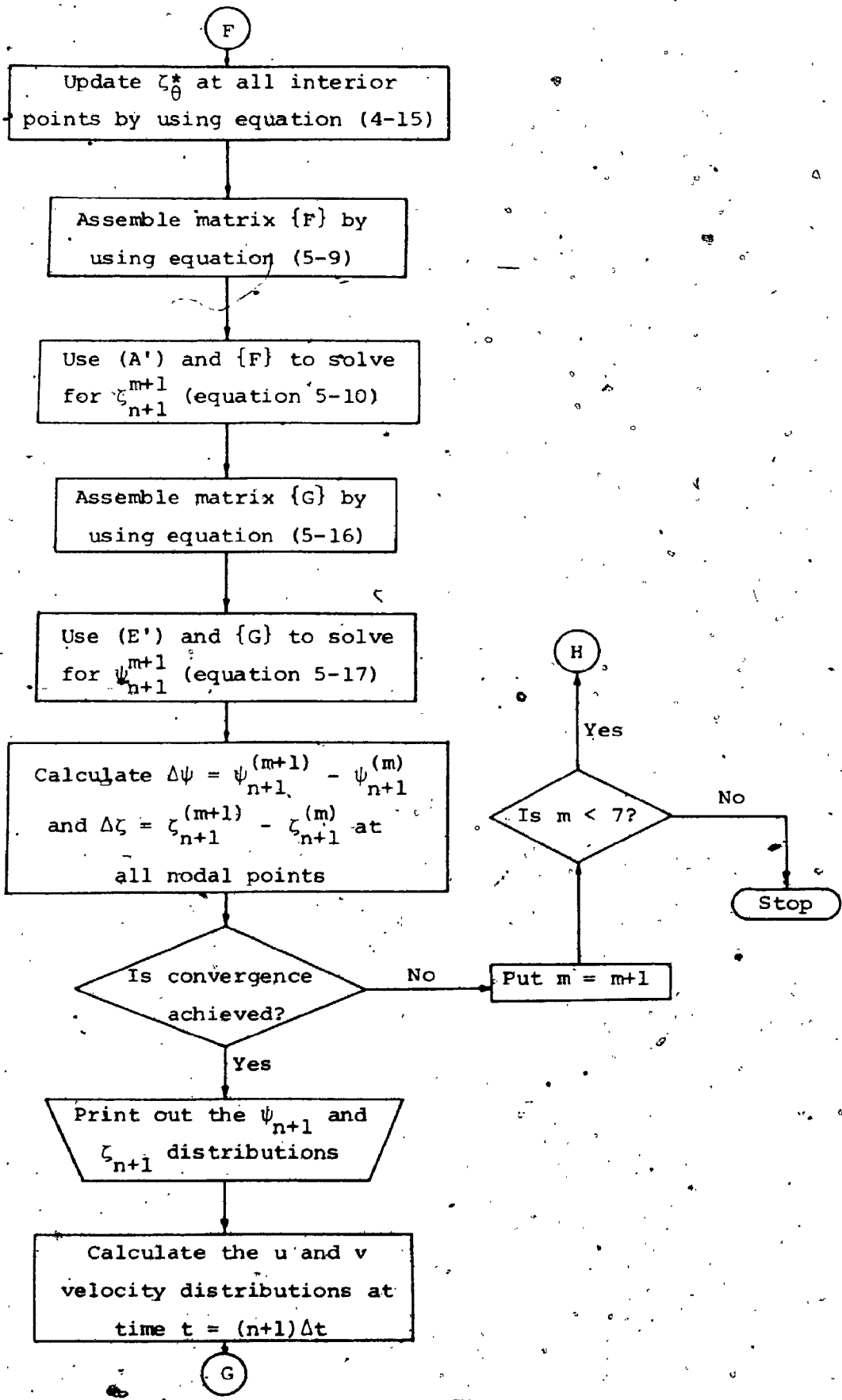


Fig. (C-3) continued

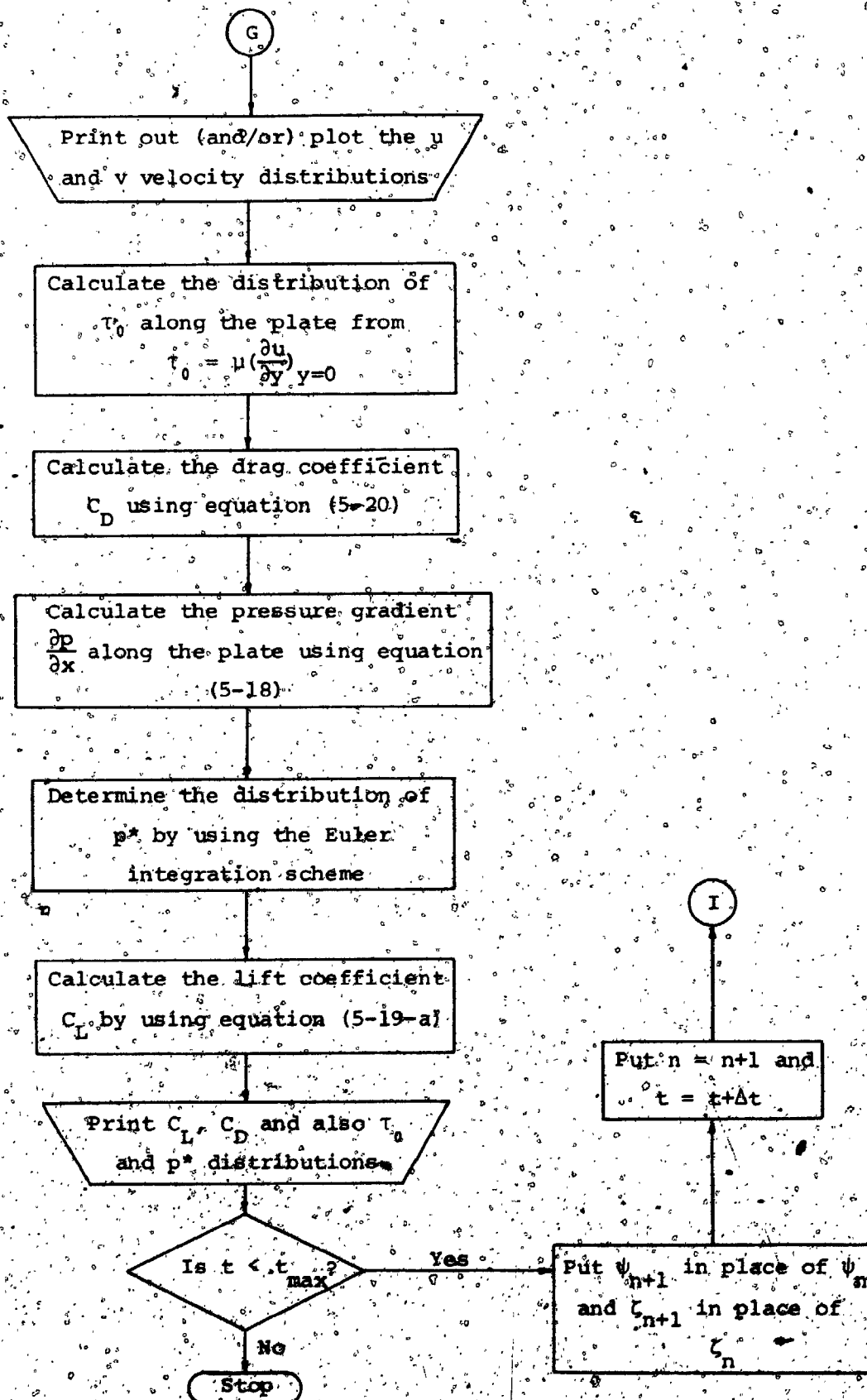


Fig. (C-3) continued

APPENDIX (D)

HOWARTH'S SOLUTION FOR THE RETARDED FLOW OVER A FLAT PLATE

In this Appendix a solution for the laminar flow over a flat plate with a linearly varying free stream velocity is discussed and was used for comparison with the finite element solution introduced in Chapter (5).

Howarth (55) investigated the laminar boundary layer over a body with a sharp leading edge for the case when the velocity distribution at the edge of the boundary layer had the particular form;

$$U = b_0 - b_1 x \quad (D-1)$$

where b_0 and b_1 are constants.

Using this assumption the steady laminar boundary layer equations were then written as;

$$u \frac{\partial u}{\partial x} + v \frac{\partial u}{\partial y} = - \frac{1}{\rho} \frac{\partial p}{\partial x} + \nu \frac{\partial^2 u}{\partial y^2} \quad (D-2)$$

where

$$- \frac{1}{\rho} \frac{\partial p}{\partial x} = - b_1 (b_0 - b_1 x) \quad (D-3)$$

To solve equations (D-2) and (D-3) Howarth assumed the

stream function ψ to have the form,

$$\psi = (b_0 xv)^{1/2} \{ f_0(\eta) - (8x^*) f_1(\eta) + (8x^*)^2 f_2(\eta) - (8x^*)^3 f_3(\eta) + \dots \} \quad (D-4)$$

where $\eta = \frac{b_0}{xy} \left(\frac{0}{xv}\right)^{1/2}$, $x^* = \frac{b_0 x}{b_0}$, $u = \frac{\partial \psi}{\partial y}$ and $v_x = -\frac{\partial \psi}{\partial x}$

Substituting this form in the boundary layer equation (D-2) and equating coefficients of various powers of x^* , it was found that

$$f_0''' + f_0 f_0'' = 0 \quad (D-5-1)$$

$$f_1''' + f_0 f_1'' - 2f_1' f_0'' + 3f_1'' f_0' = -1 \quad (D-5-2)$$

$$f_2''' + f_0 f_2'' - 4f_1' f_1'' + 5f_2'' f_0' = -\frac{1}{8} + (2f_1'^2 + 3f_1 f_1'') \quad (D-5-3)$$

$$f_3''' + f_0 f_3'' - 6f_1' f_2'' + 7f_2'' f_0' = 6f_1' f_1'' - 3f_1 f_1'' - 5f_2'' f_0' \quad (D-5-4)$$

$$f_4''' + f_0 f_4'' - 16f_1' f_3'' + 17f_3'' f_0' = (16f_1' f_1'' - 3f_1 f_1'' - 15f_2'' f_0') +$$

$$(16f_1' f_2'' - 5f_2 f_2'' - 13f_2'' f_0') + (16f_1' f_1'' - 7f_1 f_1'' - 11f_2'' f_0') +$$

$$(8f_1'^2 - 9f_1 f_1'') \quad (D-5-9)$$

where the dashes denote differentiations with respect to η and the boundary conditions were,

$$f_r = f'_r = 0 \quad \text{when } \eta = 0 \text{ for all values of } r, \quad (D-6)$$

$$f'_0 = 2, \quad f'_1 = \frac{1}{4}, \quad f''_2 = f'_3 = f'_4 = \dots = 0 \quad \text{when } \eta = \infty$$

The following results were obtained from the solution of equations (D-5),

$$\begin{array}{lll} f''_0(0) = 1.328242 & f''_1(0) = 1.02054 & f''_2(0) = -0.06926 \\ f''_3(0) = 0.0560 & f''_4(0) = -0.0372 & f''_5(0) = 0.0272 \\ f''_6(0) = -0.0212 & f''_7(0) = 0.0174 & f''_8(0) = -0.0147 \end{array}$$

The velocity distribution in the boundary layer could be obtained from the expression,

$$\begin{aligned} u &= \frac{\partial \psi}{\partial y} = \frac{\partial \psi}{\partial \eta} \frac{\partial \eta}{\partial y} \\ &= \frac{b_0}{x} \{ f'_0(\eta) - (8x^*) f'_1(\eta) + (8x^*)^2 f'_2(\eta) - \dots \} \quad (D-7) \end{aligned}$$

and the local skin friction coefficient C_f was calculated from,

$$\begin{aligned} C_f &= \frac{\tau_0}{\frac{1}{2} \rho U_\infty^2} = \mu \left(\frac{\partial u}{\partial y} \right)_0 / \frac{1}{2} \rho U_\infty^2 \\ &= \frac{b_0}{2U_\infty^2} \left(\frac{v_b}{x} \right) \{ f''_0(0) - (8x^*) f''_1(0) + (8x^*)^2 f''_2(0) - \dots \} \quad (D-8) \end{aligned}$$

The velocity distribution at the edge of the boundary layer over the flat plate in the problem considered in Chapter (5) could be approximated as,

$$U = b_0 - b_1 x$$

where $b_0 = 4.465$ and $b_1 = -0.12727$

Substituting the above values of b_0 and b_1 in equation (D-8) and using the obtained results of $f''(0)$, $f''(0)$, ..., $f''(0)$; the values given below in Table (D-1) were obtained for the variation of the local skin friction coefficient with dimensionless distance from the leading edge.

x/c	C_f
0.125	0.11318
0.250	0.08174
0.375	0.06812
0.500	0.06020
0.625	0.05491
0.750	0.05110
0.875	0.04821
1.000	0.04593
1.125	0.04409
1.250	0.04258
1.375	0.04131

Table (D-1)

Table (D-1) Variation of local skin friction coefficient with distance from the leading edge of the flat plate (based on Howarth's solution)

REFERENCES

1. Lilly, D.K., "Numerical Simulation of Two-Dimensional Turbulence", High Speed Computing in Fluid Dynamics, The Physics of Fluids Supplement II, Vol. 12, No. 12, pp. 240-249 (1969).
2. Base, T.E., "Mathematical Studies of Vortex Model to Represent Unsteady Fluid Flow", Ph.D. Thesis, I.S.V.R., The University of Southampton, England, 1970.
3. Ahmadi, G. and Goldschmidt, V.W., "Creation of a Pseudo-Turbulent Velocity Field", Developments in Mechanics, Vol. 6, Proc. of the 12th Midwestern Conf., pp. 291-304.
4. Lighthill, M.J., "The Response of Laminar Skin Friction and Heat Transfer to Fluctuations in the Stream Velocity", Royal Society of London Proceedings, Series A, Vol. 224 (1954), pp. 1-23.
5. Glauert, M.B., "The Laminar Boundary Layer on Oscillating Plates and Cylinders", Journal of Fluid Mechanics, Vol. 1, 1956, pp. 97-110.
6. Ting, L., "Boundary Layer Over a Flat Plate in Presence of Shear Flow", The Physics of Fluids, Vol. 3, No. 1 (1960), pp. 78-81.
7. Mark, R.M., "On Shear Flow Past Flat Plates", Journal of Fluid Mechanics, Vol. 14 (1962), pp. 452-462.
8. Glauert, M.B., "The Pressure Gradient Induced by Shear Flow Past a Flat Plate", Journal of the Aerospace Sciences, Vol. 29 (1962), pp. 540-542.
9. Smith, M.C. and Kuethe, A.M., "Effect of Turbulence on Laminar Skin Friction and Heat Transfer", The Physics of Fluids, Vol. 9, No. 12 (1966), pp. 2337-2344.
10. Kestin, J., "The Effect of Freestream Turbulence on Heat Rates", Advances in Heat Transfer, Vol. 3, Academic Press, New York, 1966, pp. 1-32.

11. Erens, P.J. and Chasteau, V.A.L., "Laminar Boundary Layer Response to Freestream Disturbances", A.I.A.A. Journal, Vol. 12, No. 1, January 1974, pp. 93-94.
12. Thom, A., 1928 ARC R&M No. 1194.
13. Prandtl, L., "Zur Berechnung der Grenzschichten", Zeitschrift fuer Angewandte Mathematik und Mechanik, Vol. 18, 1938, pp. 77-82; translated as "Note on the Calculation of Boundary Layers", TM, 959, NACA.
14. Rosenhead, L., Laminar Boundary Layers, Clarendon Press, Oxford, 1963.
15. Blottner, F.C., "Finite Difference Methods of Solution of the Boundary-Layer Equations", A.I.A.A. Journal, Vol. 8, No. 2 (1970), pp. 193-205.
16. Roache, P.J., Computational Fluid Dynamics, Hermosa Publishers, New Mexico, 1976.
17. Fromm, J.E. and Harlow, F.H., "Numerical Solution of the Problem of Vortex Street Development", The Physics of Fluids, Vol. 6, No. 7, 1963, pp. 975-982.
18. Fromm, J.E., "A Method for Computing Non-Steady Incompressible Viscous Fluid Flow", Los Alamos Scientific Lab., Report No. LA-2910, 1963, Los Alamos, New Mexico.
19. Donovan, L.F., "A Numerical Solution of Unsteady Flow in a Two-Dimensional Square Cavity", A.I.A.A. Journal, Vol. 8, No. 3, 1970, pp. 524-529.
20. Mills, R.D., "Numerical Solution of the Viscous Flow Equations for a Class of Closed Flows", Journal of the Royal Aeronautical Society, Vol. 69, No. 658, 1965, pp. 714-718.
21. Pan, F. and Acrivos, A., "Steady Flows in Rectangular Cavities", Journal of Fluid Mechanics, Vol. 28, Pt. 4, 1967, pp. 643-655.
22. Chien, J.C., "A General Finite-Difference Formulation with Application to Navier-Stokes Equations", Journal of Computational Physics, Vol. 20, 1975, pp. 268-278.

23. Thoman, D.C. and Szweczyk, A.A., "Time-Dependent Viscous Flow Over a Circular Cylinder", High-Speed Computing in Fluid Dynamics, The Physics of Fluids Supplement II (1969), pp. 76-86.
24. Son, J.S. and Hanratty, T.J., "Numerical Solution for the Flow Around a Cylinder at Reynolds Numbers of 40,200 and 500", Journal of Fluid Mechanics, Vol. 35, Part 2, 1969, pp. 369-386.
25. Dennis, S.C.R. and Staniforth, A.N., "A Numerical Method for Calculating the Initial Flow Past a Cylinder in a Viscous Fluid", Proceeding of the Second International Conference on Numerical Methods in Fluid Dynamics, University of California, Berkeley, September 15-19, 1970, pp. 343-349.
26. Jain, P.C. and Rao, K.S., "Numerical Solution of Unsteady Viscous Incompressible Fluid Flow Past a Circular Cylinder", High-Speed Computing in Fluid Dynamics, The Physics of Fluids Supplement II (1969), pp. 57-64.
27. Wilkes, J.O. and Churchill, S.W., "The Finite-Difference Computation of Natural Convection in a Rectangular Enclosure", A.I.Ch.E. Journal, Vol. 12, No. 1, 1966, pp. 161-166.
28. Rubel, A. and Landis, F., "Numerical Study of Natural Convection in a Vertical Rectangular Enclosure", High-Speed Computing in Fluid Dynamics, The Physics of Fluids Supplement II (1969), pp. 208-213.
29. Phillips, J.H. and Ackerberg, R.C., "A Numerical Method for Integrating the Unsteady Boundary-Layer Equations When There Are Regions of Back Flow", Journal of Fluid Mechanics, Vol. 58, Pt. 3, 1973, pp. 561-579.
30. Cebeci, T. and Smith, A.M.O., "A Finite-Difference Method for Calculating Compressible Laminar and Turbulent Boundary Layers", Trans. A.S.M.E. Journal of Basic Engineering, Vol. 92, 1970, pp. 523-535.
31. Cebeci, T., Smith, A.M.O. and Mosinskis, G., "Calculation of Adiabatic Turbulent Boundary Layers", A.I.A.A. Journal, Vol. 8, No. 11 (1970), pp. 1974-1982.

32. Blottner, F.G., "Variable Grid Scheme Applied to Turbulent Boundary Layers", *Computer Methods in Applied Mechanics and Engineering*, Vol. 4, 1974, pp. 179-194.
33. de Rivas, E.K., "On the Use of Nonuniform Grids in Finite-Difference Equations", *Journal of Computational Physics*, Vol. 10, 1972, pp. 202-210.
34. Hirsh, R.S., "Higher Order Accurate Difference Solutions of Fluid Mechanics Problems by a Compact Differencing Technique", *Journal of Computational Physics*, Vol. 19, 1975, pp. 90-109.
35. Dwyer, H.A. and McCroskey, W.J., "Computational Problems in Three and Four-Dimensional Boundary Layer Theory", *Proceeding of the 3rd International Conference on Numerical Methods in Fluid Dynamics*, July 1972, pp. 138-145.
36. Singleton, R.E. and Nash, J.F., "Methods for Calculating Unsteady Turbulent Boundary Layers in Two and Three-Dimensional Flows", *A.I.A.A. Journal*, Vol. 12, No. 5 (1974), pp. 590-595.
37. Cooper, P. and Reshotko, E., "Turbulent Flow Between a Rotating Disk and a Parallel Wall", *A.I.A.A. Journal*, Vol. 13, No. 5 (1975), pp. 573-578.
38. Cebeci, T., "Calculation of Three-Dimensional Boundary Layers. II. Three-Dimensional Flow in Cartesian Coordinates", *A.I.A.A. Journal*, Vol. 13, No. 8 (1975), pp. 1056-1064.
39. Smith, G.D., Numerical Solution of Partial Differential Equations, Oxford University Press, London, 1969.
40. Plotkin, A. and Flugge-Lotz, I., "A Numerical Solution for the Laminar Wake Behind a Finite Flat Plate", *Journal of Applied Mechanics*, Trans. A.S.M.E., Vol. 90, 1968, pp. 625-630.
41. Cheng, R.T., "Numerical Solution of the Navier-Stokes Equations by the Finite Element Method", *The Physics of Fluids*, Vol. 15, No. 12, 1972, pp. 2098-2105.

42. Smith, S.L. and Brebbia, C.A., "Finite Element Solution of Navier-Stokes Equations for Transient Two-Dimensional Incompressible Flow", *Journal of Computational Physics*, Vol. 17, 1975, pp. 235-245.
43. Pao, Y.H. and Daugherty, R.J., "Time-Dependent Viscous Incompressible Flow Past a Finite Flat Plate", Boeing Scientific Research Laboratories, D1-82-0822, January 1969.
44. Kawaguti, M., "Numerical Solutions of the Navier-Stokes Equations for the Flow in a Channel with a Step", MRC TSR 574, Mathematics Research Center, Madison, Wisconsin, 1965.
45. Thoman, D. and Szewczyk, A.A., "Numerical Solutions of Time Dependent Two-Dimensional Flow of a Viscous, Incompressible Fluid Over Stationary and Rotating Cylinders", Tech. Rept. 66-14, Heat Transfer and Fluid Mech. Lab., Dept. of Mech. Eng., University of Notre Dame, Notre Dame, Indiana, 1966.
46. Kinney, R.B. and Paolino, M.A., "Flow Transient Near the Leading Edge of a Flat Plate Moving Through a Viscous Fluid", *Trans. A.S.M.E. Journal of Applied Mechanics*, Vol. 41, Series E, No. 4, December 1974.
47. Allen, D.N. and Southwell, R.V., "Relaxation Methods Applied to Determine the Motion in Two Dimensions, of a Viscous Fluid Past a Fixed Cylinder", *Quarterly J. of Mech. and Appl. Math.*, Vol. 8, pp. 129-145, 1955.
48. Michael, P., "Steady Motion of a Disk in a Viscous Fluid", *The Physics of Fluids*, Vol. 9, No. 3, pp. 466-471, 1966.
49. Katsanis, T., "A Computer Program for Calculating Velocities and Streamlines for Two-Dimensional Incompressible Flow in Axial Blade Rows", NASA TN D-3762, January 1967.
50. Friedman, M., "Flow in a Circular Pipe with Recessed Walls", *Journal of Applied Mechanics*, Vol. 37, No. 1, 1970, pp. 5-8.
51. Lee, J.S. and Fung, U.C., "Flow in Locally Constricted Tubes at Low Reynolds Numbers", *Journal of Applied Mechanics*, Vol. 37, No. 1, pp. 9-17 (1970).

52. Paris, J. and Whitaker, S., "Confined Wakes; A Numerical Solution of the Navier-Stokes Equations", A.I.Ch.E. Journal, Vol. 11, No. 6, pp. 1033-1041 (1965).
53. Hall, M.G., "The Boundary Over an Impulsively Started Flat Plate", Proc. Roy. Soc. of London, Series A, Vol. 310, 1969, pp. 401-414.
54. Schlichting, H., Boundary Layer Theory, McGraw-Hill, New York, 1968.
55. Howarth, L., "On the Solution of the Laminar Boundary Equations", Proc. Roy. Soc. of London, Series A, Vol. 164, 1937, pp. 547-579.
56. de Vries, G. and Norrie, D.H., "The Application of the Finite-Element Technique to Potential Flow Problems", Trans. A.S.M.E., Series E, Journal of Applied Mechanics, Vol. 38, 1971, pp. 798-802.
57. Vooren, J.V. and Labrujere, T.E., "Finite Element Solution of the Incompressible Flow Over an Airfoil in a Non-uniform Stream", Proc. of the Int. Conf. for Numerical Methods in Fluid Dynamics held at the University of Southampton, England, September 26-28, 1973.
58. Doctors, L.J., "An Application of the Finite Element Technique to Boundary Value Problems of Potential Flow", International Journal for Numerical Methods in Engineering, Vol. 2, pp. 243-252 (1970).
59. Atkinson, B., Brocklebank, M., Card, C. and Smith, J., "Low Reynolds Number Developing Flows", A.I.Ch.E. Journal, Vol. 15, No. 4, 1969, pp. 548-553.
60. Atkinson, B., Card, C. and Irons, B., "Application of the Finite Element Method to Creeping Flow Problems", Trans. Inst. Chem. Engrs., Vol. 48, 1970, pp. T276-T284.
61. Thompson, E.G. and Hauque, M.I., "A High Order Finite Element for Completely Incompressible Creeping Flow", Int. Journal for Numerical Methods in Engg., Vol. 6, pp. 315-321, 1973.

62. Yamada, Y., Ito, K., Yokouchi, Y., Tamano, T. and Ohtsubo, T., "Finite Element Analysis of Steady Fluid and Metal Flow", Finite Element Methods in Flow Problems, edited by Oden et al., UAH press, Huntsville, Alabama, 1974, pp. 465-469.
63. Lyness, J.F., Owen, D. and Zienkiewicz, O.C., "Finite Element Analysis of the Steady Flow of Non-Newtonian Fluids Through Parallel Sided Conduits", Finite Element Methods in Flow Problems, edited by Oden et al., UAH press, Huntsville, Alabama, 1974, pp. 489-503.
64. Zienkiewicz, O.C. and Godbole, A.N., "Viscous, Incompressible Flow with Special Reference to Non-Newtonian (Plastic) Fluids", Finite Element Methods in Flow Problems, edited by Oden et al., UAH press, Huntsville, Alabama, 1974, pp. 461-464.
65. Crocco, L., "A Suggestion for the Numerical Solution of the Steady Navier-Stokes Equations", A.I.A.A. Journal, Vol. 3, No. 10, 1965, pp. 1824-1832.
66. Olson, M.D., "Variational-Finite Element Methods for Two-Dimensional and Axisymmetric Navier-Stokes Equations", Finite Element Methods in Flow Problems, edited by Oden et al., UAH press, Huntsville, Alabama, 1974, pp. 103-106.
67. Tong, P., "On the Solution of the Navier-Stokes Equations in Two-Dimensional and Axial Symmetric Problems", Finite Element Methods in Flow Problems, edited by Oden et al., UAH press, Huntsville, Alabama, 1974, pp. 57-66.
68. Gartling, D.K. and Becker, E.B., "Finite Element Analysis of Viscous Incompressible Fluid Flow", Computer Methods in Applied Mech. and Engg., Vol. 8, 1976, pp. 51-60.
69. Kawahara, M., Yoshimura, N. and Nakagawa, K., "Analysis of Steady Incompressible Viscous Flow", Finite Element Methods in Flow Problems, edited by Oden et al., UAH press, Huntsville, Alabama, 1974, pp. 107-120.
70. Guymon, G.L., "Finite Element Solution for General Fluid Motion", J. Hydr. Div., A.S.C.E., Vol. 99, 1972, pp. 913-919.
71. Baker, A.J., "Finite Element Solution Algorithm for Viscous Incompressible Fluid Dynamics", Int. J. for Numerical Methods in Engg., Vol. 6, pp. 89-101 (1973).

72. Baker, A.J., "Finite Element Solution Algorithm for Incompressible Fluid Dynamics", Finite Element Methods in Flow Problems, edited by Oden et al., UAH press, Huntsville, Alabama, 1974, pp. 51-56.
73. Bilgen, E. and Too, J.J., "On the Finite Element Formulation of Navier-Stokes Equations", Trans. C.S.M.E., Vol. 2, No. 4, 1973, pp. 205-208.
74. Hood, P. and Taylor, C., "Navier-Stokes Equations Using Mixed Interpolation", Finite Element Methods in Flow Problems, edited by Oden et al., UAH press, Huntsville, Alabama, 1974, pp. 121-132.
75. Taylor, C. and Hood, P., "A Numerical Solution of the Navier-Stokes Equations Using the Finite Element Technique", Computers and Fluids, Vol. 1, 1973, pp. 73-100.
76. Bratanow, T., Ecer, A. and Kobiske, M., "Finite Element Analysis of Unsteady Incompressible Flow Around Oscillating Obstacle of Arbitrary Shape", A.I.A.A. Journal, Vol. 11, No. 11, 1973, pp. 1471-1477.
77. Bratanow, T., Ecer, A. and Kobiske, M., "Numerical Calculations of Velocity and Pressure Distribution Around Oscillating Aerofoils", NASA CR-2368, February 1974.
78. Kobiske, M.H., "An Application of the Finite Element Method in Determining Pressure Distributions Around Pitching and Plunging Rotor Blade Airfoils", M.Sc. Thesis, University of Wisconsin, Milwaukee, January 1973.
79. Bratanow, T. and Ecer, A., "Analysis of Three-Dimensional Unsteady Viscous Flow Around Oscillating Wings", A.I.A.A. Journal, Vol. 12, No. 11, 1974, pp. 1577-1584.
80. Bratanow, T. and Ecer, A., "On the Application of the Finite Element Method in Unsteady Aerodynamics", A.I.A.A. Journal, Vol. 12, No. 4, 1974, pp. 503-510.
81. Kawahara, M., Yoshimura, N., Nakagawa, K. and Ohsaka, H., "Steady and Unsteady Finite Element Analysis of Incompressible Viscous Fluid", Int. J. for Numerical Methods in Engg., Vol. 10, pp. 437-456 (1976).

82. Ikenouchi, M. and Kimura, N., "An Approximate Numerical Solution of the Navier-Stokes Equations by Galerkin Method", Finite Element Methods in Flow Problems, edited by Oden et al., UAH press, Huntsville, Alabama, 1974, pp. 99-100.
83. Aral, M.M., "Application of the Finite Element Analysis in Fluid Mechanics", Ph.D. Thesis, Georgia Institute of Technology, Atlanta, Ga., September 1971.
84. Lieber, P., Wen, K. and Attia, A., "Finite Element Method as an Aspect of the Principle of Maximum Uniformity: New Hydrodynamical Ramifications", Finite Element Methods in Flow Problems, edited by Oden et al., UAH press, Huntsville, Alabama, 1974, pp. 85-96.
85. Argyris, J.H. and Mareczek, G., "Finite Element Analysis of Slow Incompressible Viscous Fluid Motion", Ingenieur-Archiv., Vol. 43, 1974, pp. 92-109.
86. Tay, A.O. and Davis, G.D., "Application of the Finite Element Method to Convection Heat Transfer Between Parallel Planes", Int. J. Heat and Mass Transfer, Vol. 14, pp. 1057-1069 (1971).
87. Skiba, E., Unny, T.E. and Weaver, D.S., "A Finite Element Solution for a Class of Two-Dimensional Viscous Fluid Dynamics Problems", Computer Aided Engineering, edited by G.M.L. Glaswell, University of Waterloo, Waterloo, Ontario, 1971, pp. 493-507.
88. Zienkiewicz, O.C., The Finite Element Method in Engineering Science, McGraw-Hill, London, 1971.
89. Huebner, K.H., The Finite Element Method for Engineers, John Wiley & Sons, New York, 1975.
90. Dasai, C.S. and Abel, J.F., Introduction to the Finite Element Method, Van Nostrand Reinhold Comp., New York, 1972.
91. Finlayson, B.A., "Existence of Variational Principles for the Navier-Stokes Equations", The Physics of Fluids, Vol. 15, No. 6, 1972, pp. 963-967.

92. Bratanow, T. and Ecer, A., "Analysis of Moving Body Problems in Aerodynamics", Finite Element Methods in Flow Problems, edited by Odén et al., UAH press, Huntsville, Alabama, 1974, pp. 225-241.
93. Base, T.E. and Davies, P.O.A.L., "A Vortex Model to Relate Eulerian and Lagrangian "Turbulent" Velocity Fields", The Canadian Journal of Chemical Engineering, Vol. 52, pp. 11-16, February 1974.

TABLE 1: DETAILS OF VORTEX MODEL PARAMETER

Flow Statistics

Mean Flow Velocity, $u_{\infty} = 4$ cm./sec.

Turbulence Intensity, $\frac{\langle u^2 \rangle^{1/2}}{u_{\infty}} = .357$

Length Scale, $L_{11}(x_1) = 9.85$ mm.

Flatness Factor of u_1 Velocity Component = 3
(Gaussian Distributed).

Vortex Model

Mean Convection Velocity (u_c) = 40 mm./sec.

Model Width (b) = 25 mm.

Model Stage Length (s) = 20 mm.

Number of Vortices per 'box' = 4

Vortex Core Radius (r_c) = 2.8 mm.

Mean Distance Between Vortices (λ) = 11.2 mm.

Vortex Circulation Constant (Γ_1) = 40 mm.²/sec.

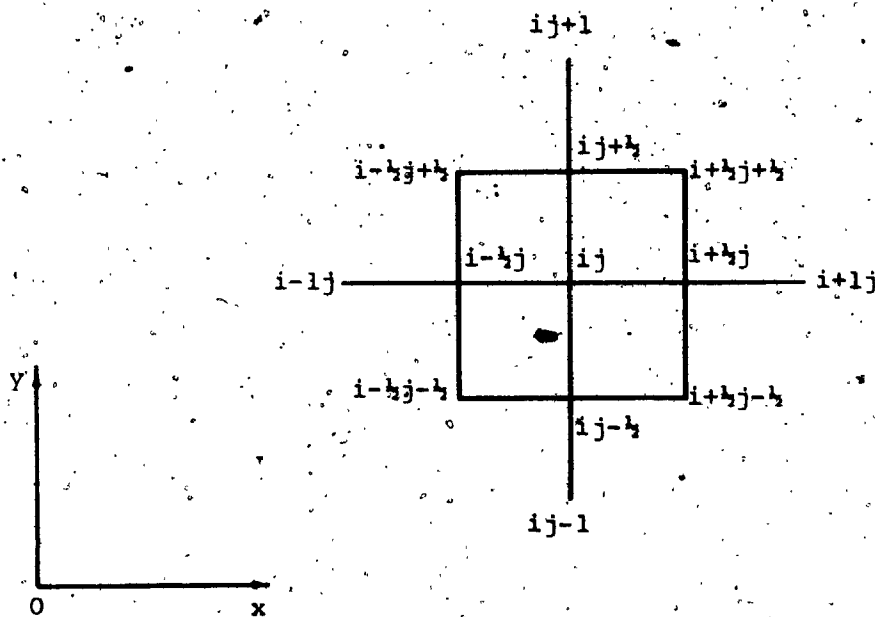


Fig. 1 Finite-difference notations

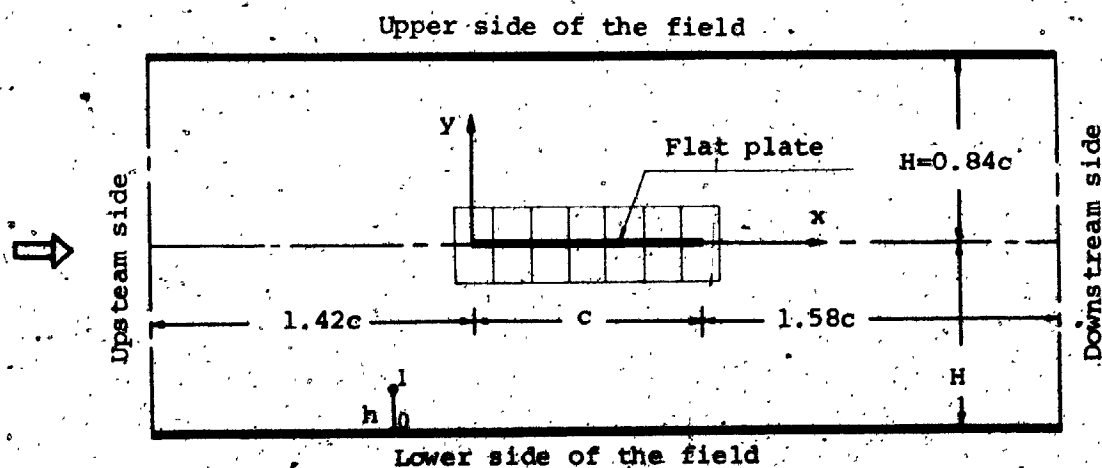


Fig. 2 Schematic diagram showing the flow field with the finite-difference mesh near the flat plate

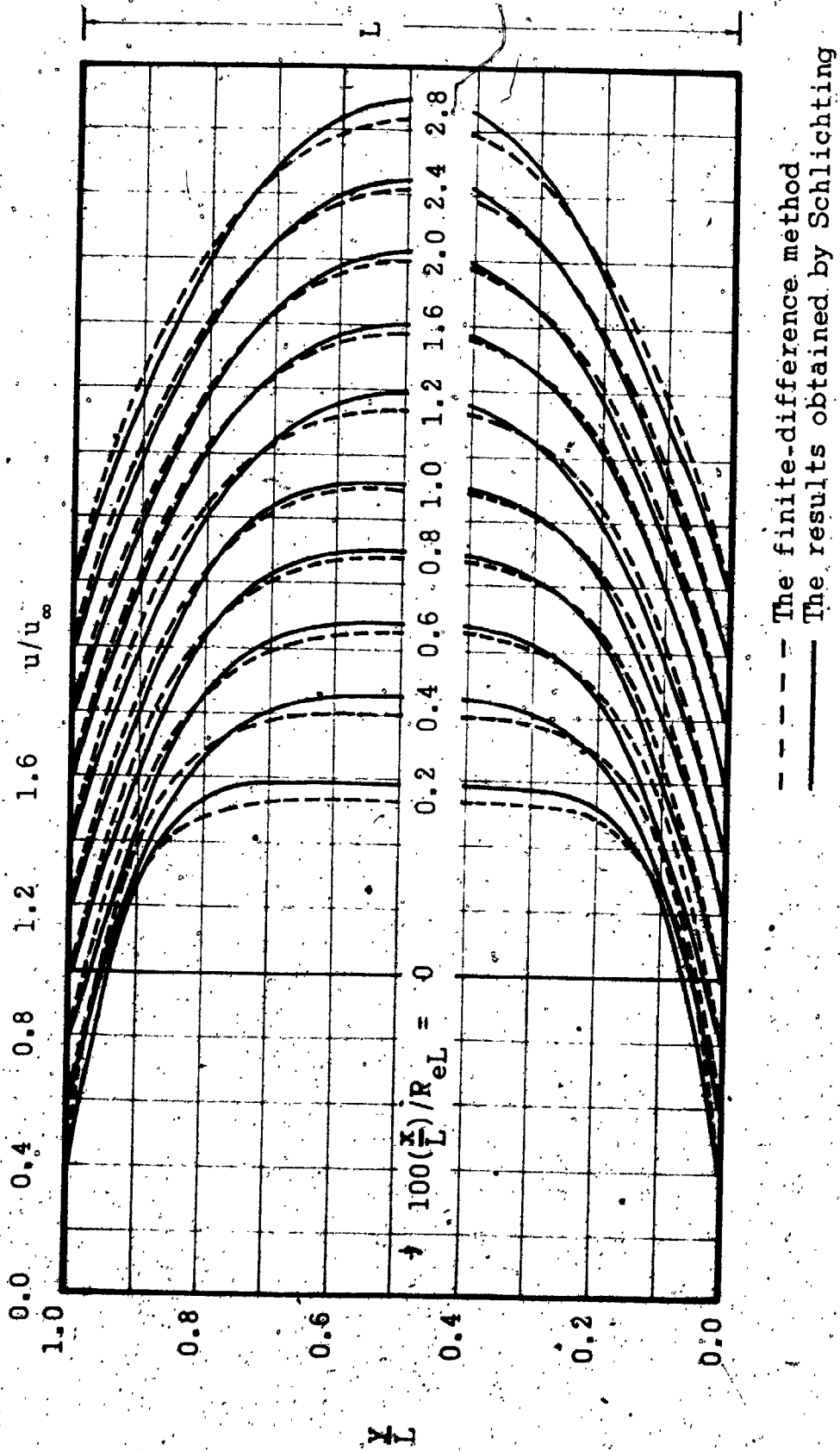


Fig. 3 Comparison between the velocity profiles at the entrance region of a channel by using the finite-difference method of solution and the results obtained by Schlichting (54)

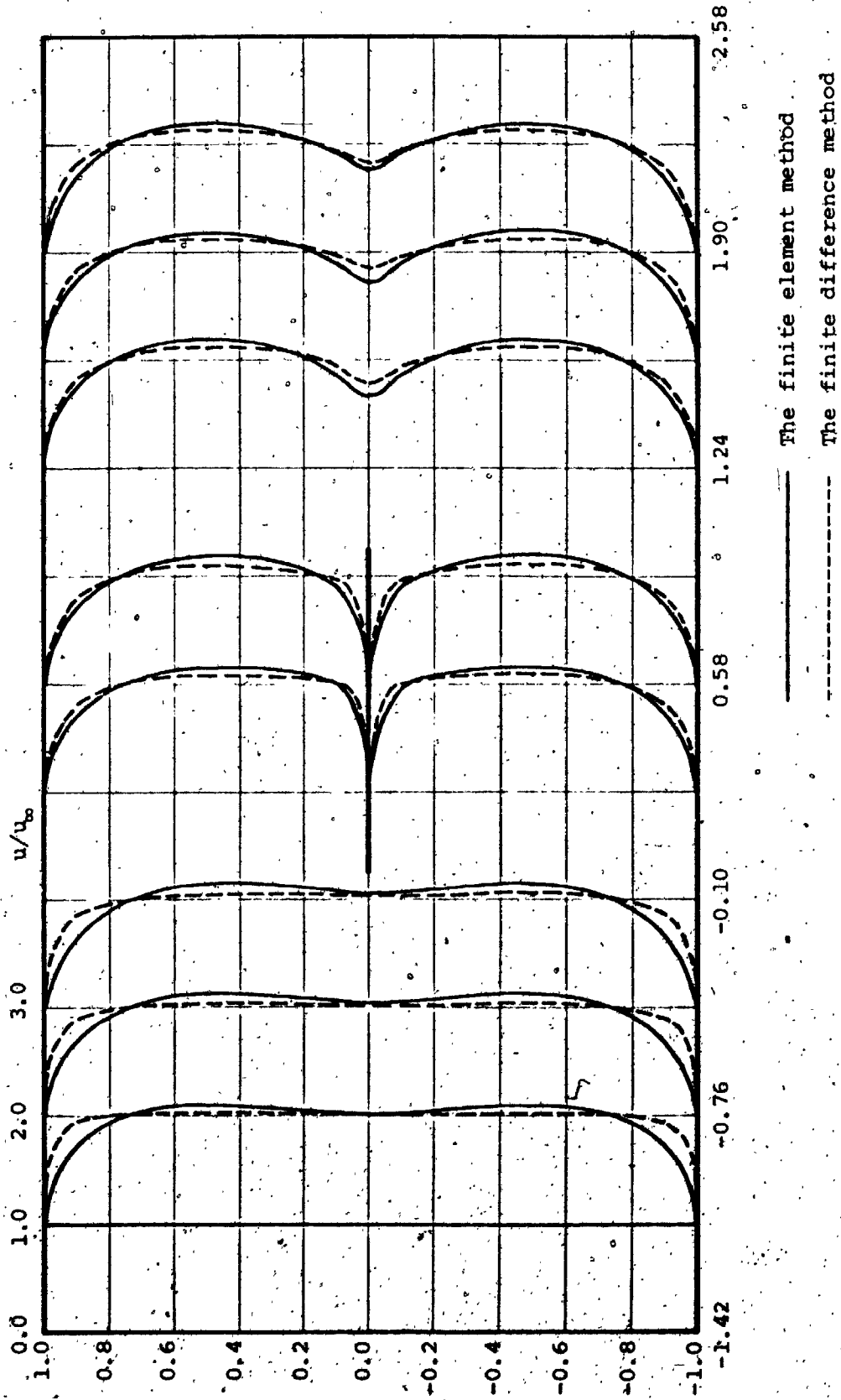


Fig. 4 Comparison between the steady velocity profiles obtained by using the finite difference method and the finite element method.

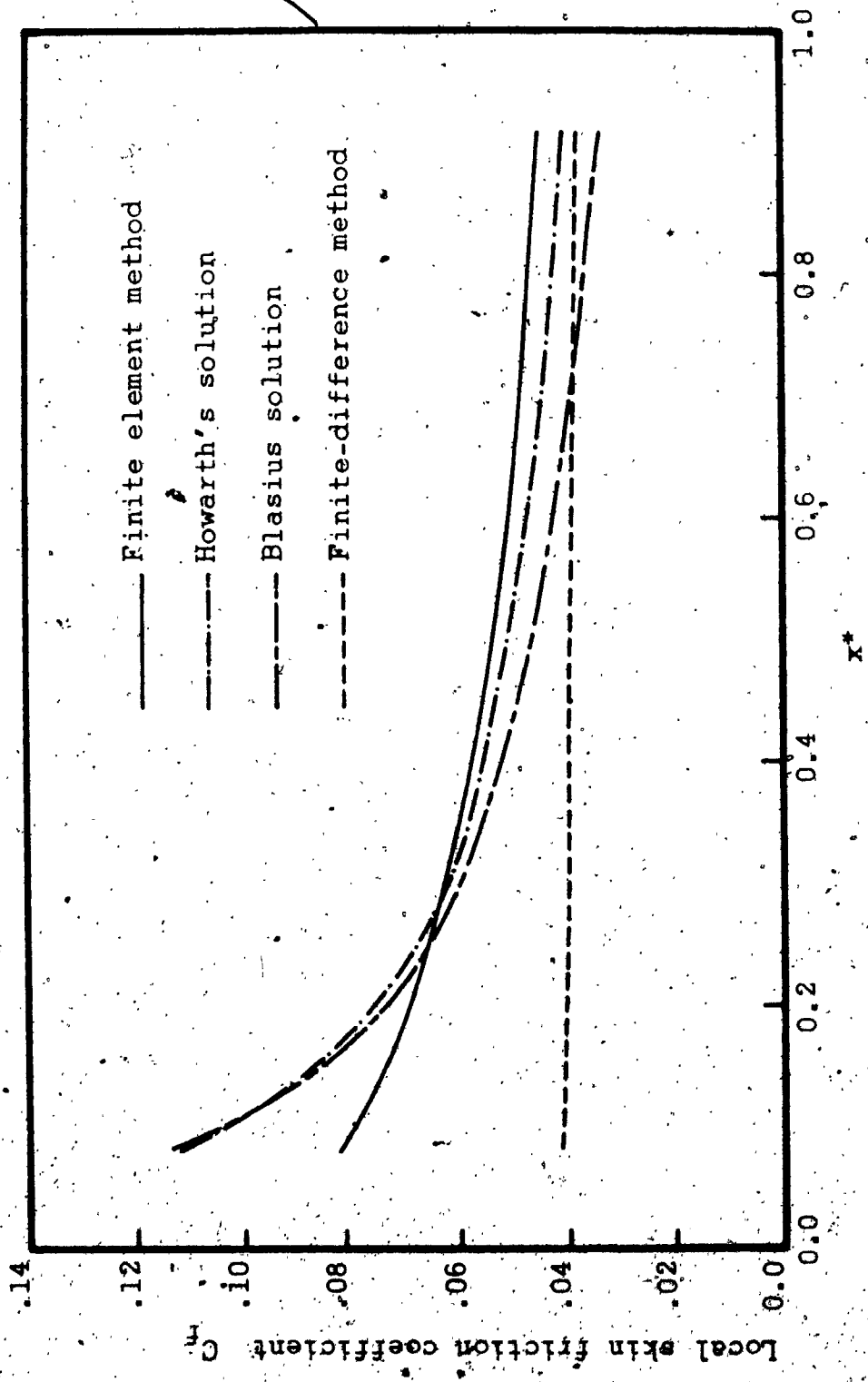


Fig. 5 Comparison between the local skin friction coefficient obtained by the finite element method and by the finite-difference method and by using Blasius and Howarth's solutions.

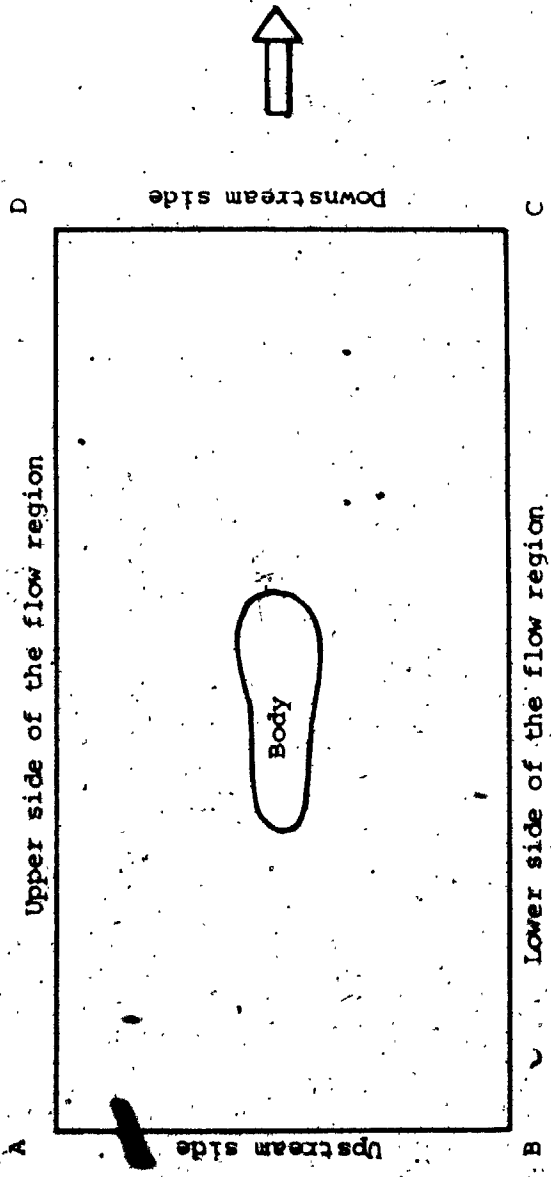
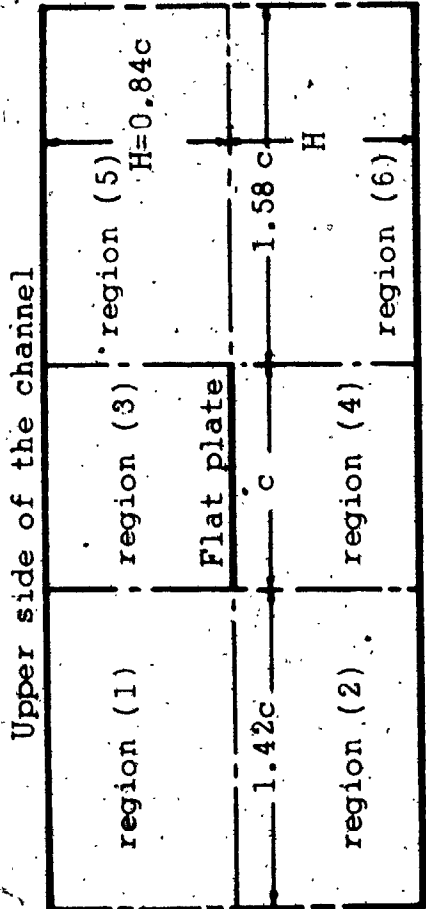
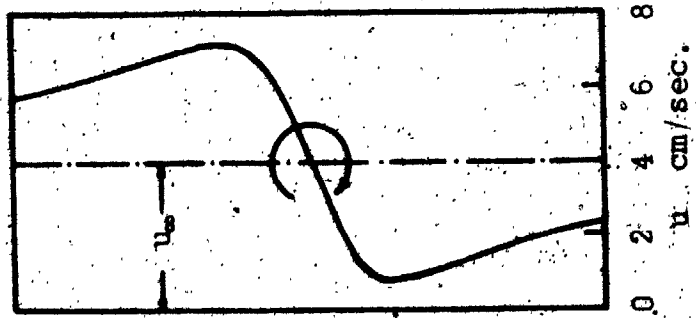


Fig. 6 A four-sided flow region with a body of arbitrary cross-section inside



Details of plate and modified Rankine vortex

- chord of plate (c) = 1.5 cm.
- vortex core radius (r_c) = 0.5 cm.
- vortex strength (Γ) = 10 cm²/sec.
- convection velocity (u_c) = 4 cm/sec.

Fig. 7 Schematic diagram showing the flow domain with the vortex approaching

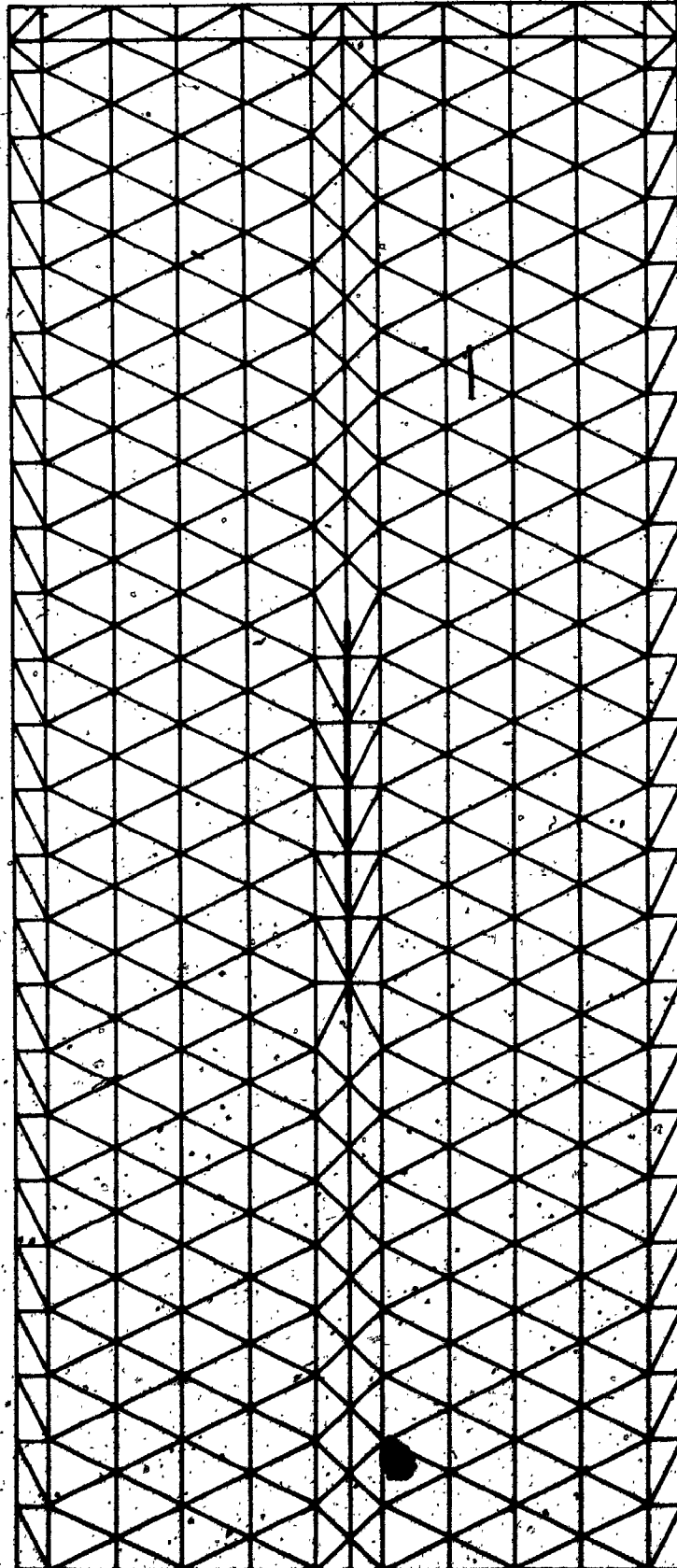


Fig. 8. The finite element mesh

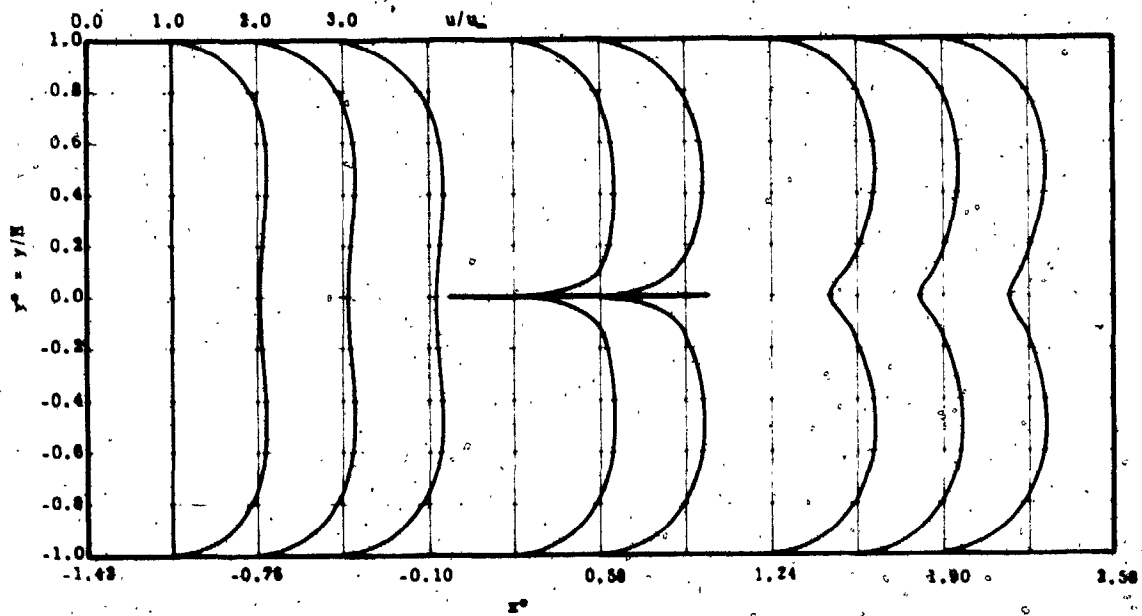


Fig. 9-a Spatial variation of the velocity field at time $t=0$

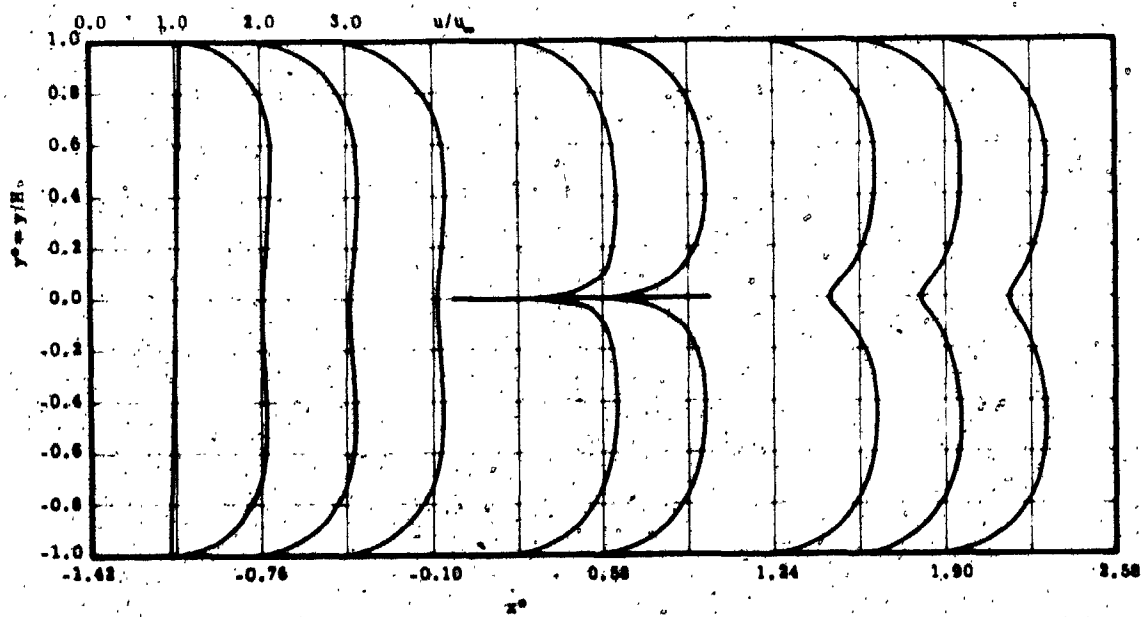


Fig. 9-b Spatial variation of the velocity field at time $t=0.4$ sec.

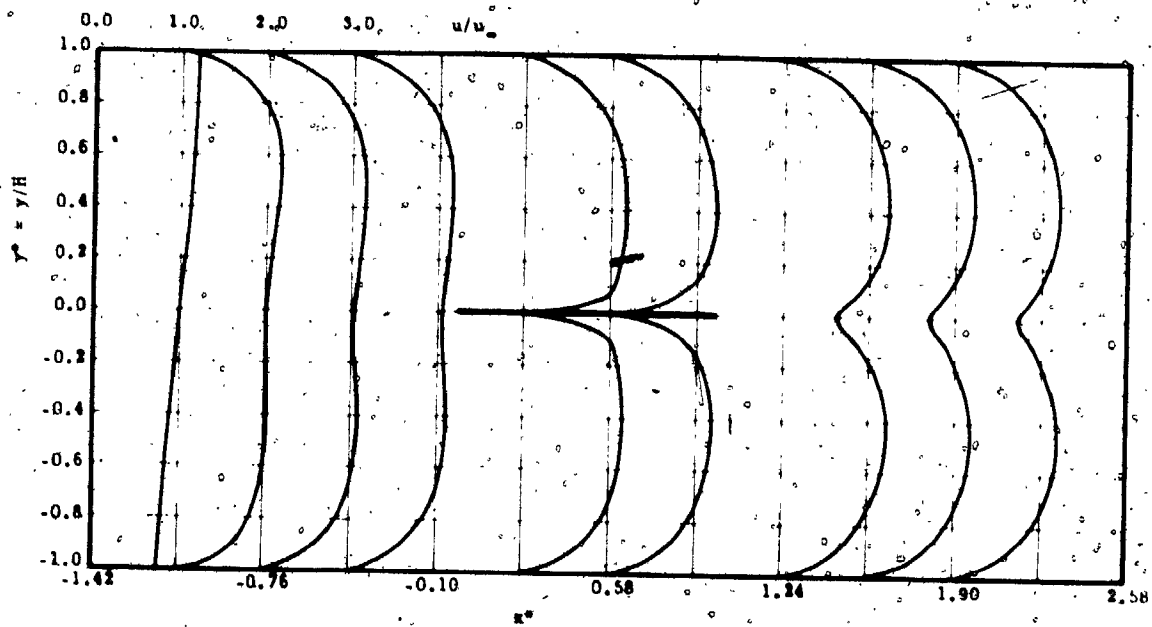


Fig. 9-c Special variation of the velocity field at $t=0.8$ sec.

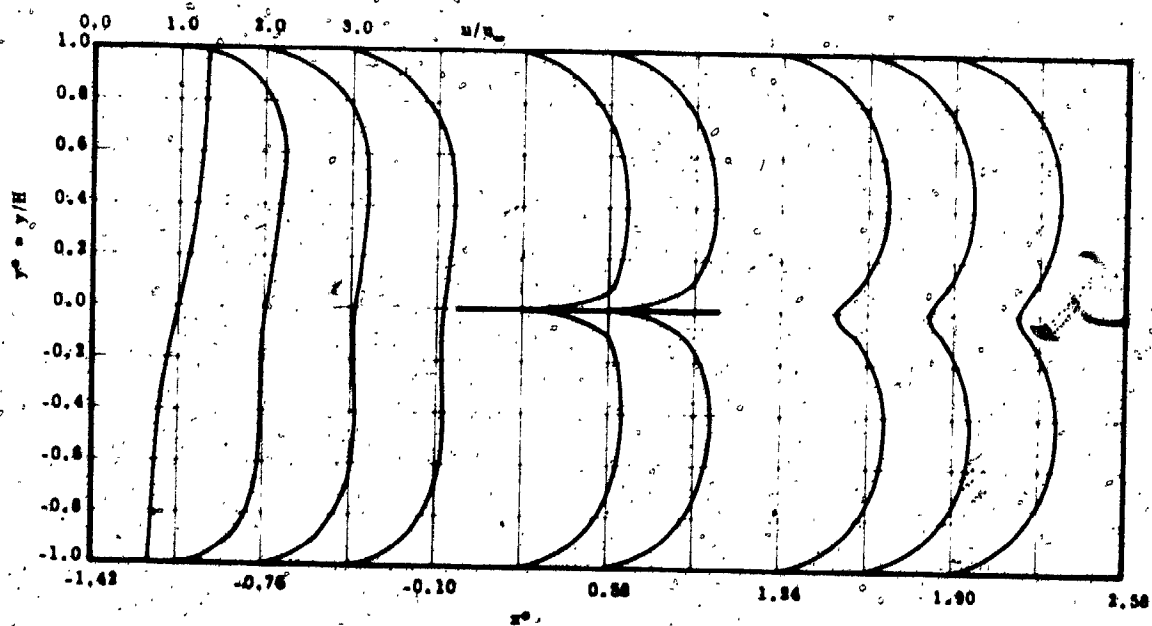


Fig. 9-d Special variation of the velocity field at $t=0.96$ sec.

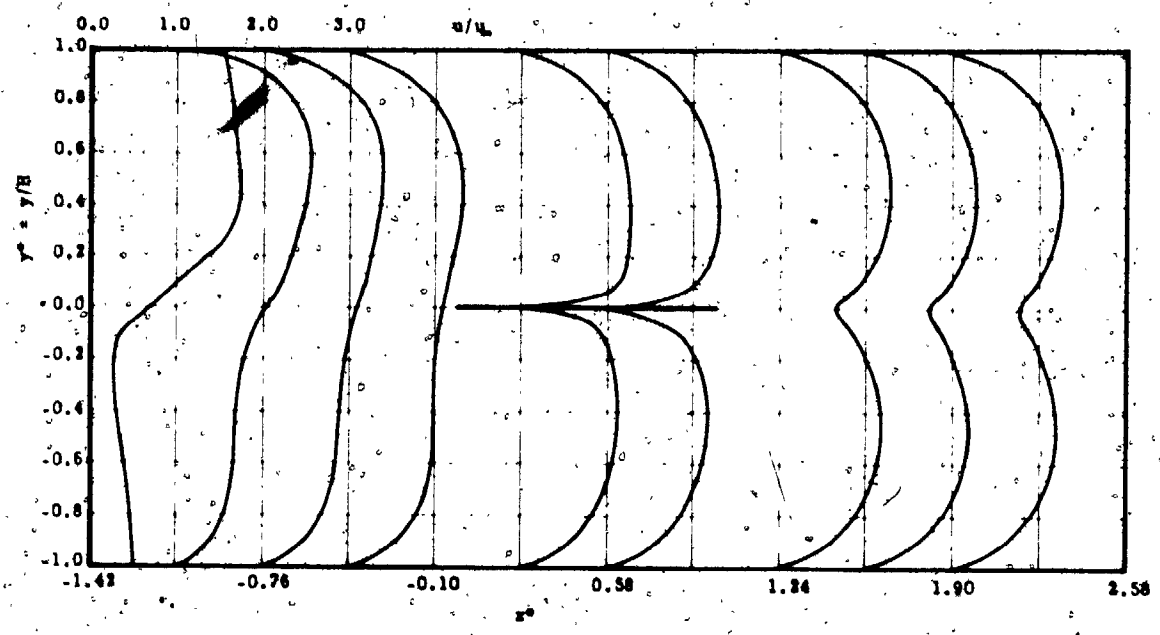


Fig. 9-d Special variation of the velocity field at $t=1.2$ sec.

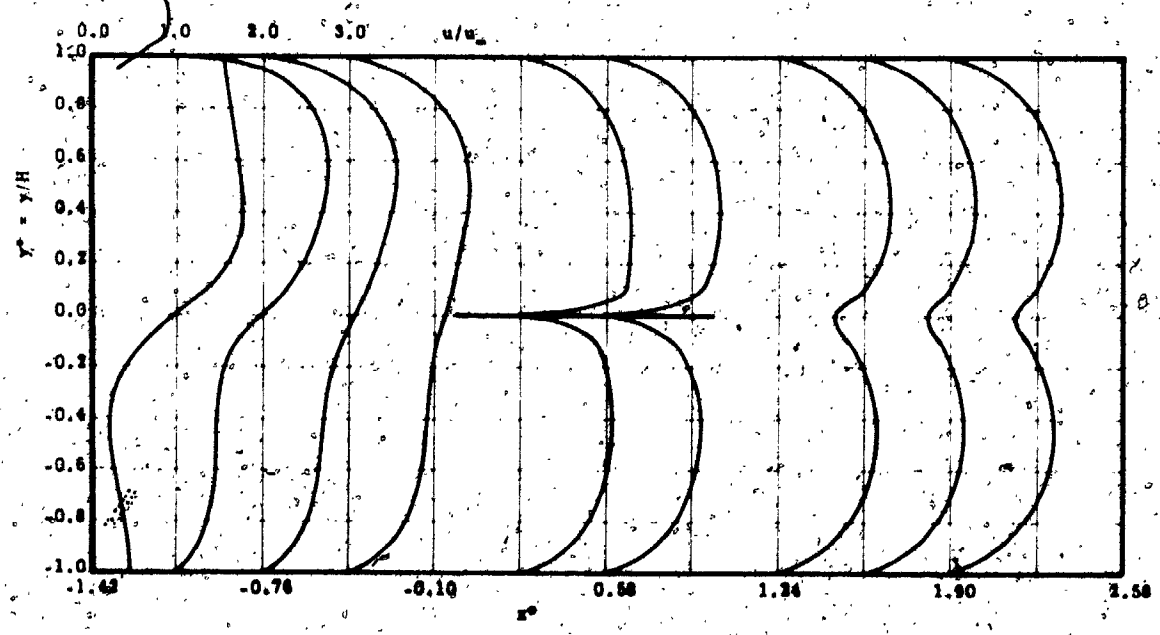


Fig. 9-f Special variation of the velocity field at $t=1.28$ sec.

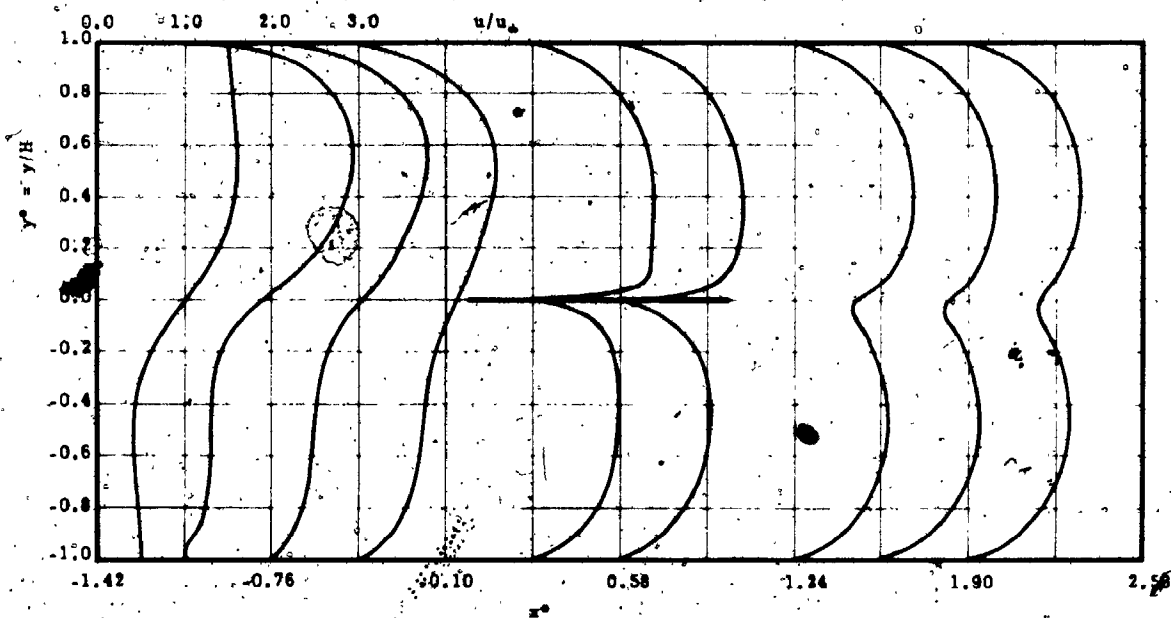


Fig. 9-g Spatial variation of the velocity field at $t=1.36$ sec.

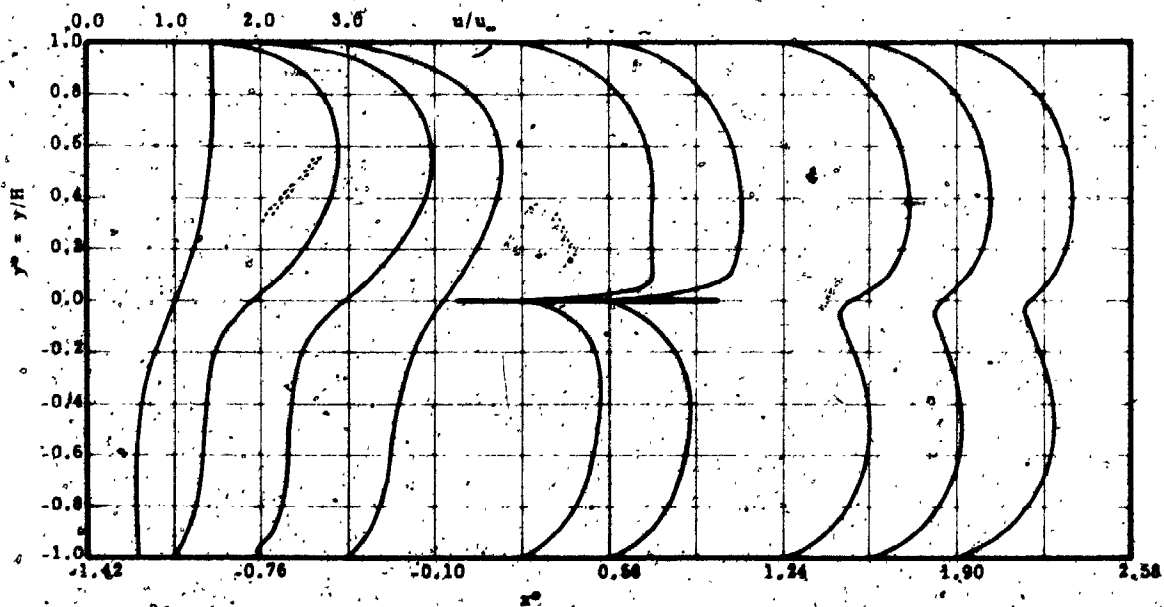


Fig. 9-h Spatial variation of the velocity field at $t=1.44$ sec.

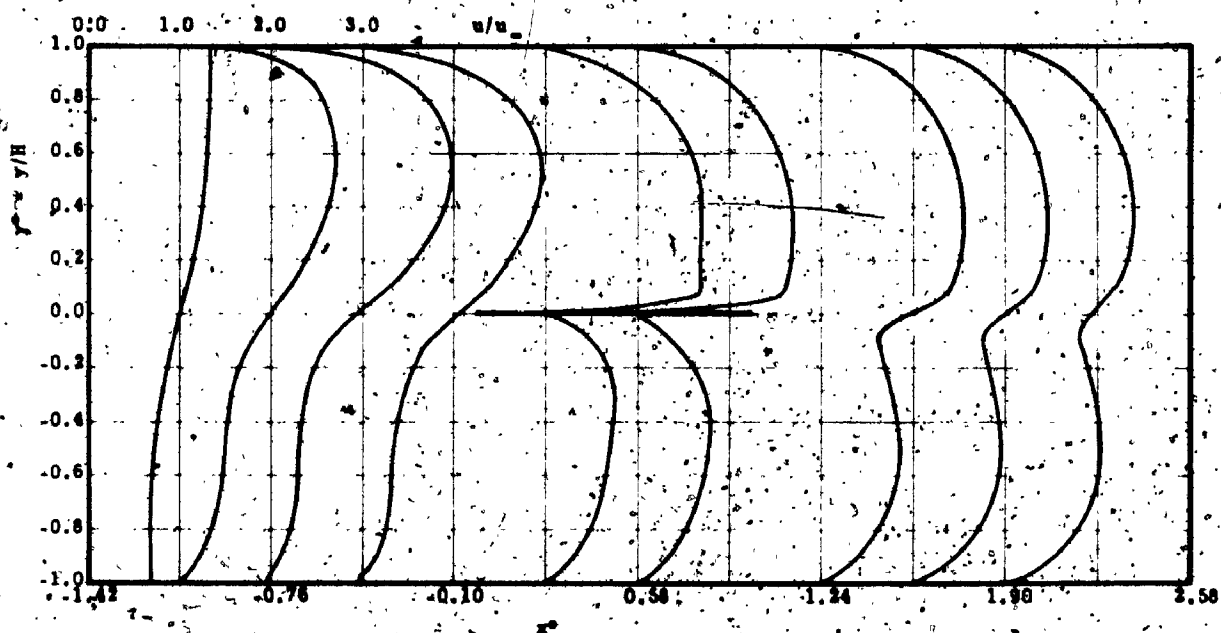


Fig. 9-1 Spatial variation of the velocity field at $t=1.52$ sec.

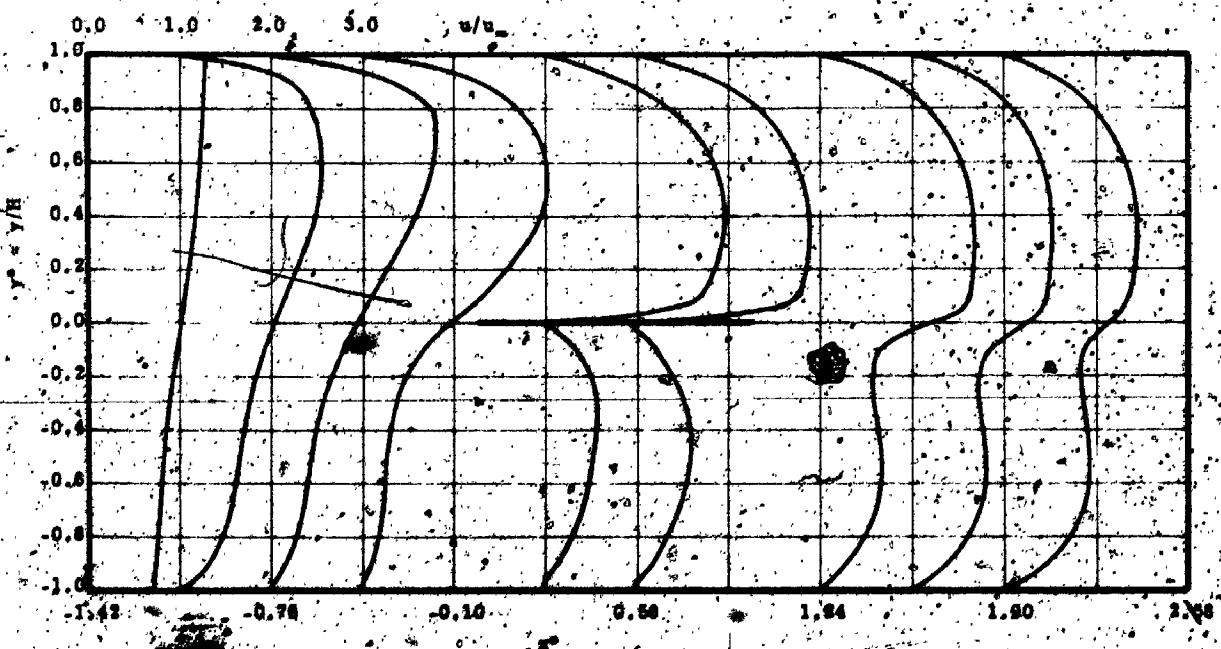


Fig. 9-2 Spatial variation of the velocity field at $t=1.6$ sec.

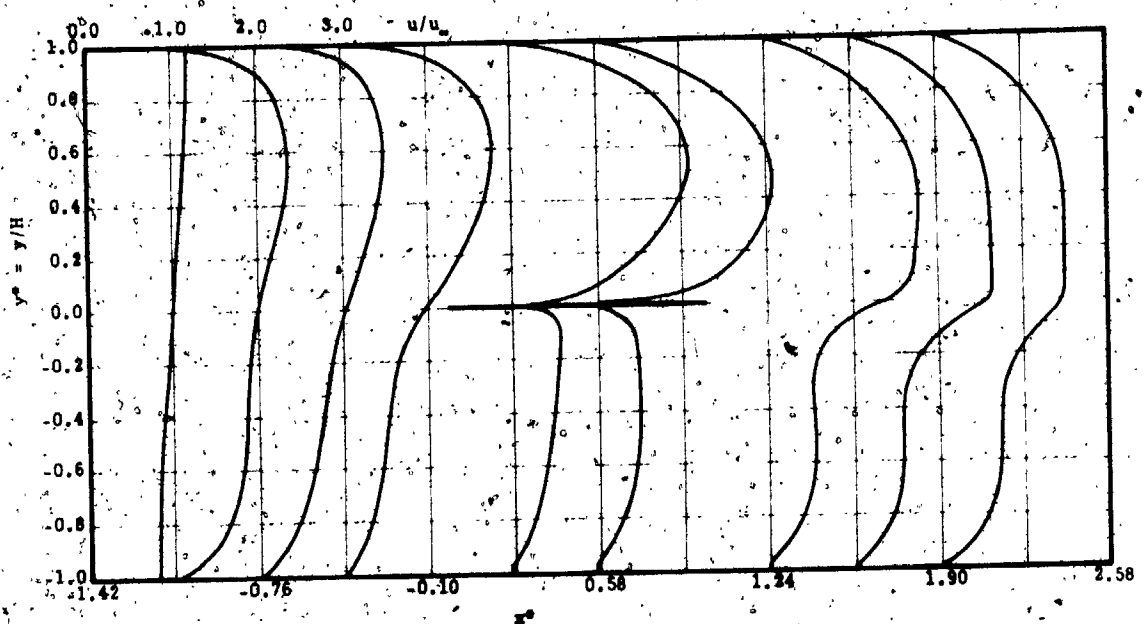


Fig. 9-k Spatial variation of the velocity field at time $t=1.72$ sec.

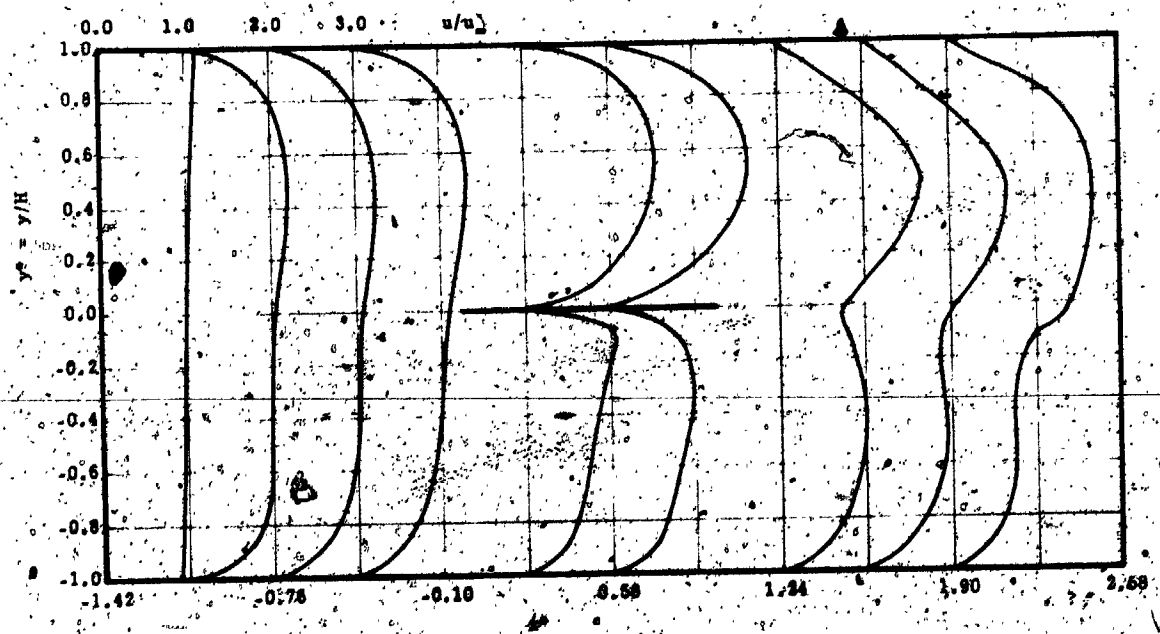


Fig. 9-l Spatial variation of the velocity field at $t=1.96$ sec.

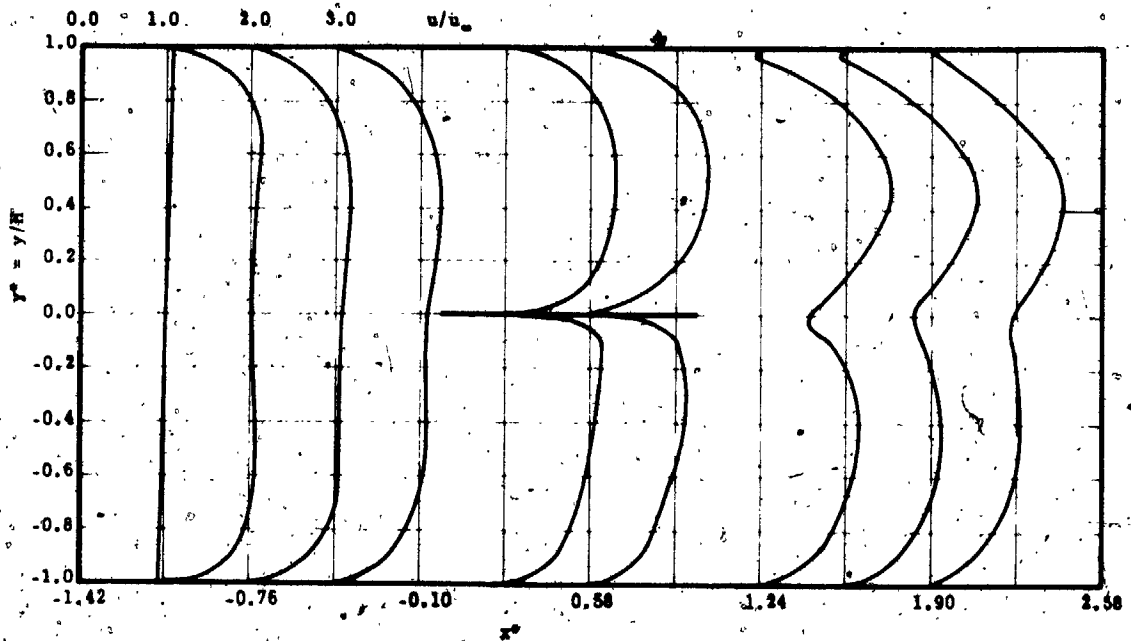


Fig. 9-m Spatial variation of the velocity field at $t=2.12$ sec.

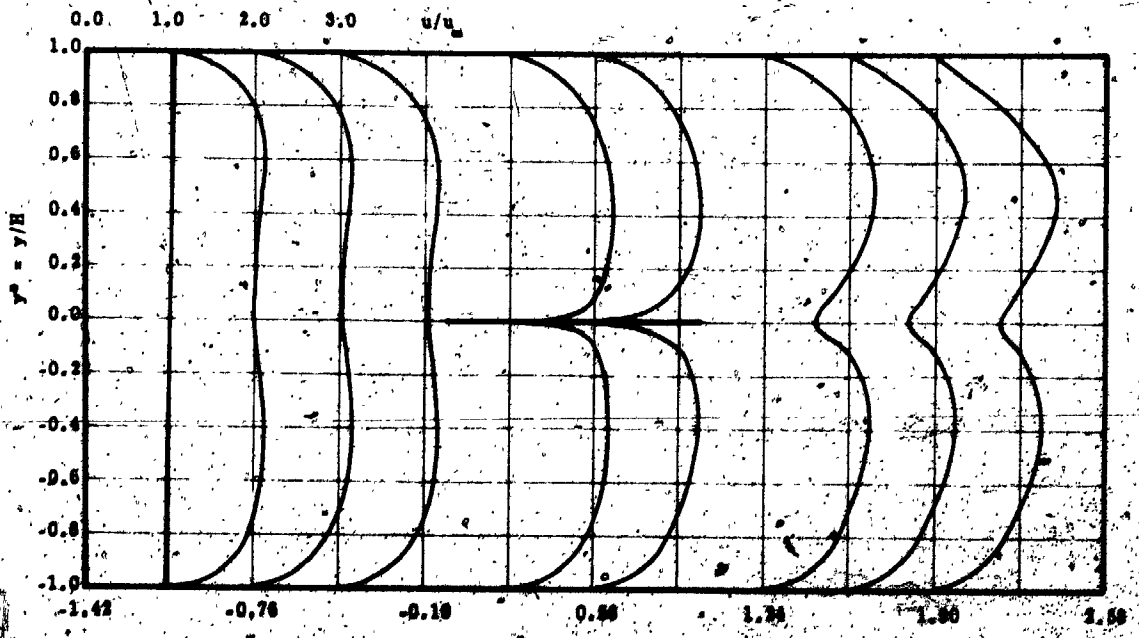


Fig. 9-n Spatial variation of the velocity field at $t=4.44$ sec.

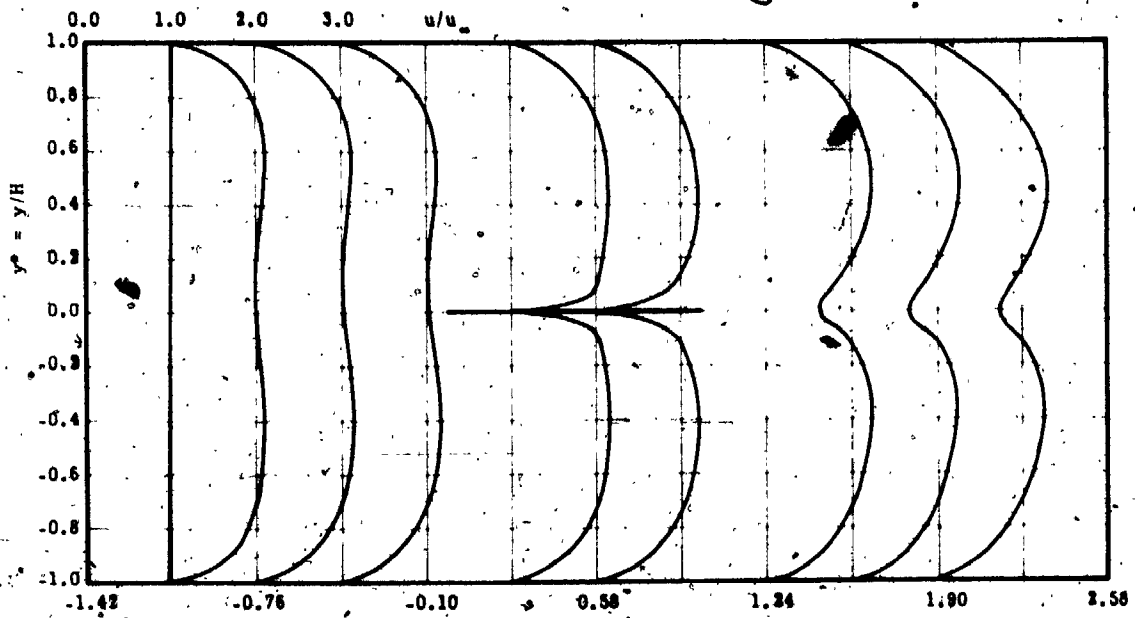


Fig. 9-o Special variation of the velocity field at $t=2.6$ sec.

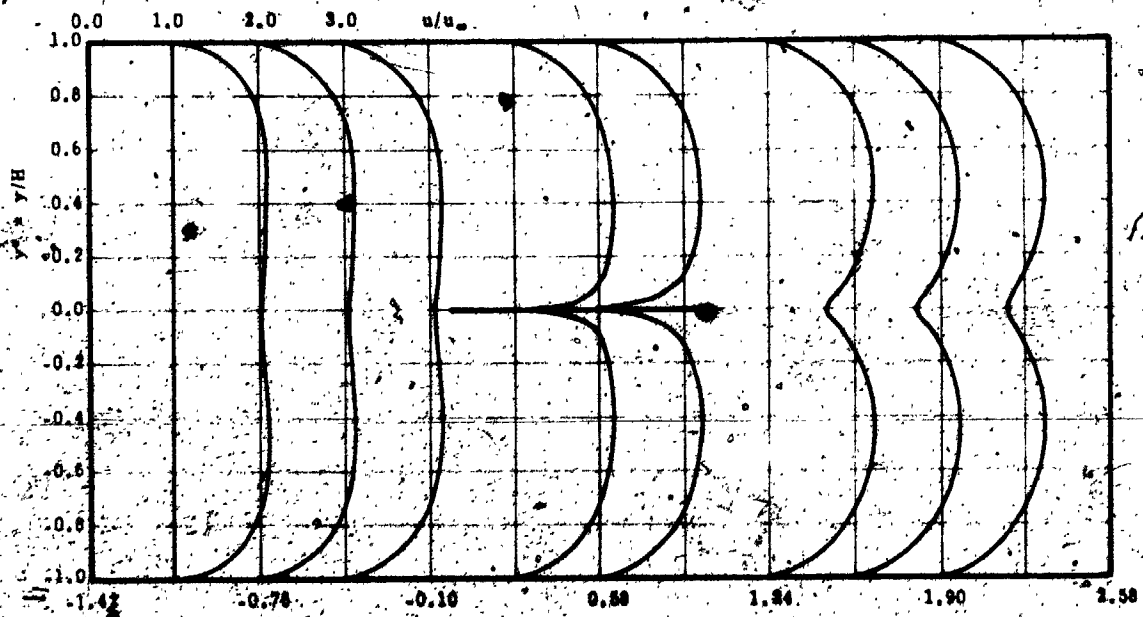


Fig. 9-p Special variation of the velocity field at $t=3.51$ sec.

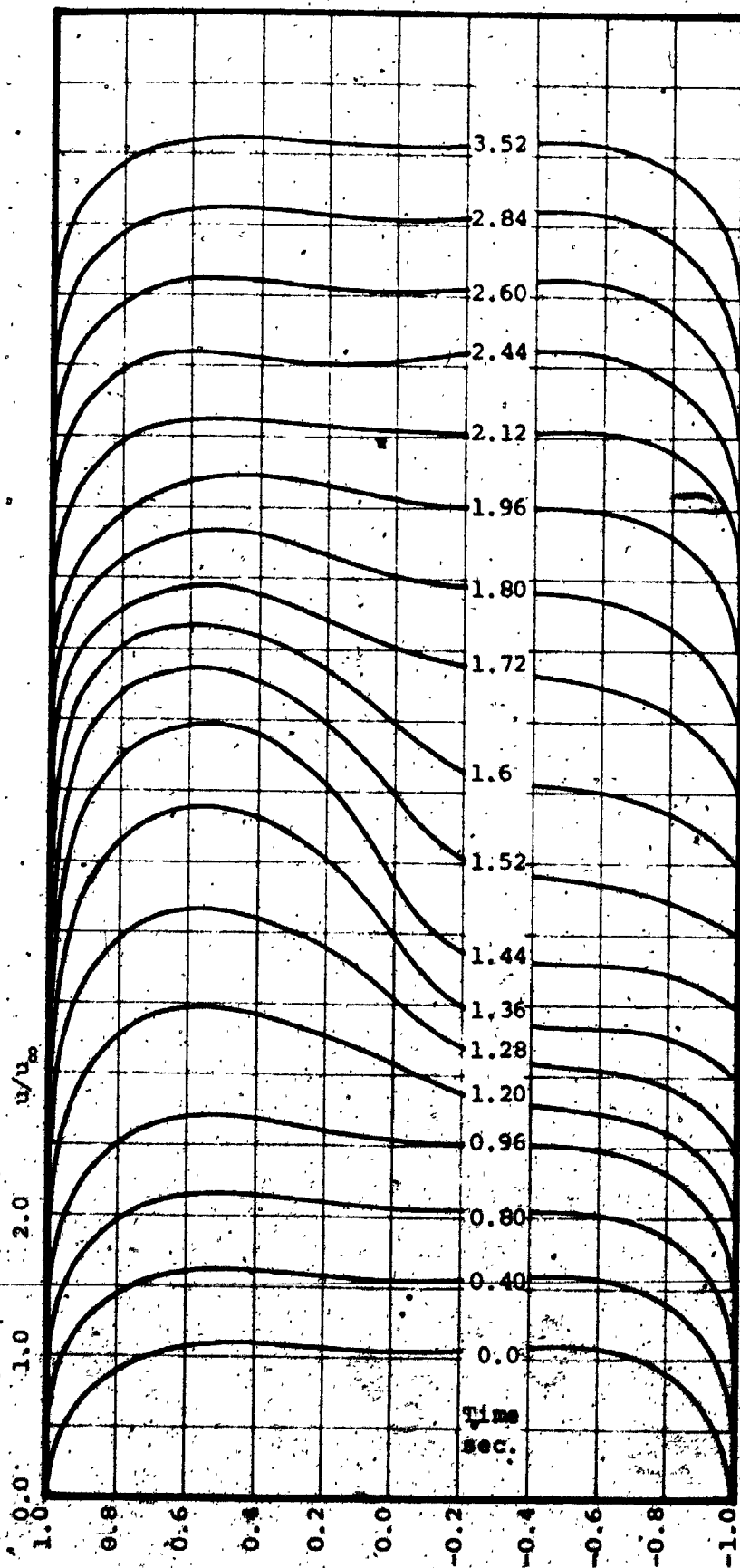


Fig. 10-a Variation of velocity profiles 'u component' with time at a section $x^* = -0.92$

$y/\lambda = x$

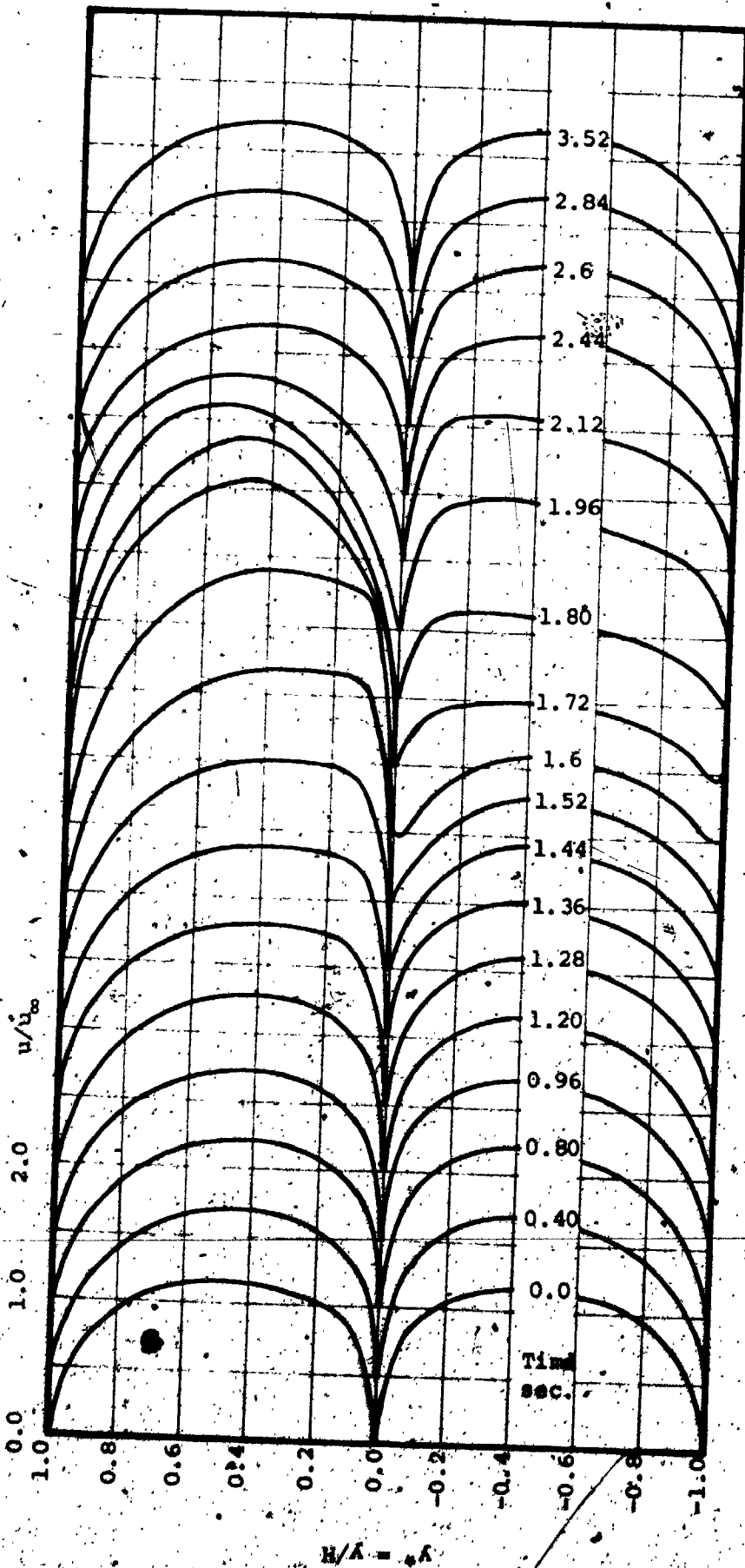


Fig. 10-b Variation of velocity profiles 'u component' with time at a section $x^* = 0.5$

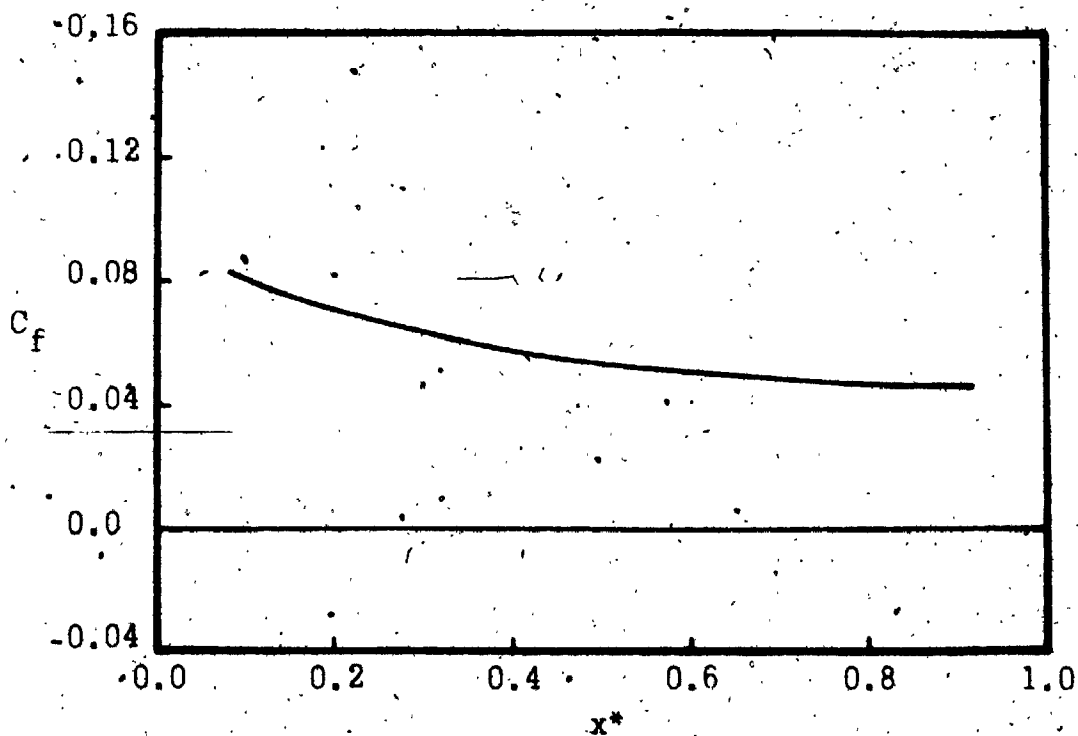


Fig. 11-a Local skin friction coefficient on the two sides of the plate at time $t=0$

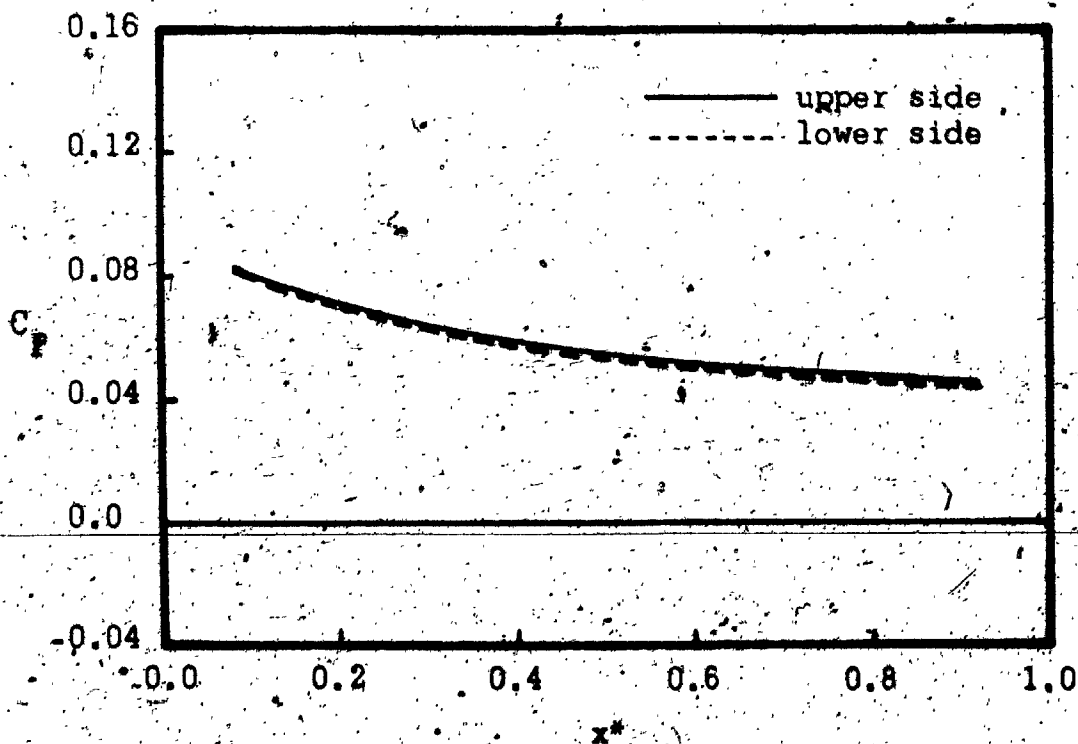


Fig. 11-b Local skin friction coefficient on the two sides of the plate at time $t=0.4$ sec.

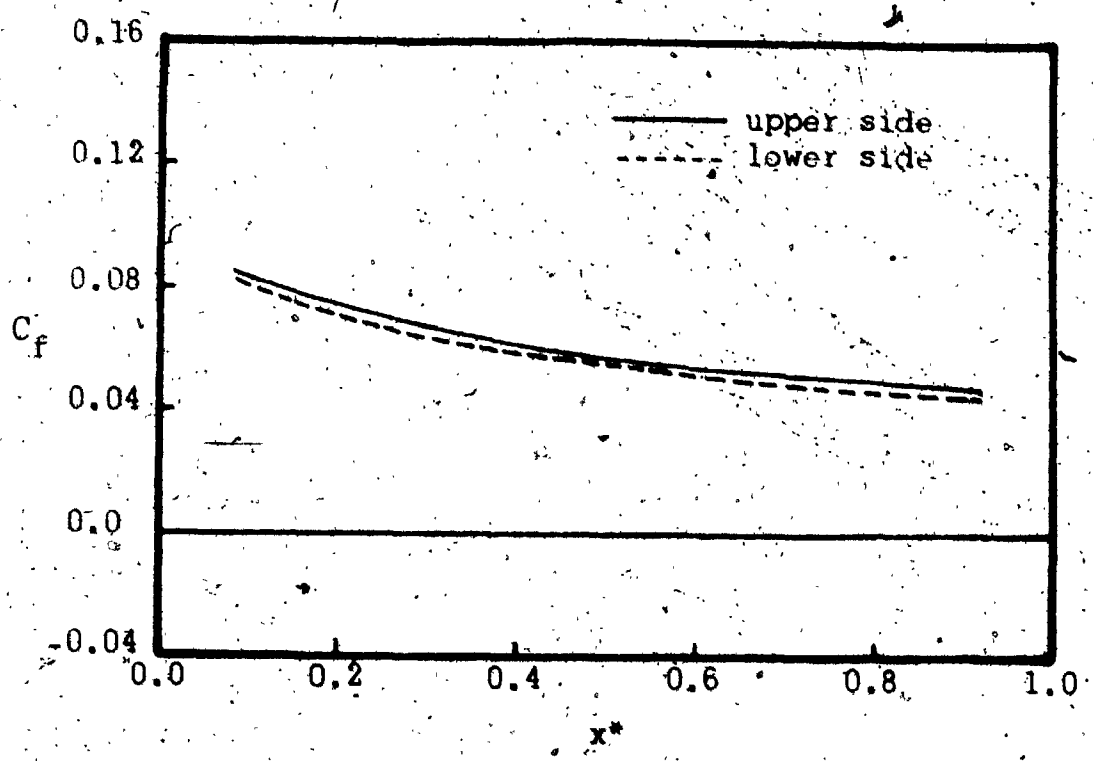


Fig. 11-c Local skin friction coefficient on the two sides of the plate at $t=0.64$ sec.

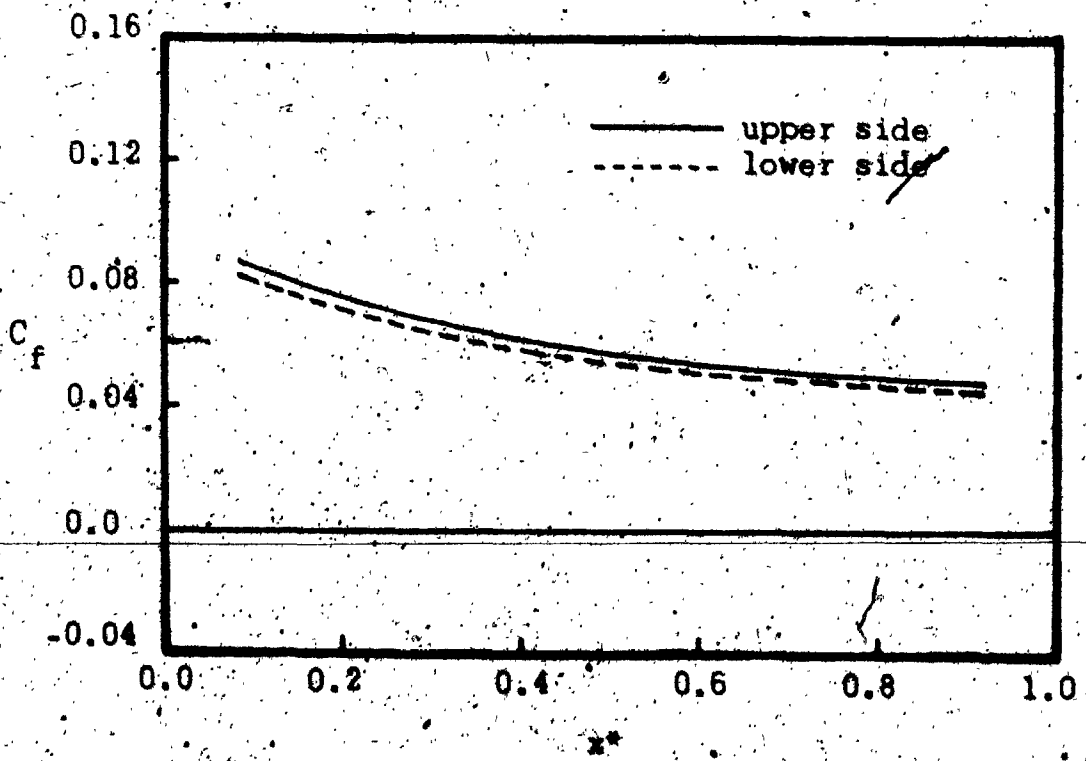


Fig. 11-d Local skin friction coefficient on the two sides of the plate at $t=0.8$ sec.

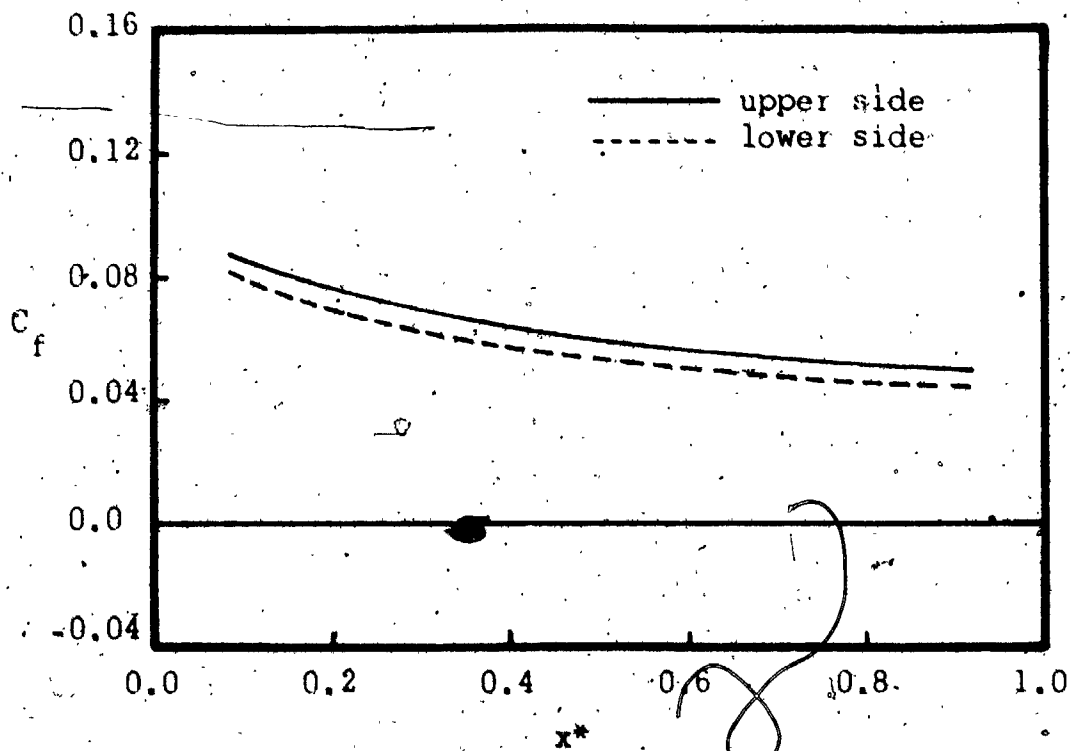


Fig. 11-e Local skin friction coefficient on the two sides of the plate at $t=0.96$ sec.

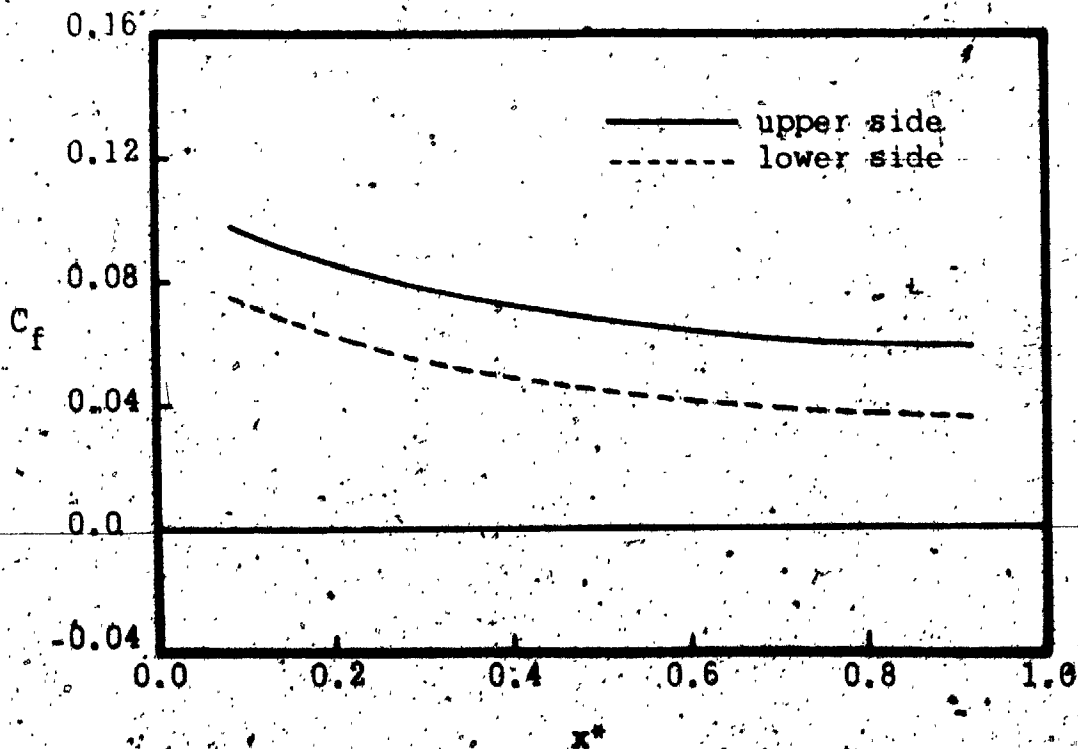


Fig. 11-f Local skin friction coefficient on the two sides of the plate at $t=1.2$ sec.

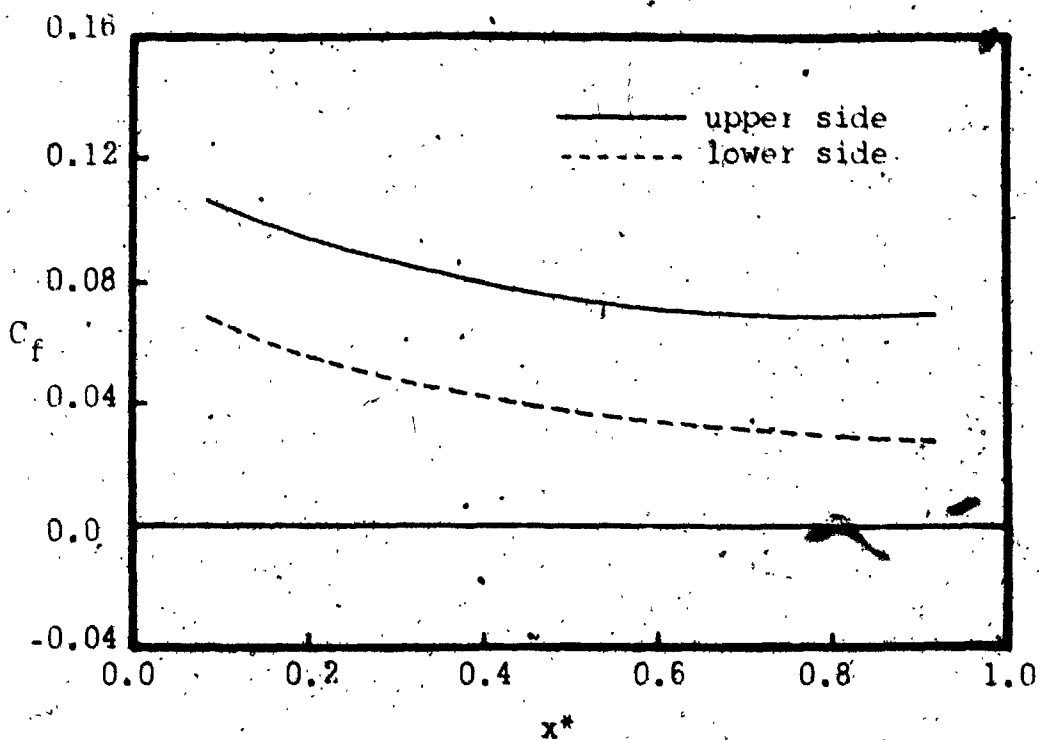


Fig. 11-g Local skin friction coefficient on the two sides of the plate at $t=1.28$ sec.

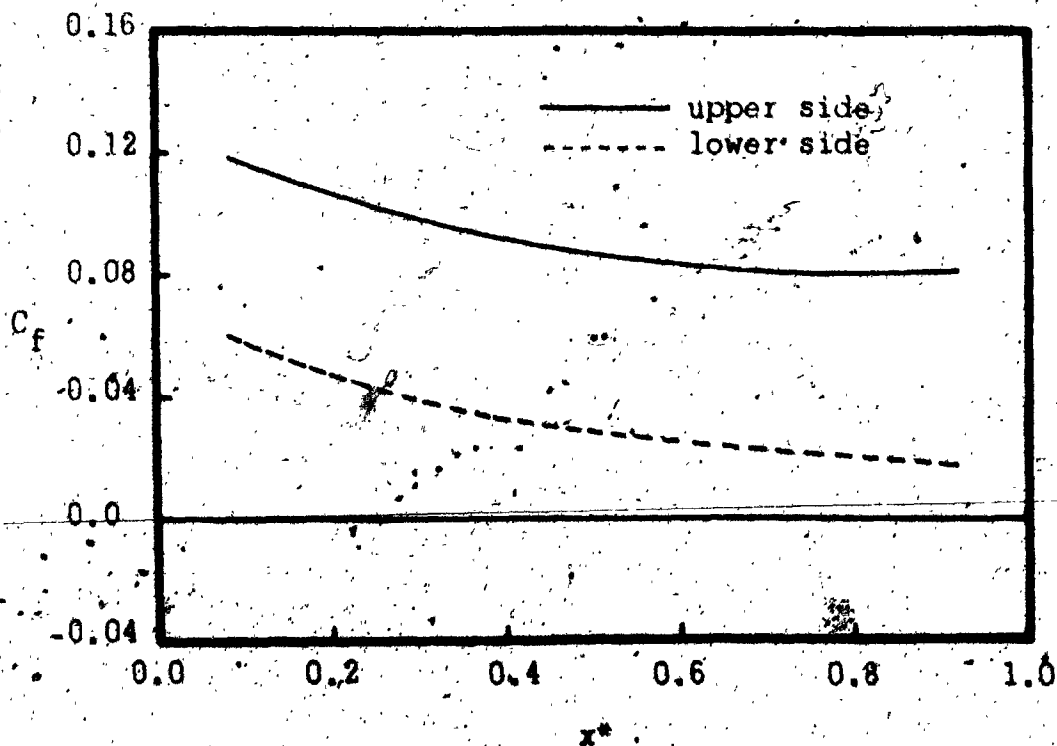


Fig. 11-h Local skin friction coefficient on the two sides of the plate at $t=1.35$ sec.

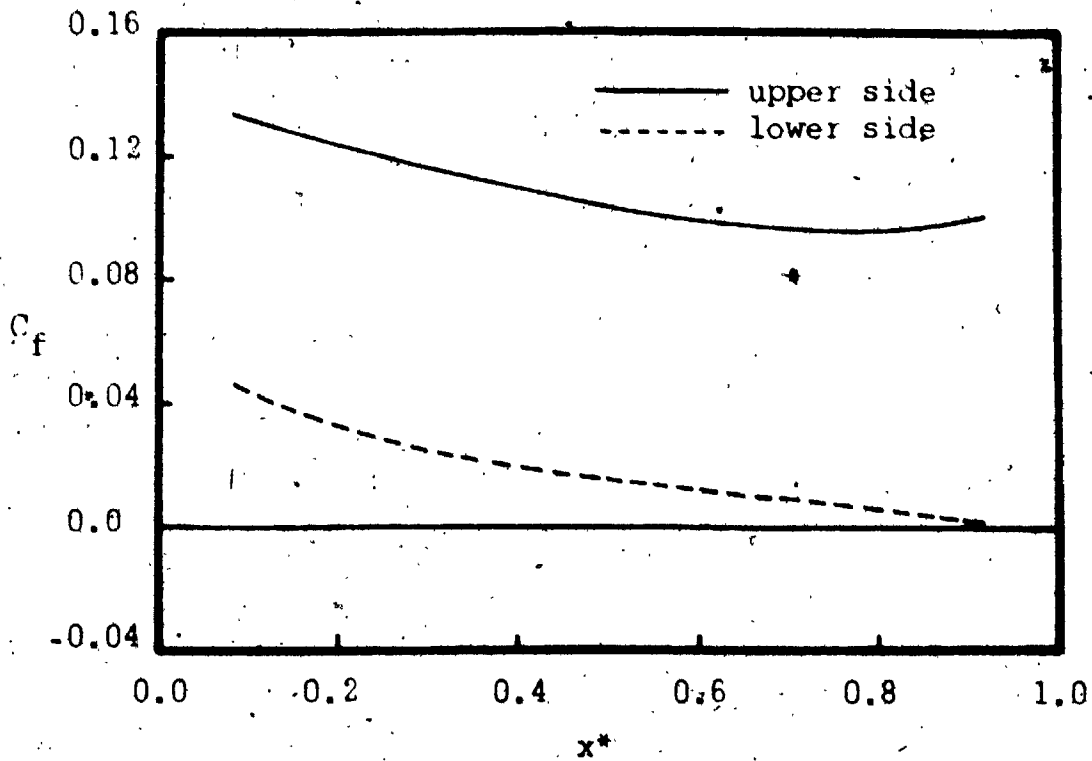


Fig. 11-i Local skin friction coefficient on the two sides of the plate at $t=1.44$ sec.

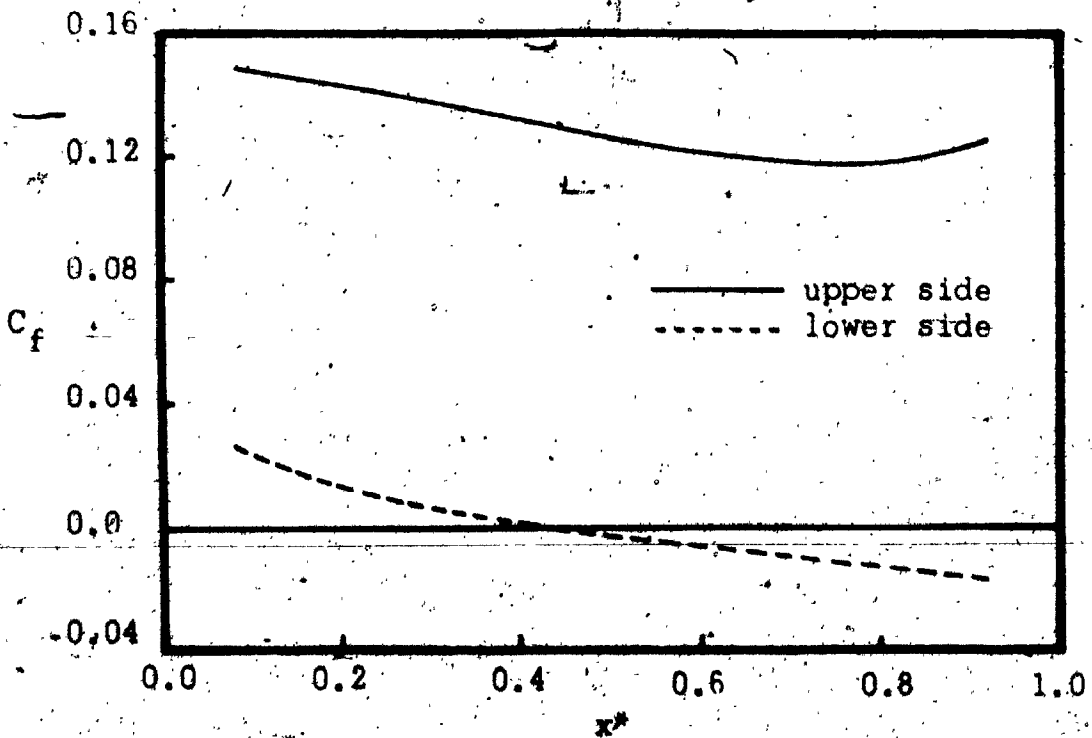


Fig. 11-j Local skin friction coefficient on the two sides of the plate at $t=1.52$ sec.

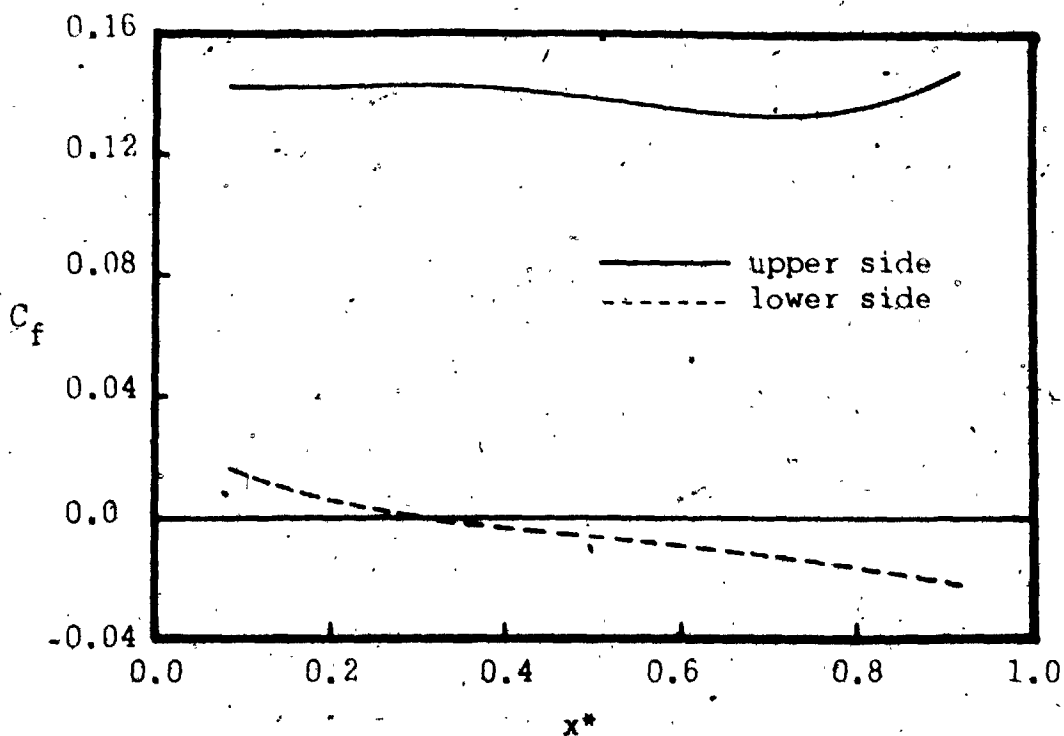


Fig. 11-k Local skin friction coefficient on the two sides of the plate at $t=1.6$ sec.

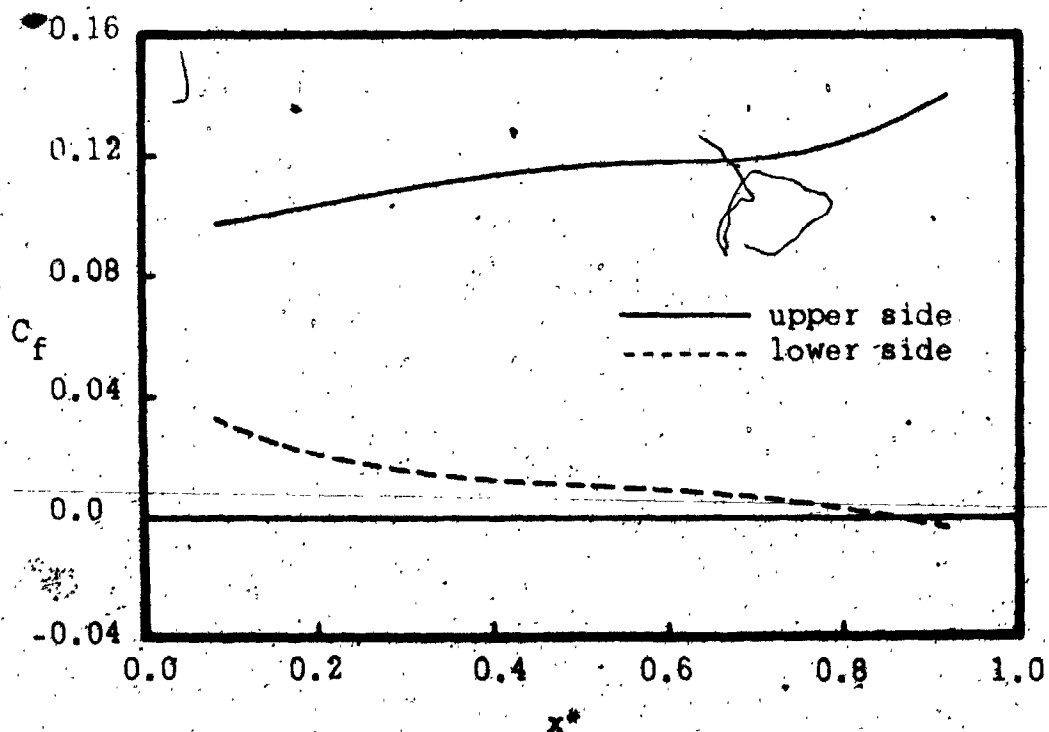


Fig. 11-l Local skin friction coefficient on the two sides of the plate at $t=1.66$ sec.

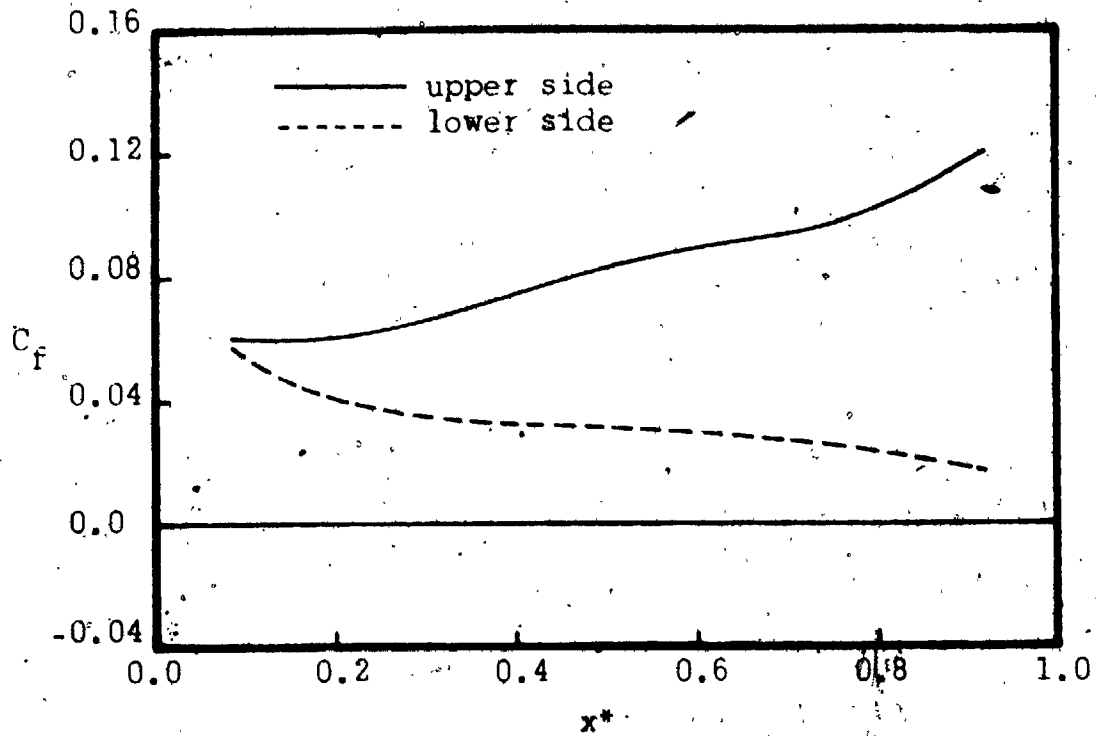


Fig. 11-m Local skin friction coefficient on the two sides of the plate at $t=1.72$ sec.

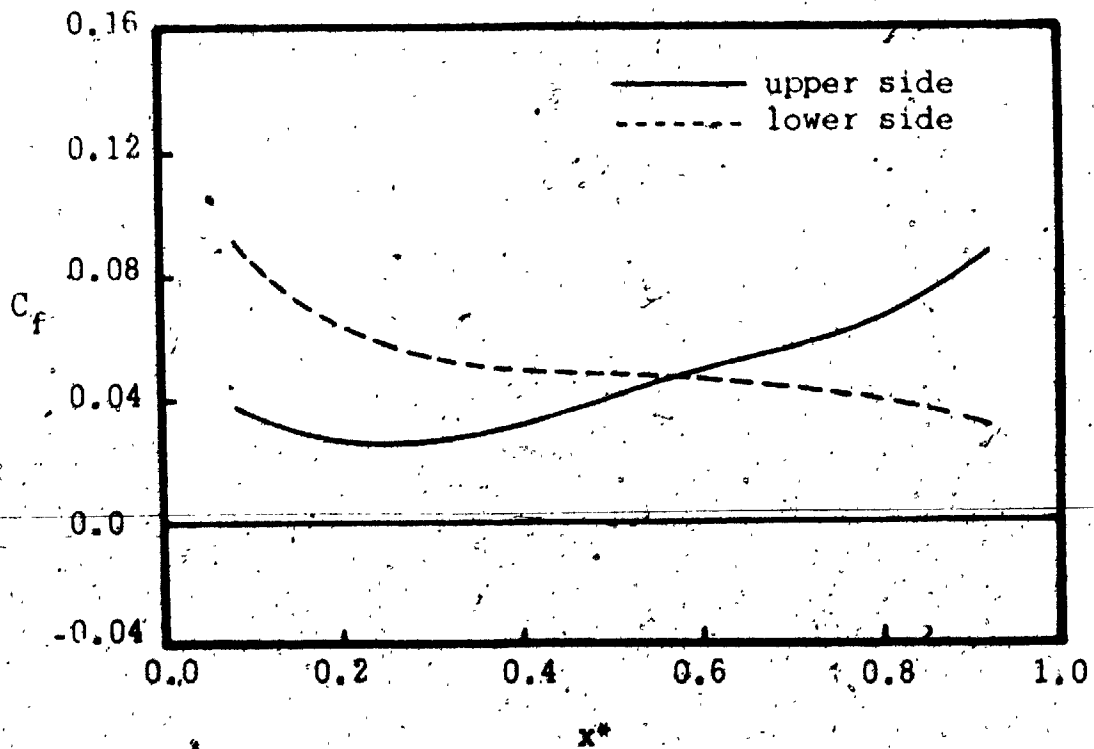


Fig. 11-n Local skin friction coefficient on the two sides of the plate at $t=1.8$ sec.

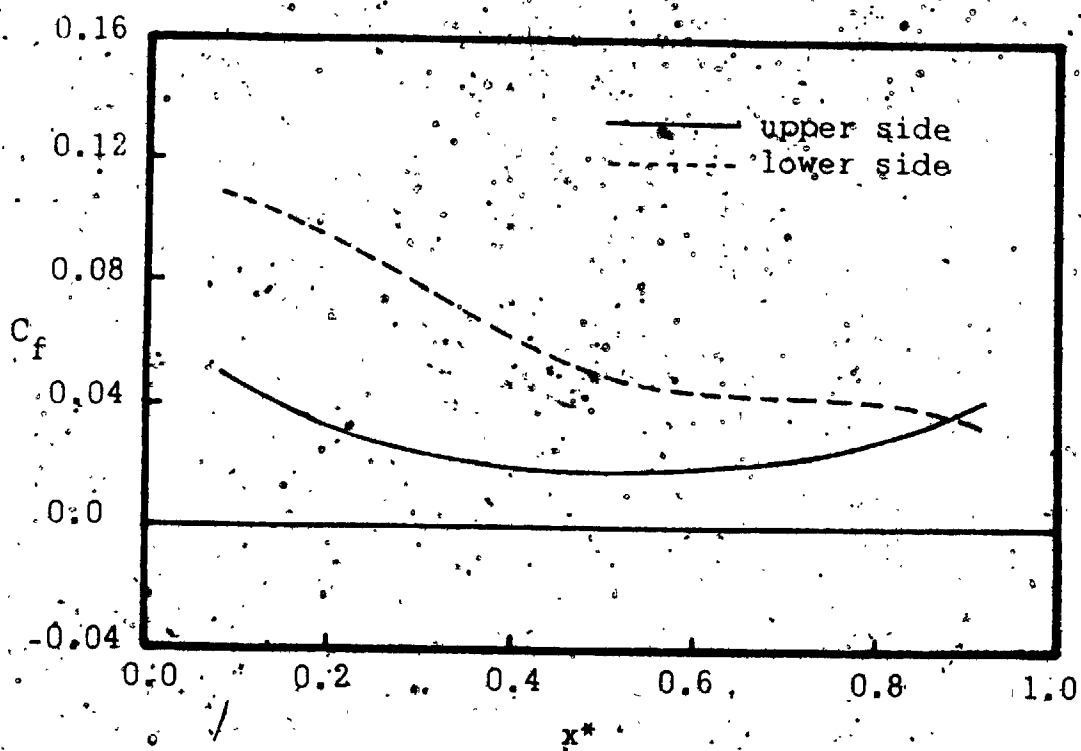


Fig. 11-o Local skin friction coefficient on the two sides of the plate at $t=1.96$ sec.

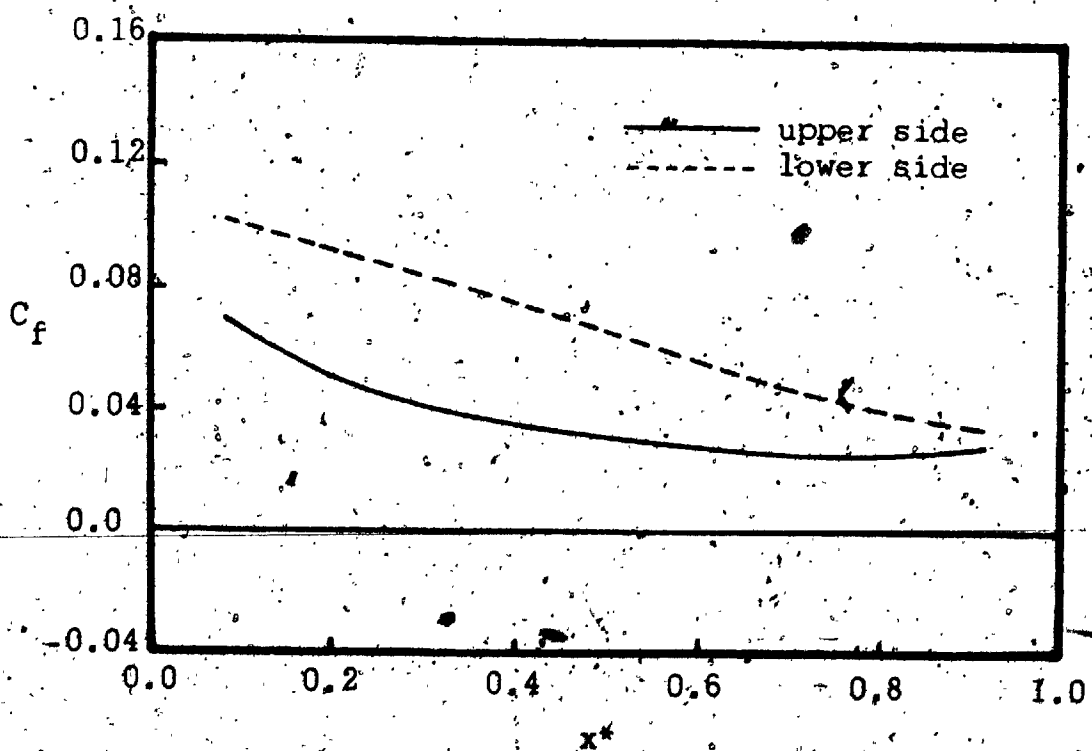
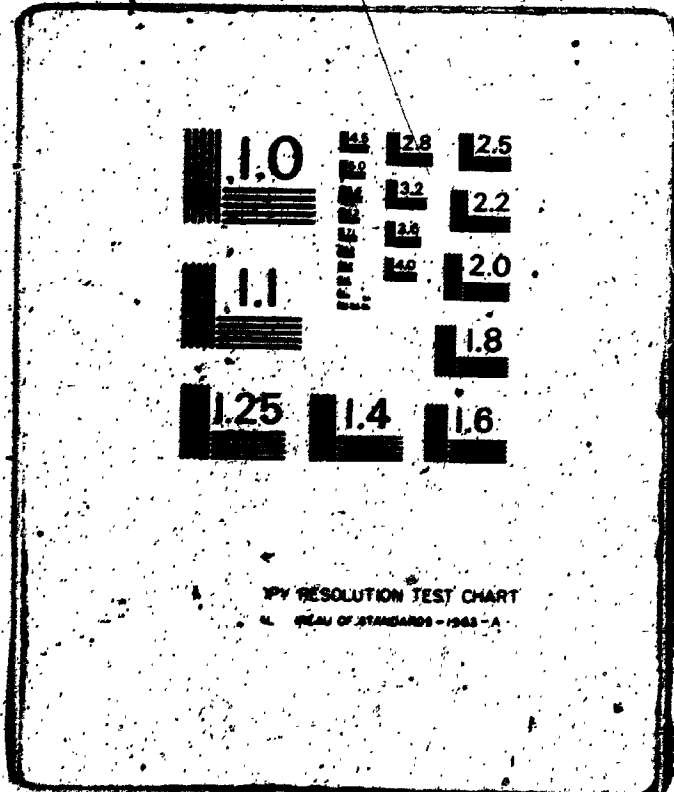


Fig. 11-p Local skin friction coefficient on the two sides of the plate at $t=2.12$ sec.

3 OF/DE 3



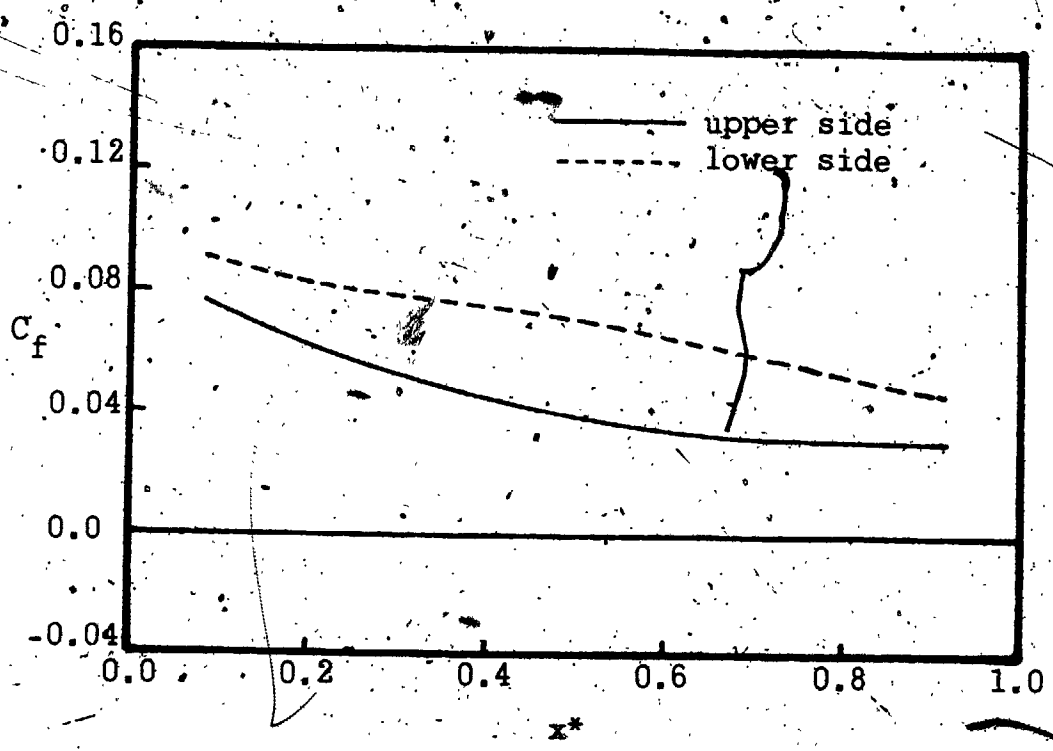


Fig. 11-q Local skin friction coefficient on the two sides of the plate at $t=2.28$ sec.

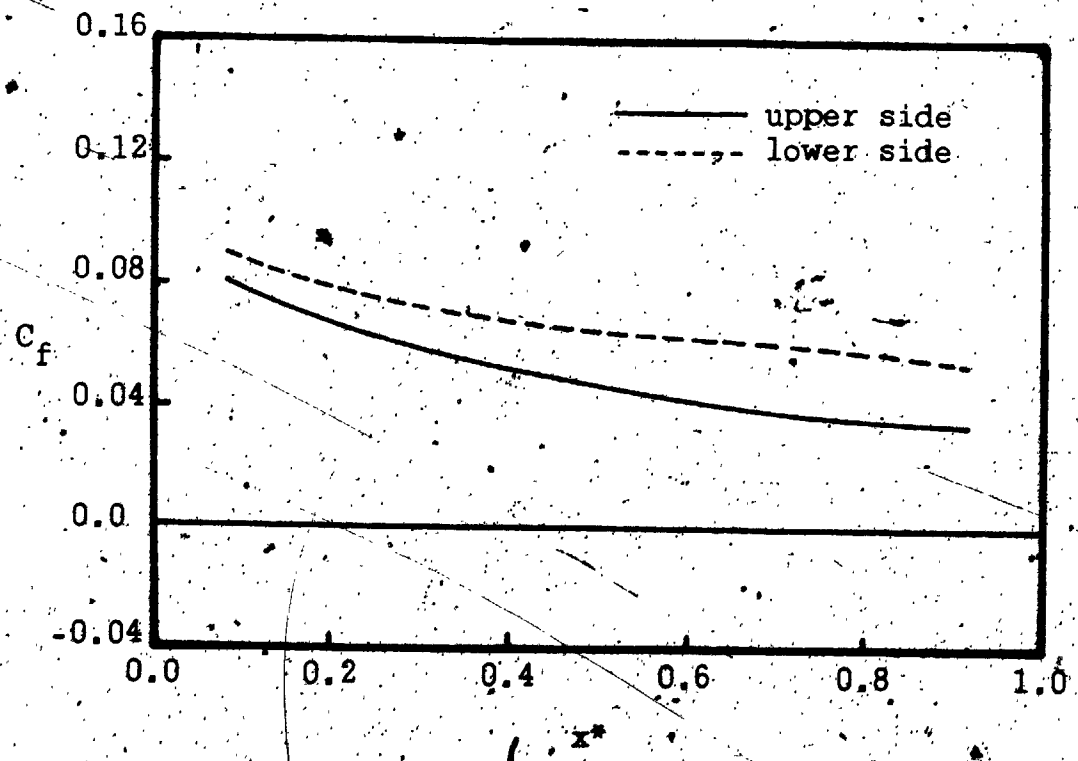


Fig. 11-r Local skin friction coefficient on the two sides of the plate at $t=2.44$ sec.

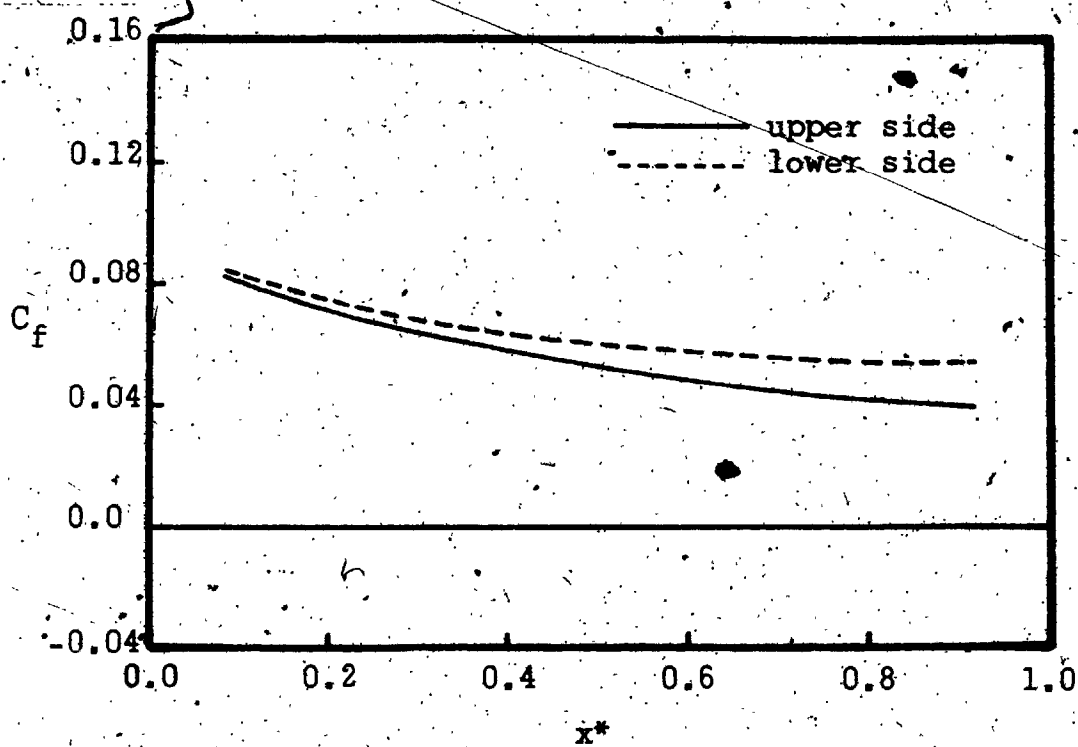


Fig. 11-s Local skin friction coefficient on the two sides of the plate at $t=2.6$ sec.

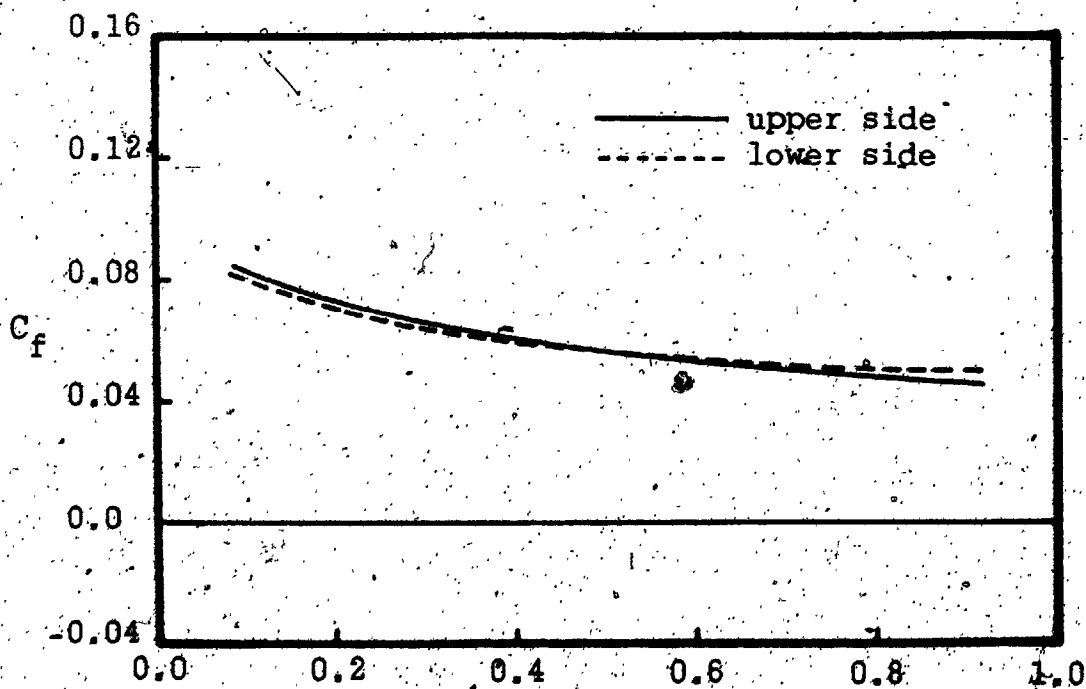


Fig. 11-t Local skin friction coefficient on the two sides of the plate at $t=2.84$ sec.

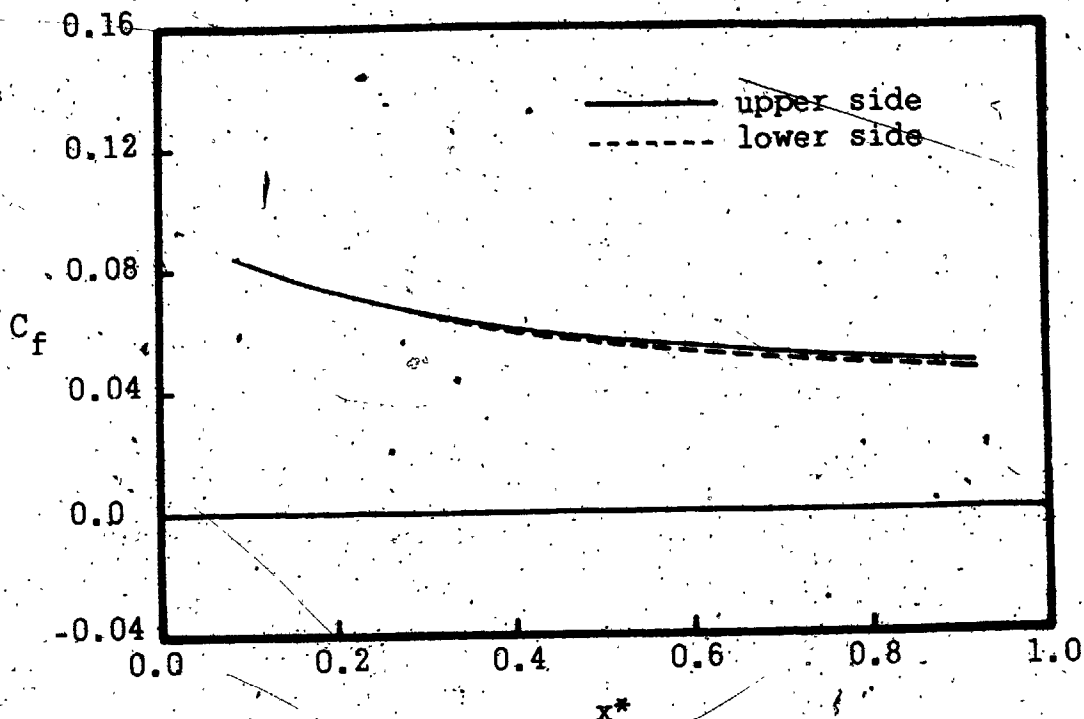


Fig. 11-u Local skin friction coefficient on the two sides of the plate at $t=3.24$ sec.

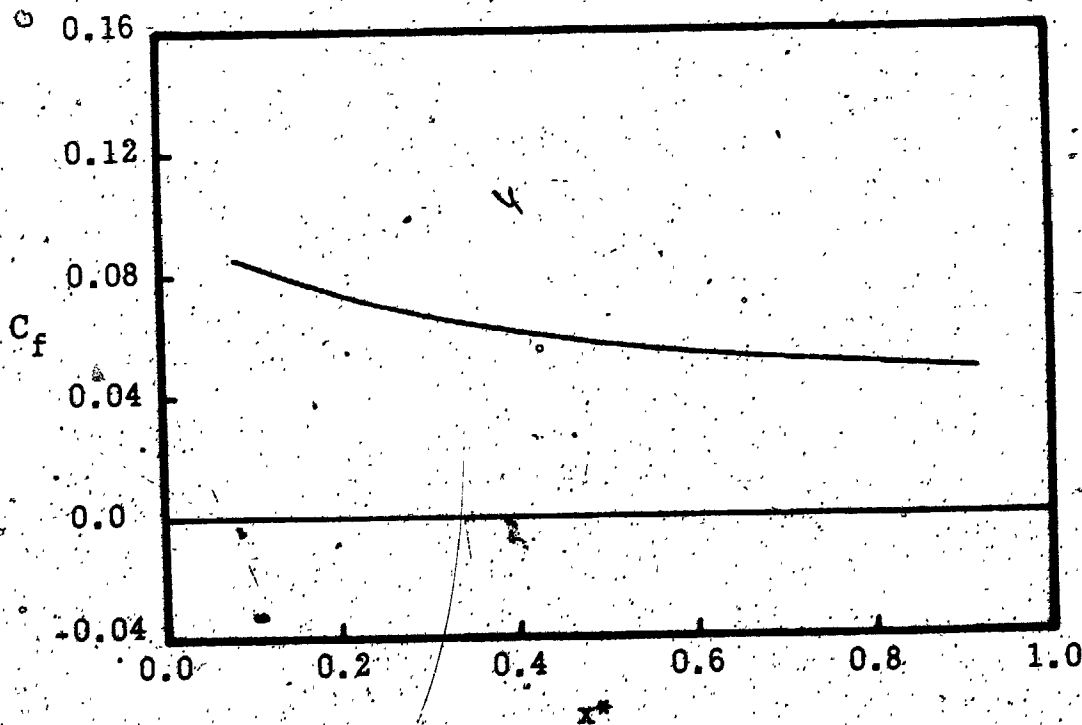


Fig. 11-v Local skin friction coefficient on the two sides of the plate at $t=3.52$ sec.

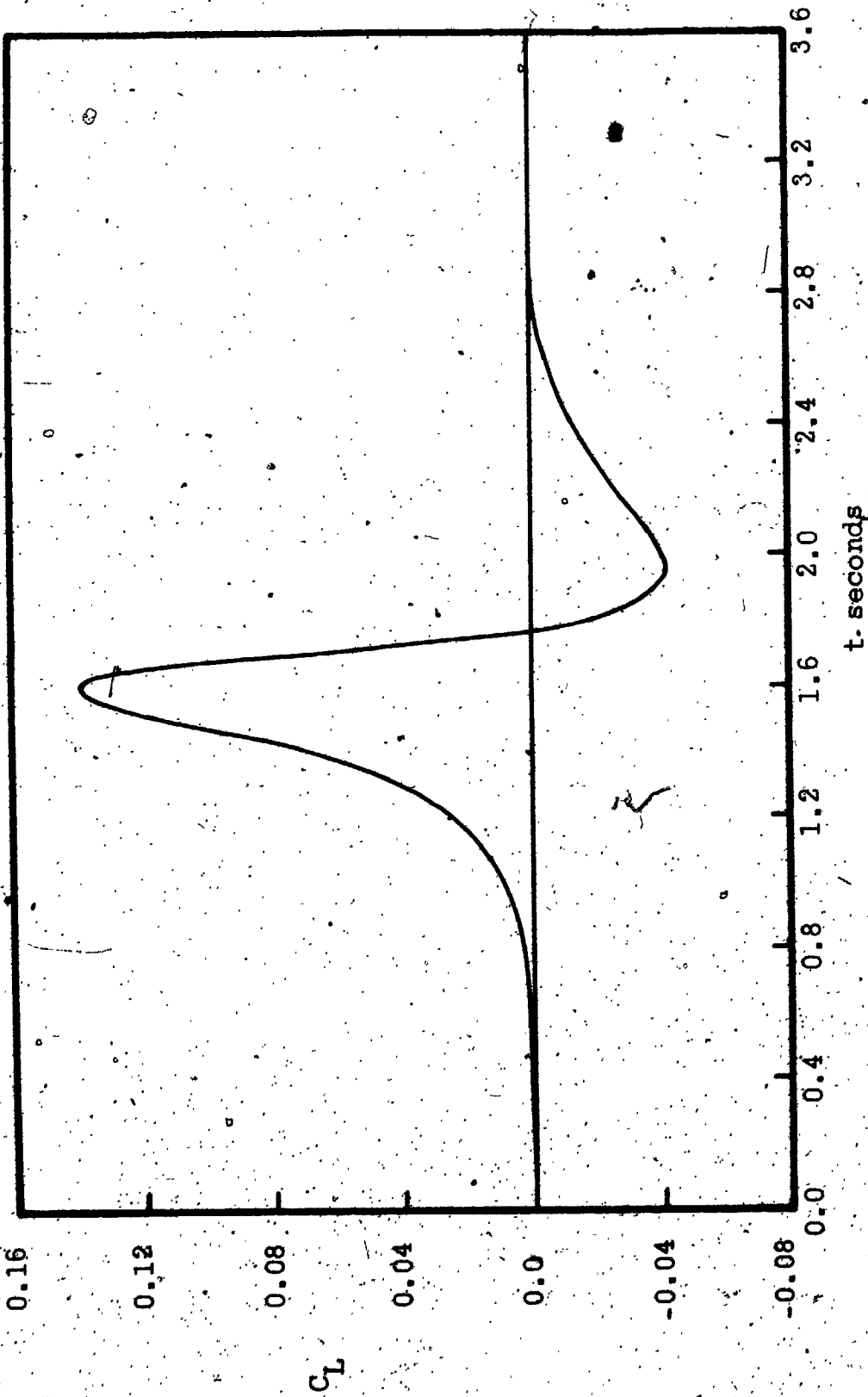


Fig. 12 Variation of lift coefficient with time

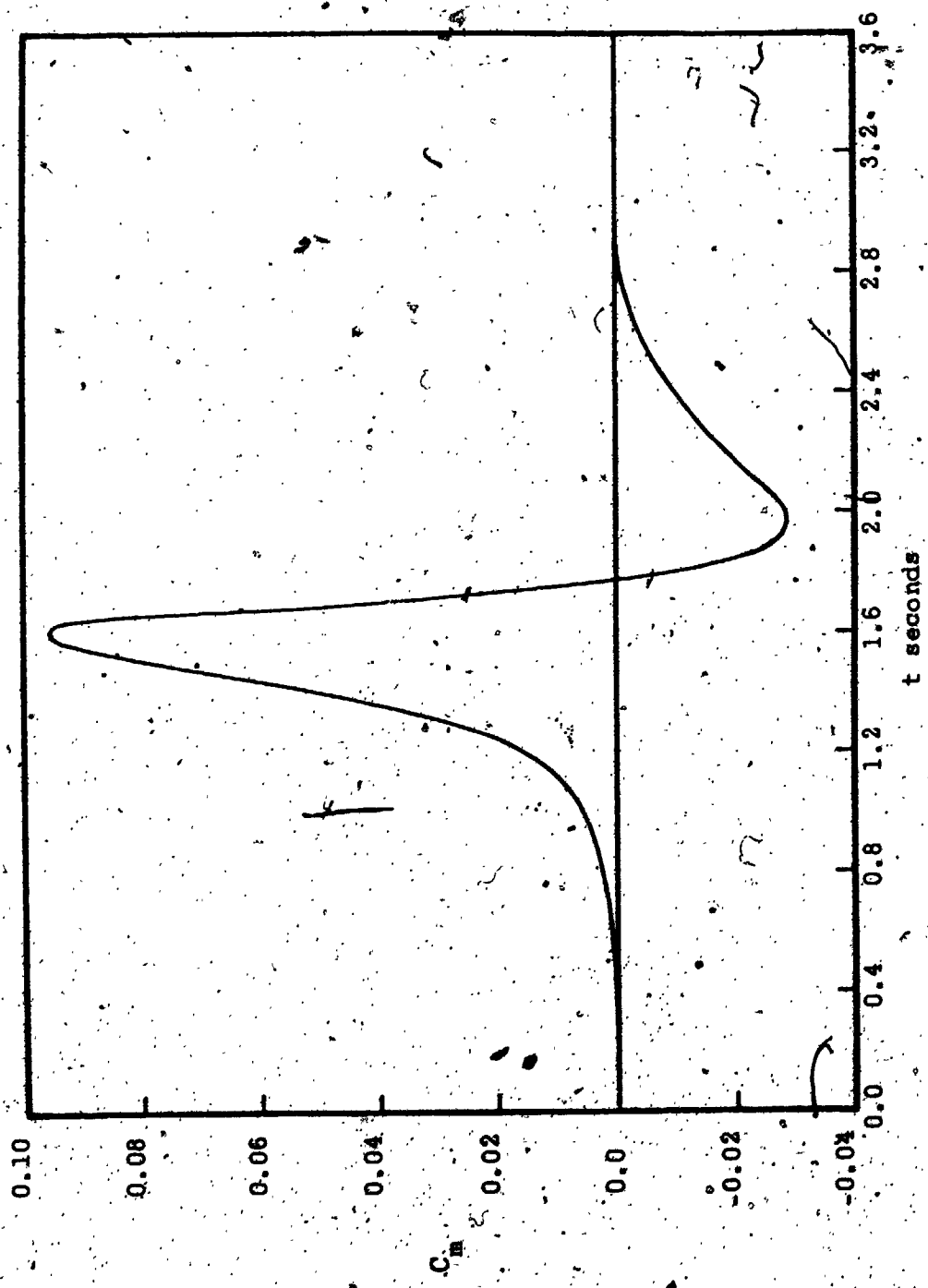


Fig. 13 Variation of the pitching moment coefficient about the leading edge with time

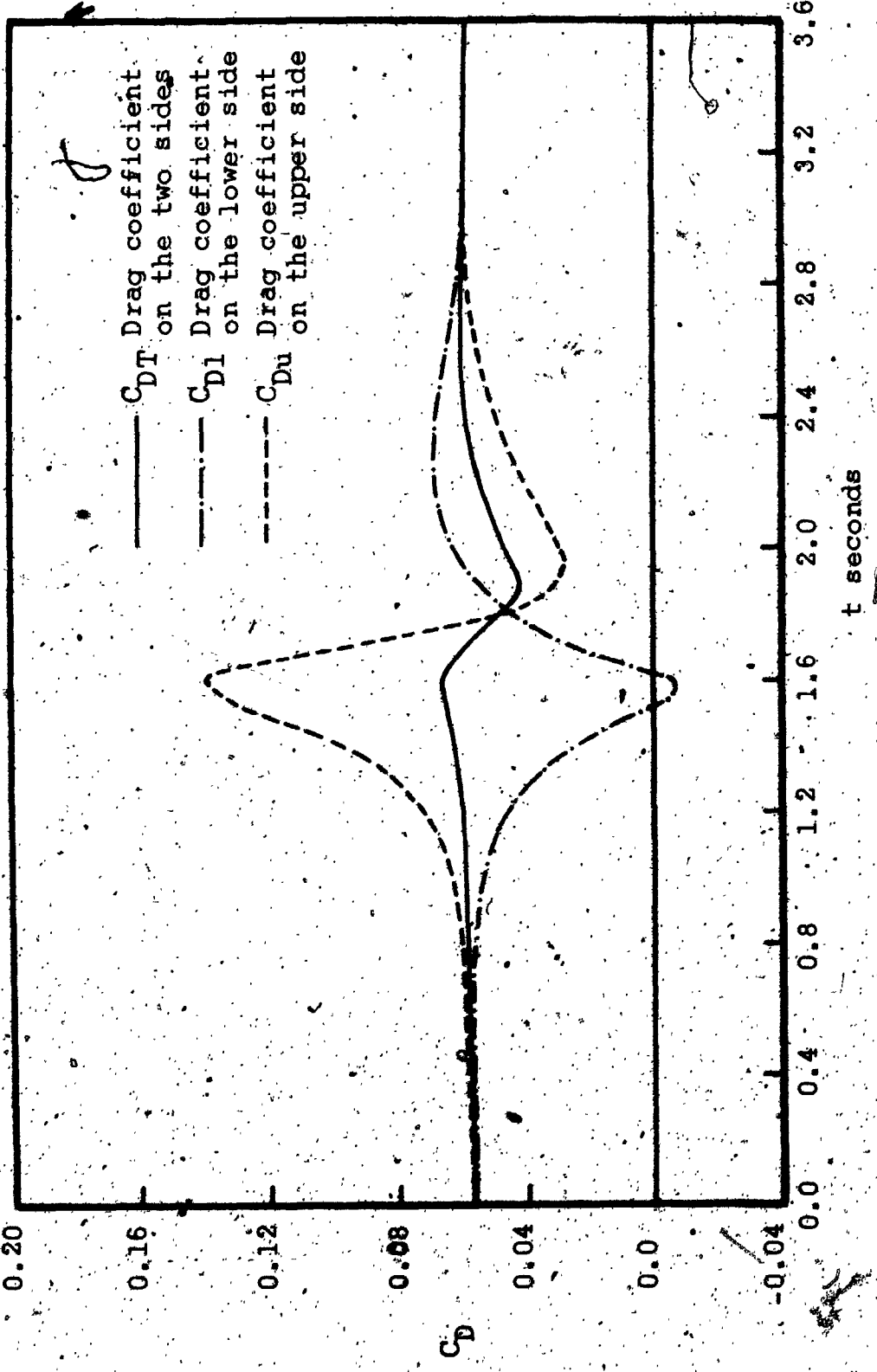


Fig. 14 Variation of drag coefficients with time

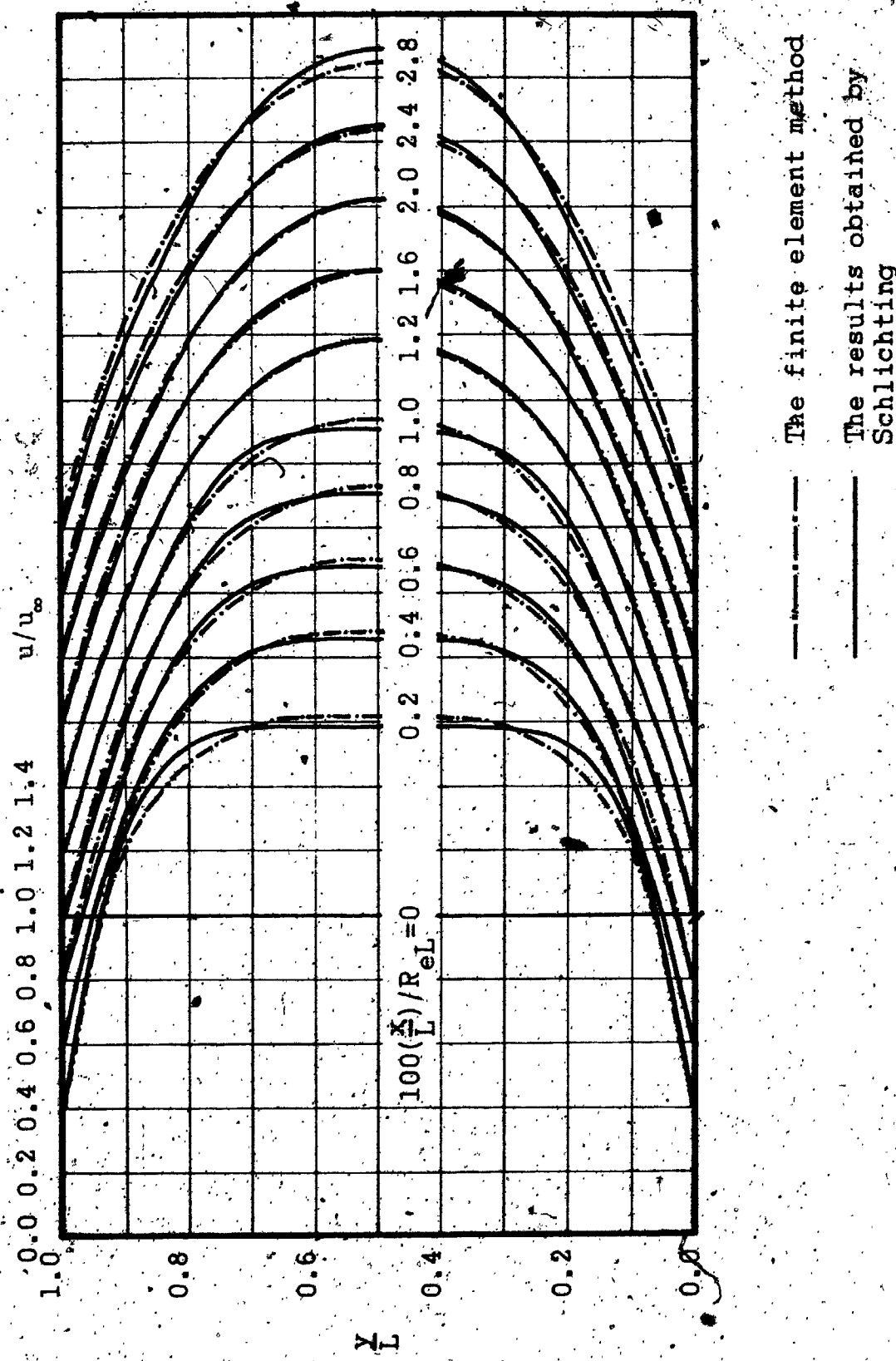


Fig. 15 Comparison between the velocity profiles at the entrance region of a channel by using the finite element method of solution and the results obtained by Schlichting (54)

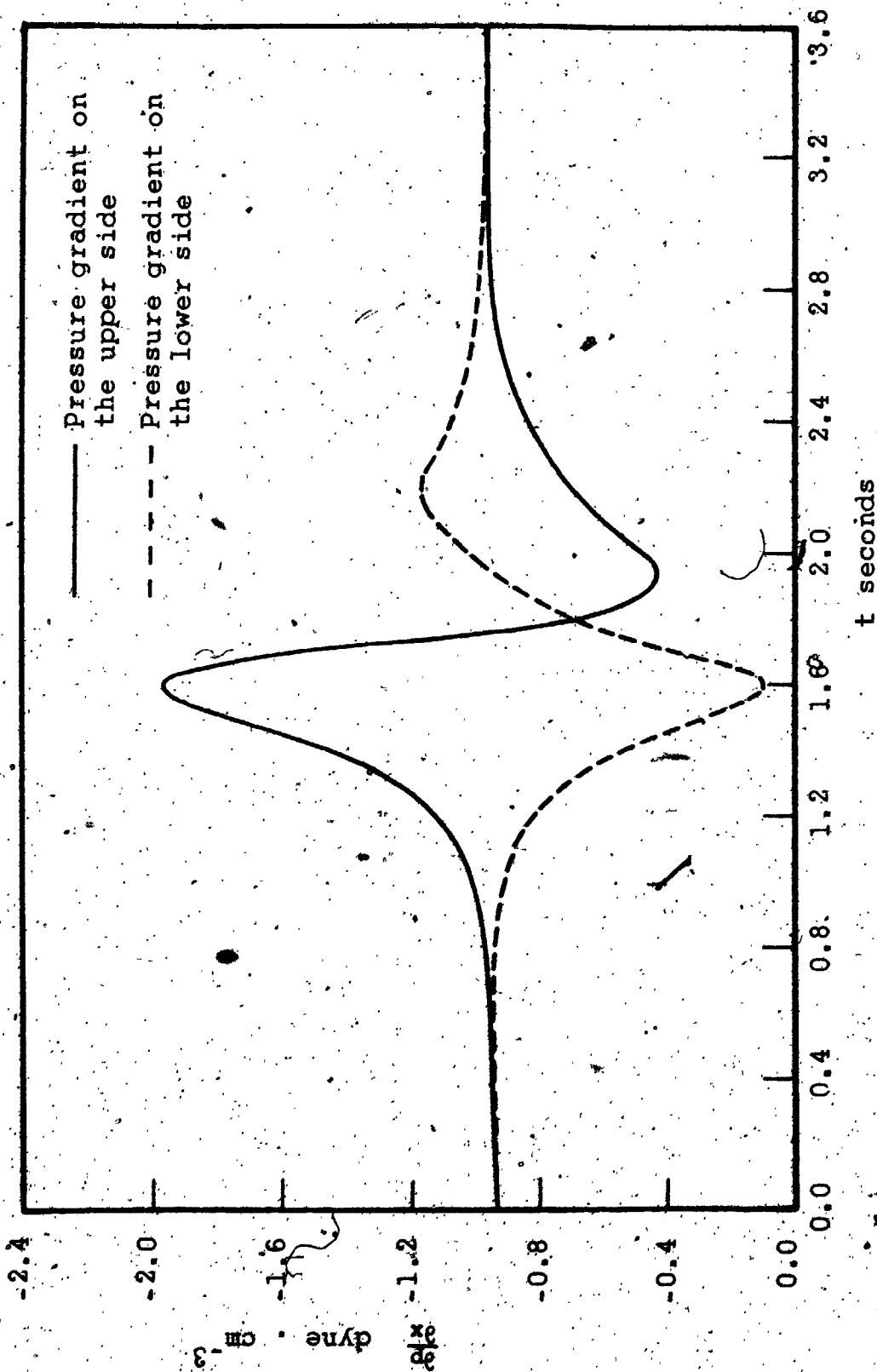


Fig. 16 Variation of the pressure gradient with time at $x^* = x/c = 0.5$

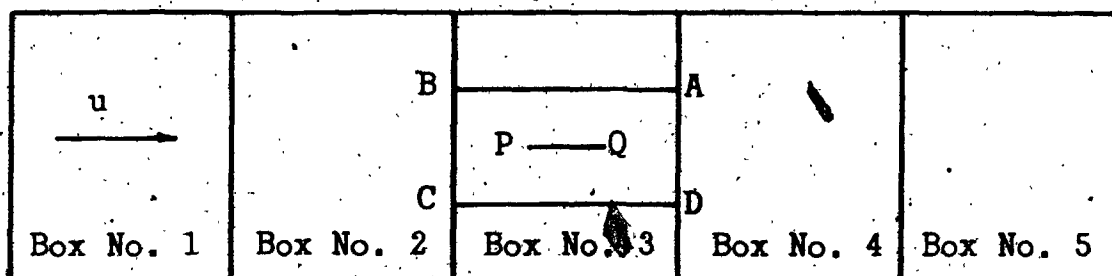


Fig. 17-a Schematic diagram showing five boxes for the real vortices with the flat plate (PQ) mounted inside the flow domain (ARCD)

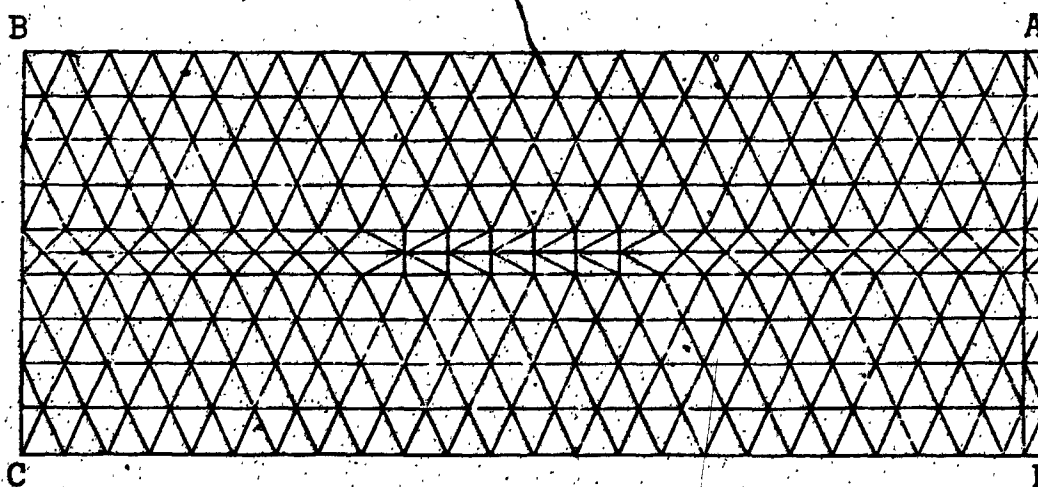
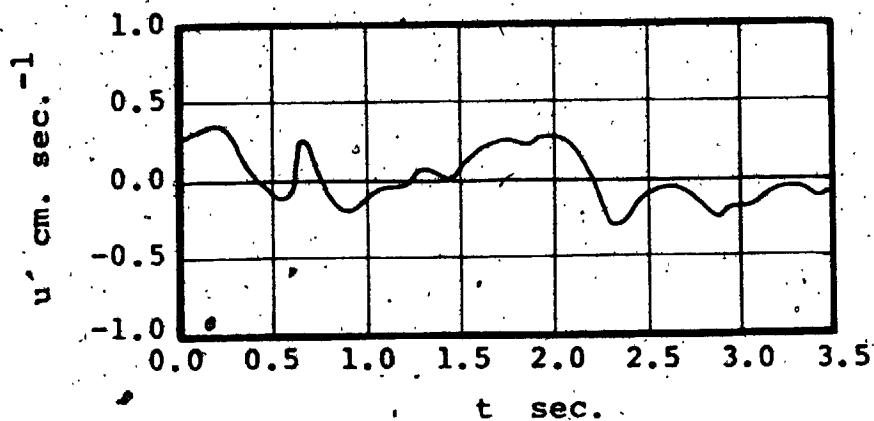
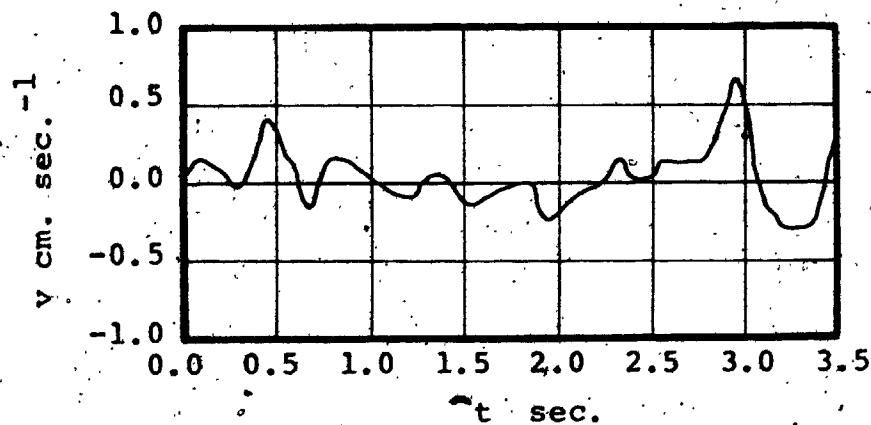


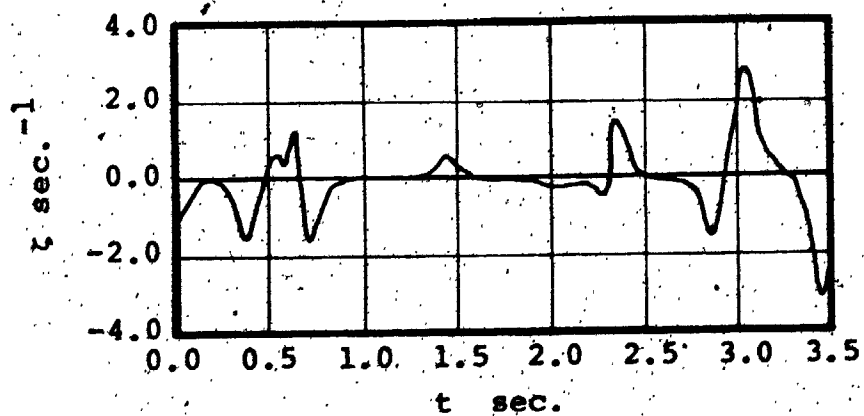
Fig. 17-b The finite element mesh inside the flow domain (ABCD)



Variation of longitudinal velocity component (u')

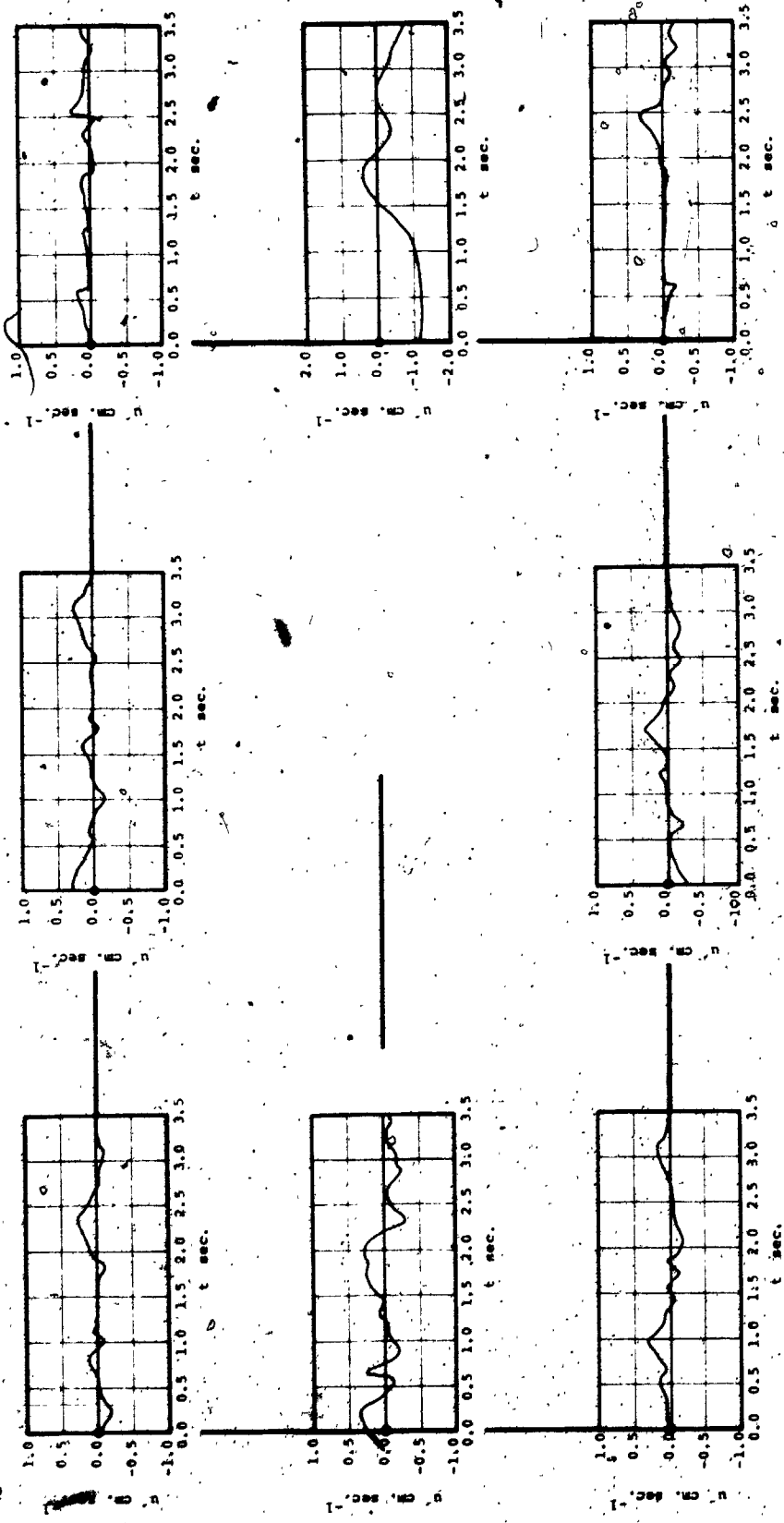


Variation of lateral velocity component (v)



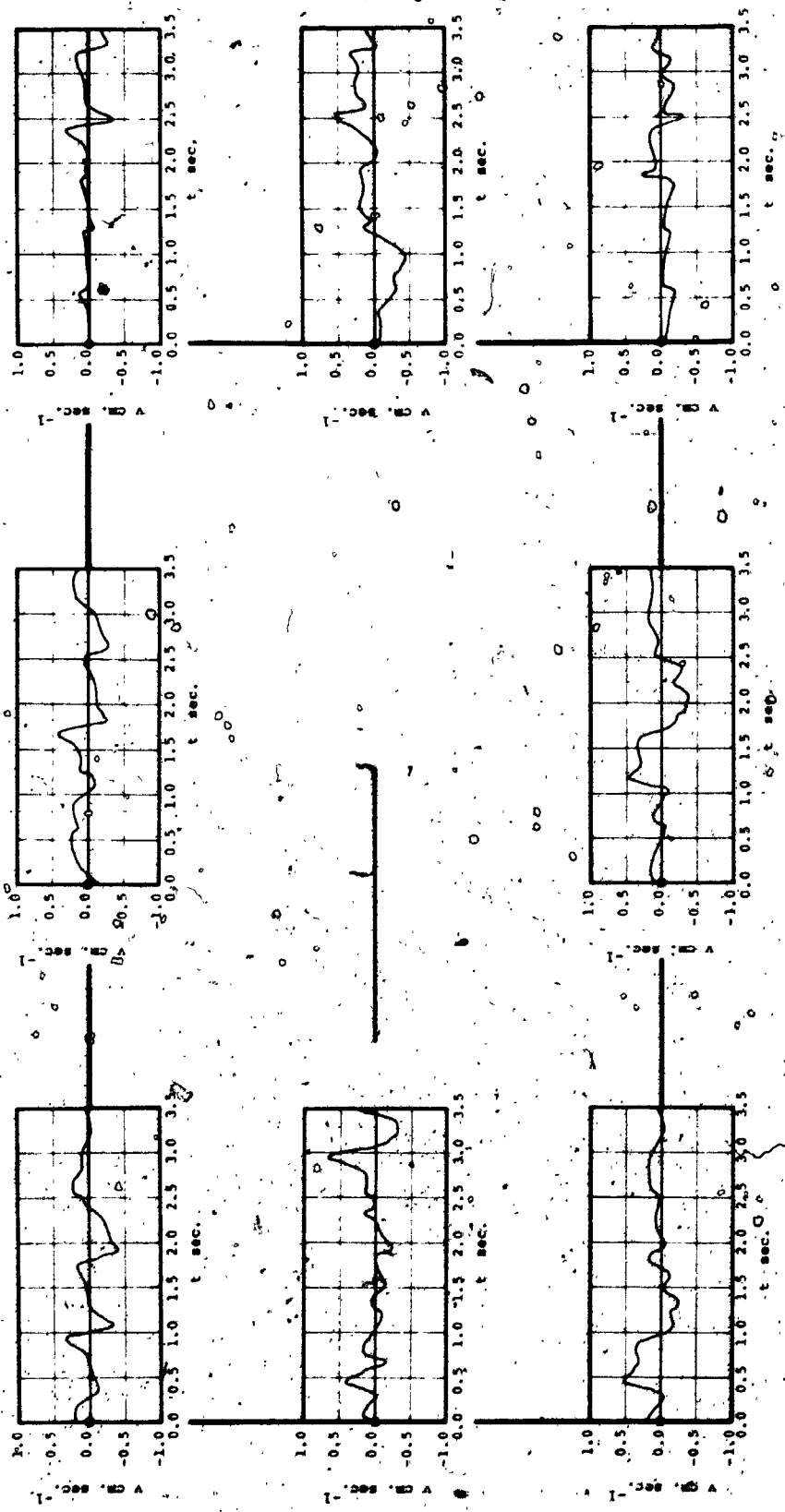
Variation of vorticity component (ζ)

Fig. 18 Typical traces of velocity and vorticity variations with time



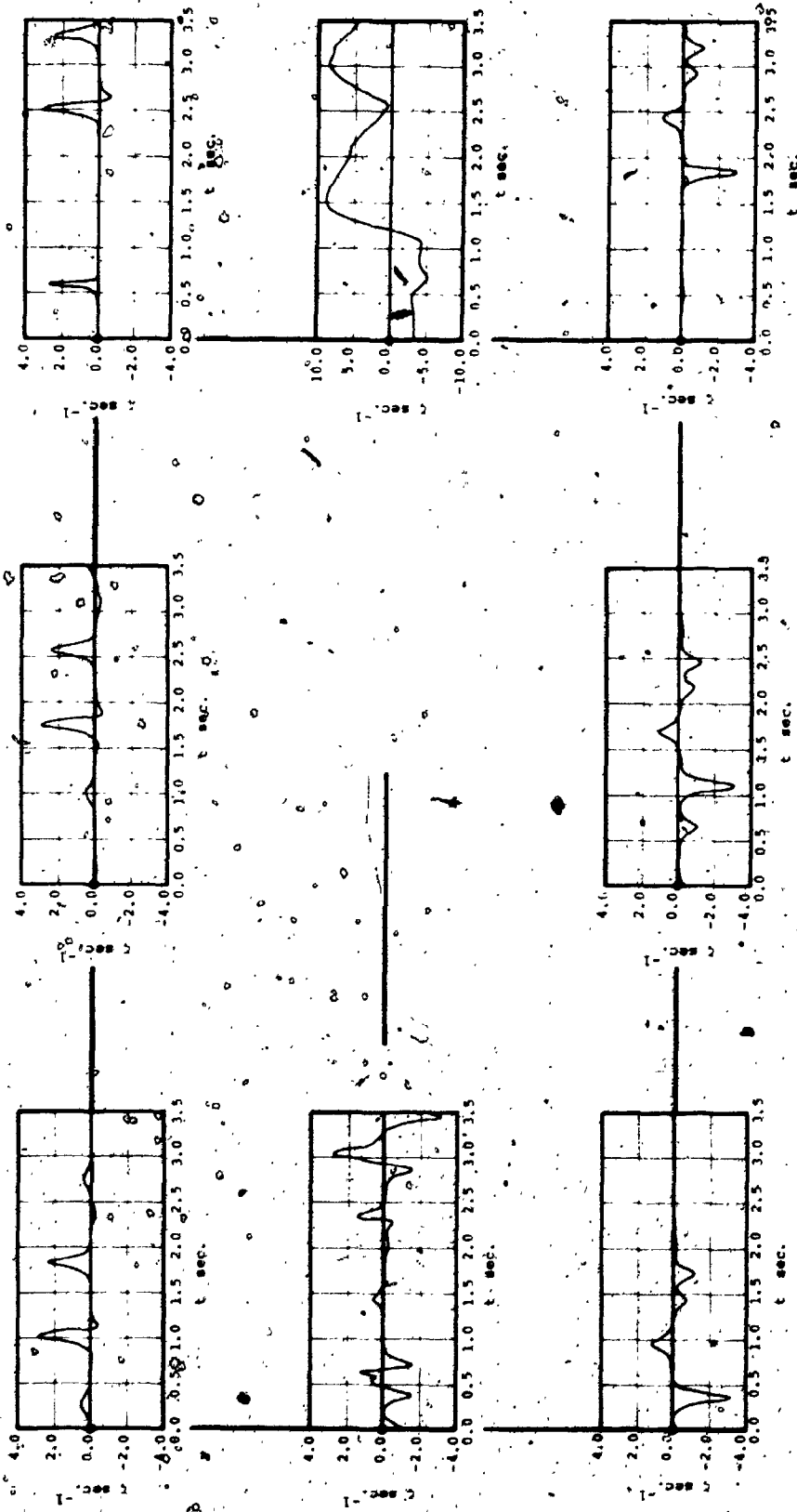
Legend • marks the position in space for the particular u' - t trace.

Fig. 19 Variation of the fluctuating component of the velocity u' with time at some points in the flow field.



Legend • marks the position in space for the particular v-t trace.

Fig. 20 Variation of the v component of the velocity with time at some points in the flow field.



Legend • marks the position in space for the particular -t trace.

Fig. 21 Variation of the vorticity with time at some points in the flow field.

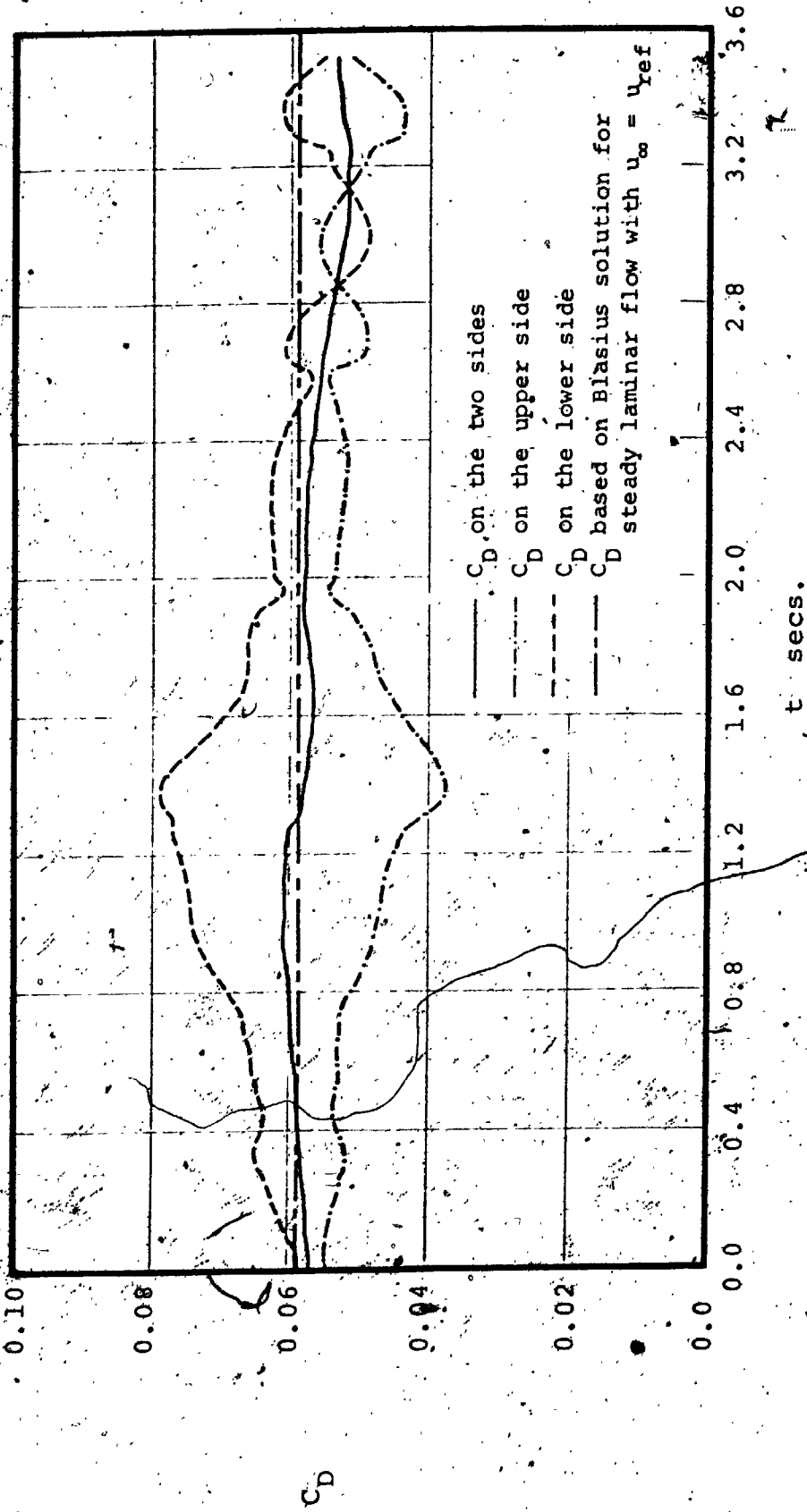


Fig. 22 Variation of Plate Drag Coefficients with Time

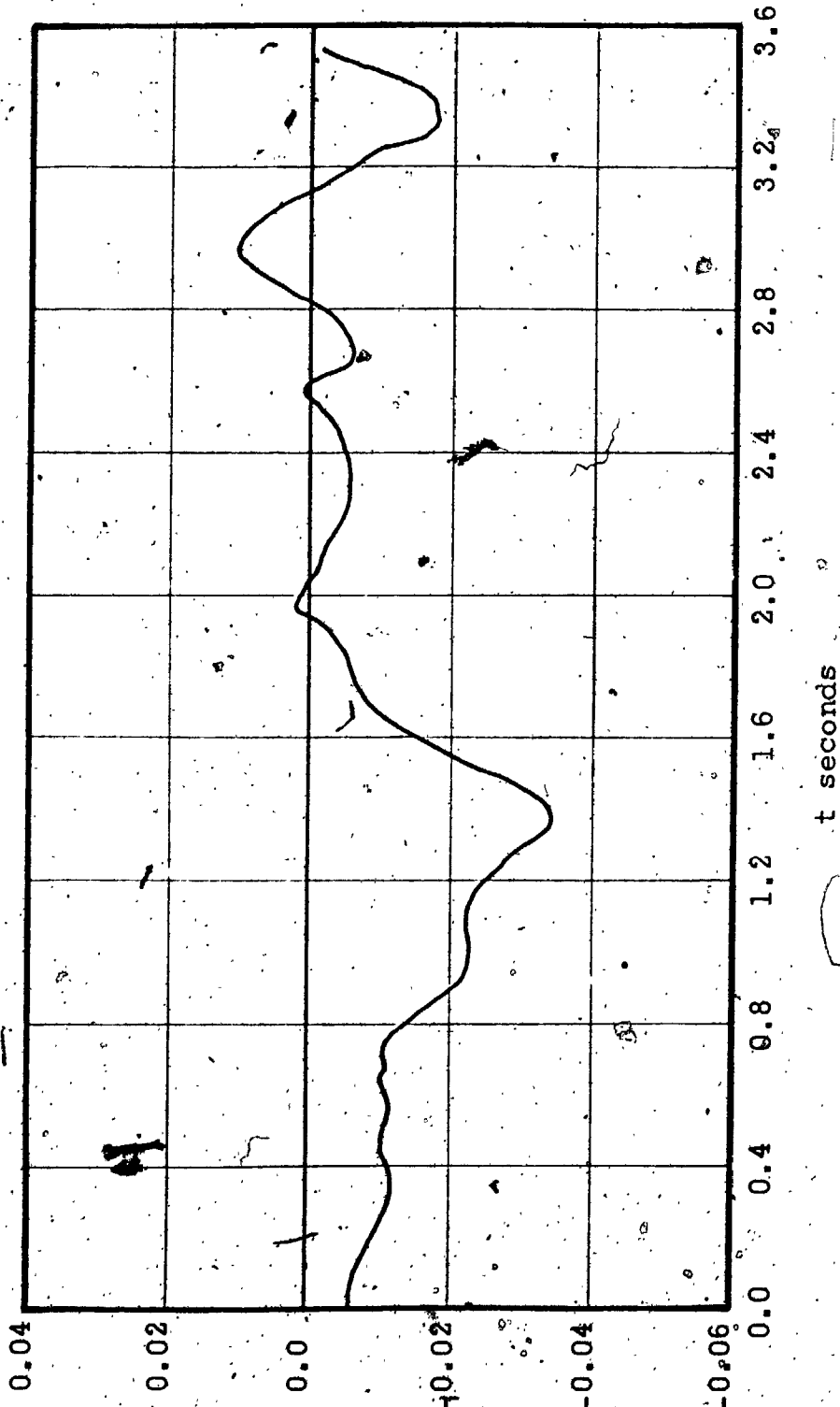


Fig. 23 Variation of lift coefficient with time